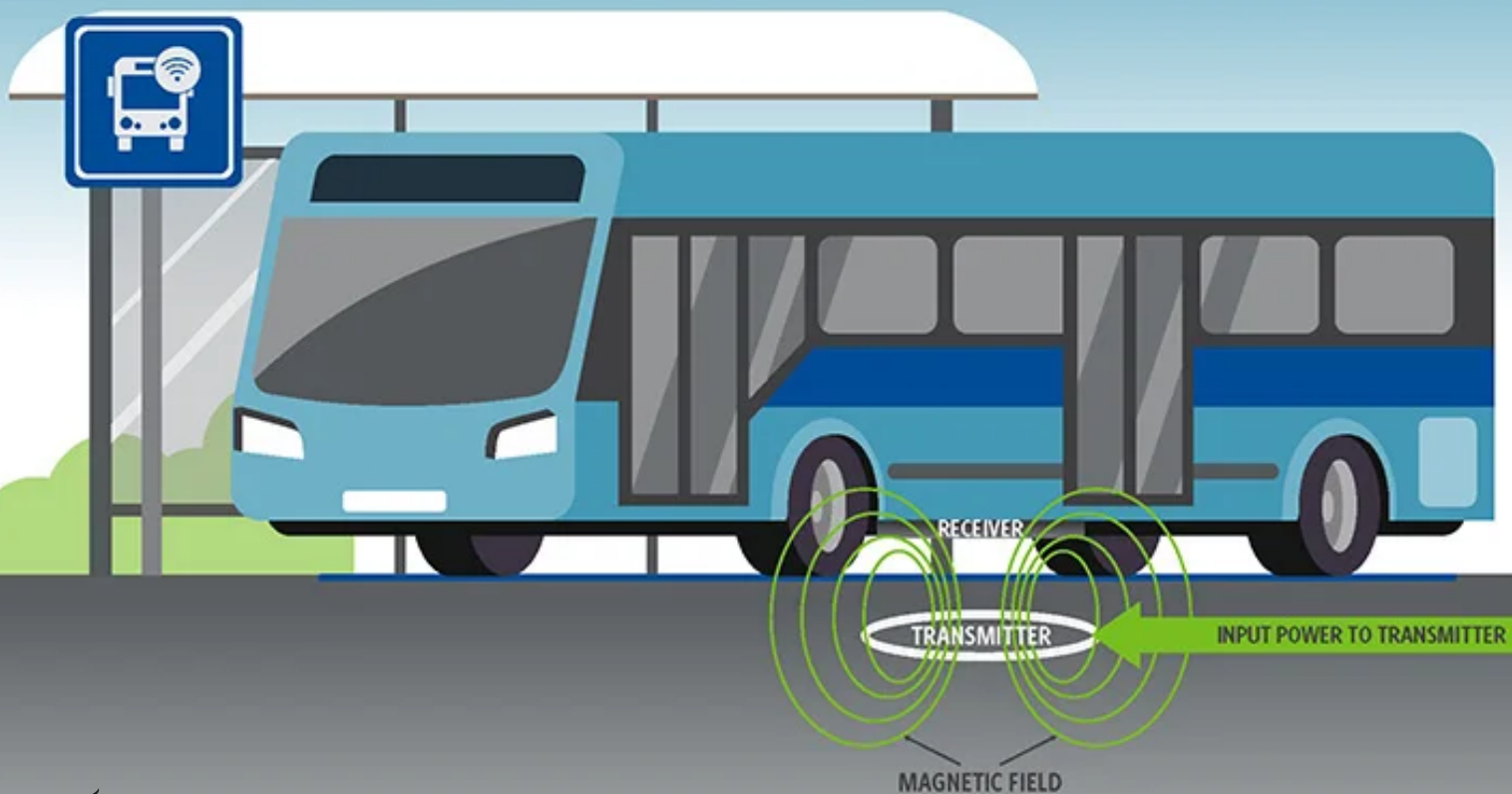


# Thesis:

Opportunity charging:

A case study based on real-life public transportation scenarios

Talha Kuruoglu





# Thesis:

## Opportunity charging: A case study based on real-life public transportation scenarios

by

Talha Kuruoglu

to obtain the degree of Master of Science  
at the Delft University of Technology,  
to be defended publicly on Thursday June 8, 2023 at 14:00.

Student number: 4718569  
Project duration: September 1, 2023 – June 8, 2023  
Thesis committee: Prof. dr. ir. P. Bauer, TU Delft, Responsible professor  
Dr. J. Dong, TU Delft, Supervisor  
Dr. ir. R. Santbergen, TU Delft

An electronic version of this thesis is available at <http://repository.tudelft.nl/>.



# Abstract

Emissions caused by regular vehicles with fossil fuels are problematic for the environment. The integration of electric vehicles in public transportation can potentially cause zero emissions. This paper will focus on the implementation of electric buses together with inductive chargers at bus stops. These chargers will charge the bus battery while passengers enter or leave the bus. This is also known as opportunity charging. Opportunity charging could result in the easier implementation of electric buses within public transportation since it solves the range problem that electric vehicles have.

The first parts of this paper will provide a discussion about the powertrain model made in Matlab/Simulink. The powertrain model input is the driving cycles from the Arnhem Trolleybus data. The outputs are the energy consumption during the driving cycle and the state of charge of the bus battery. The opportunity charger will then be added to the model to analyze the effects of opportunity charging on the bus. The implementation of opportunity charging increases the operational range of the electric bus, while also lowering the energy consumption.

The chargers will operate at a high power rating which spans from 100 kW to 200 kW. These power ratings could cause congestion of the grid. This is why the feasibility of PV systems at bus stops is analyzed using a PV model. A PV system is insufficient to power the chargers on its own. The PV system can still provide a significant percentage of the charger power demand.



# Preface

This preface is written to show gratitude to the people that supported me during my master's thesis. Firstly I would like to thank my daily supervisor Calvin Riekerk for his guidance and feedback which helped me with my progress in the master thesis. I would also like to thank Dr.Jianning Dong for giving his insight and feedback which improved the quality of the thesis. I would also like to thank Ibrahim Diab for the providence of the driving cycle and PV model data which were used within this thesis. Finally, I would like to thank Prof.dr.ir.P.Bauer and Dr.ir.Rudi Santbergen to take the time to be on my thesis committee.

*Talha Kuruoglu  
Delft, June 2023*



# Contents

<b>Abstract</b>	<b>iii</b>
<b>1 Introduction</b>	<b>1</b>
1.1 Motivation . . . . .	1
1.2 Driving Cycles . . . . .	1
1.3 Thesis Objectives. . . . .	2
1.4 Thesis Outline . . . . .	3
<b>2 Powertrain components and models</b>	<b>5</b>
2.1 Electric Vehicle Configuration . . . . .	5
2.1.1 Bus company configurations. . . . .	6
2.1.2 Configuration choice . . . . .	6
2.2 Electrical machine . . . . .	6
2.3 Battery . . . . .	7
2.3.1 Battery model. . . . .	7
2.3.2 Parameter identification . . . . .	7
<b>3 Bus Characteristics</b>	<b>11</b>
3.1 Bus dynamics. . . . .	11
3.2 Vehicle Resistance . . . . .	11
3.2.1 Rolling Resistance . . . . .	11
3.2.2 Aerodynamic Drag . . . . .	12
3.2.3 Grading Resistance . . . . .	12
3.3 Battery parameters . . . . .	12
3.4 Bus Dimensions . . . . .	13
3.5 Bus Performance . . . . .	14
3.5.1 Top speed. . . . .	14
3.5.2 Road angle . . . . .	14
3.5.3 Acceleration and Deceleration. . . . .	14
3.6 Gear ratio and EM parameters. . . . .	14
3.6.1 Gear. . . . .	14
3.6.2 EM parameters and inverter efficiency . . . . .	15
3.7 Auxiliary and HVAC. . . . .	15
<b>4 Simulation of electric powertrain of electric buses</b>	<b>17</b>
4.1 Vehicle model. . . . .	17
4.1.1 Driver model . . . . .	17
4.1.2 Forward movement. . . . .	18
4.1.3 Braking strategy model. . . . .	18
4.1.4 Vehicle speed. . . . .	20
4.1.5 Battery input power. . . . .	20
4.2 Battery model. . . . .	21
4.2.1 Single cell current demand. . . . .	21
4.2.2 DP model . . . . .	21
4.2.3 Output of battery model . . . . .	22
<b>5 Opportunity Charging</b>	<b>23</b>
5.1 Inductive charger . . . . .	23
5.1.1 Wireless charger overview. . . . .	23
5.1.2 System Efficiency. . . . .	24

5.2	Different opportunity charging case implementations. . . . .	24
5.2.1	Opportunity charging at every stop . . . . .	24
5.2.2	Minimum amount of stops needed. . . . .	25
5.3	Battery sizing . . . . .	26
5.4	Charging model. . . . .	28
5.4.1	SOC check . . . . .	29
5.4.2	Stoppick. . . . .	29
5.4.3	Savedstops . . . . .	29
<b>6</b>	<b>PV system for opportunity charging</b>	<b>31</b>
6.1	PV power output model . . . . .	31
6.2	PV system placement and assumptions. . . . .	32
6.2.1	PV module placement . . . . .	32
6.2.2	Assumptions . . . . .	32
6.3	Simulation Model . . . . .	32
6.4	Energy-Neutrality Ratio . . . . .	33
<b>7</b>	<b>Results &amp; Discussion</b>	<b>35</b>
7.1	Opportunity charging at every stop . . . . .	35
7.2	Discussion of the minimum battery size . . . . .	38
7.3	Results of the minimum amount of stops . . . . .	38
7.3.1	Minimum stops at 200kW . . . . .	38
7.3.2	Minimum stops at 150kW . . . . .	39
7.3.3	Minimum stops at 125kW . . . . .	40
7.3.4	Minimum stops at 100kW . . . . .	41
7.4	Discussion of the minimum amount of stops . . . . .	43
7.5	PV Results . . . . .	43
7.5.1	PV system sizing . . . . .	43
7.5.2	Standalone PV system or grid-tied PV system . . . . .	47
7.6	PV discussion. . . . .	50
7.7	Energy Consumption results and discussion . . . . .	51
<b>8</b>	<b>Conclusion</b>	<b>53</b>
<b>A</b>	<b>Appendix</b>	<b>55</b>
A.1	Driving Cycles . . . . .	55
A.2	Energy Consumption. . . . .	59

# Introduction

## 1.1. Motivation

In recent years, there has been a growing interest in electric buses as a more sustainable and environmentally friendly alternative to traditional diesel-fueled buses. However, one of the major challenges facing the adoption of electric buses is the limited range of their batteries, which can lead to concerns about their practicality for use in public transportation systems. Opportunity charging utilizing inductive power transfer is a technology developed to address this challenge. It offers a solution that enables electric buses to recharge their batteries while parked at bus stops, without manual intervention or long charging times.

The technology works by using wireless charging, also known as inductive charging. This involves the transfer of electrical energy through an electromagnetic field from a charging pad on the ground to a receiver on the underside of the bus. The charging pad is installed at the bus stop, and the bus parks directly over it to initiate the charging, while taking in passengers.

Opportunity charging utilizing inductive power transfer has several advantages compared to other charging methods. Inductive charging systems have no mechanical components [28]. This makes the charging systems maintenance-free for many years [28]. This advantage causes to save maintenance and personnel costs [28]. In addition, inductive opportunity charging can help extend the range of electric buses, allowing them to travel long distances without needing to recharge. This can increase the adoption of electric buses, particularly in urban areas where range anxiety is a significant concern.

The possibility of grid congestion becomes present by adding chargers that need a high power rating at bus stops. Congestion in the grid is an unwanted electricity supply and demand limitation because of capacity constraints [8]. Natural resources like solar could be used by installing PV modules at bus stops. This addition could result in the reduction or elimination of the energy demand from the grid. Another advantage of a solar source is the positive effect on the environment since it is a source that does not produce air pollution.

Overall, inductive opportunity charging has the potential to transform the public transportation industry by making electric buses more reliable, efficient, and environmentally friendly. As more cities around the world look to reduce their carbon footprint and improve the sustainability of their transportation systems, the adoption of inductive opportunity charging technology is likely to continue to grow.

## 1.2. Driving Cycles

The driving cycle data in this report is from the trolleybus grid of Arnhem [16],[39]. This data is used because it represents bus routes based on real-life driving cycles of different buses. This enables the chance to look at multiple driving cycles, which means more variety of data to analyze in this paper. The data used are different routes that different buses use in the trolleybus grid. This is shown in



## **1.4. Thesis Outline**

This paper will discuss the modeling of the powertrain of the electric bus. The electric bus model calculates the energy consumption of an electric bus at a specific driving cycle. The powertrain model is discussed in Chapters 2 to 5. The implementation of opportunity charging with different power ratings and charging times is discussed afterwards in Chapter 6. This is followed up by the feasibility investigation of implementing PV systems at bus stops that serve as input for the chargers in Chapter 7. The paper is finally finished with the results, discussion, and conclusion covered in Chapters 8 and 9.



# 2

## Powertrain components and models

The powertrain is the combination of every component that causes a vehicle to move. This chapter will describe the powertrain configuration and the powertrain components of the electric bus model which is used in this paper.

### 2.1. Electric Vehicle Configuration

Electric vehicles (EVs) like electric buses have a variety of configurations that are possible. Figure 2.1 shows possible EV configurations which could be picked for the electric bus model.

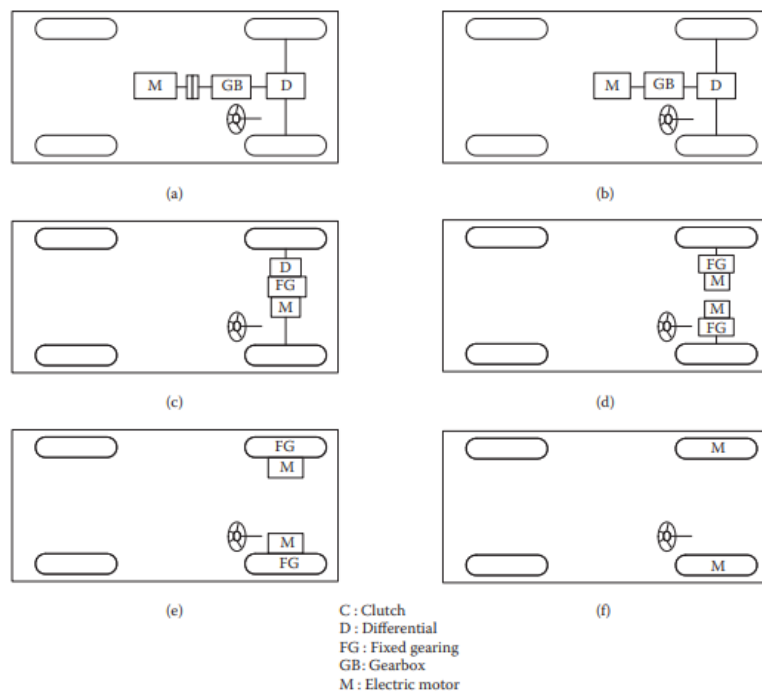


Figure 2.1: Electric vehicle configurations [18].

Figure 2.1(a) is more similar to a conventional vehicle with the engine replaced by an electric machine [18]. Figure 2.1(b) has a fixed gearing and removes the clutch. This becomes possible because the electric machine has a constant power in a long speed range [18]. Figure 2.1(c) is similar to figure 2.1(b). The whole drivetrain is simplified and compacted [18]. The configurations mentioned will be called **single machine powertrain** in this paper.

Figure 2.1(d) shows a configuration in which the mechanical differential is replaced by using two traction motors [18]. The configuration mentioned will be called **dual machine powertrain**.

The last configurations in figure 2.1 are configurations that use in-wheel drive [18]. This paper will mention the configurations as **in-wheel powertrain**.

### 2.1.1. Bus company configurations

Different literature papers and data sheets of bus companies are analyzed to find the EV configuration which will be used for the electric bus design. The configurations used by the bus companies are determined from the provided datasheet and they are listed in table 2.1.

Table 2.1: Bus companies and the powertrain configuration that companies use in their battery electric buses.

Bus company	Configuration
BYD bus	In-wheel powertrain [10]
Proterra	Single machine and dual machine powertrain [35]
Saietta	In-wheel powertrain [37]
Optare	Dual machine powertrain [34]
Solaris	Single machine powertrain [41]
King Long	Single machine and dual machine powertrain [30]
Mercedes Benz	Dual machine powertrain [31]

### 2.1.2. Configuration choice

Table 2.1 shows that almost all configurations are used in real-life buses. This thesis will implement the configuration shown in figure 2.1(b). The thesis is only interested in the power consumption of the powertrain, detailed implementation is not of concern for the study. The energy consumption of the configurations given in figure 2.1 have an energy consumption difference in the range of  $\pm 4\%$  [29] when compared to each other. Thus configurations will have similar values for energy consumption. The most simple configuration is chosen to be implemented.

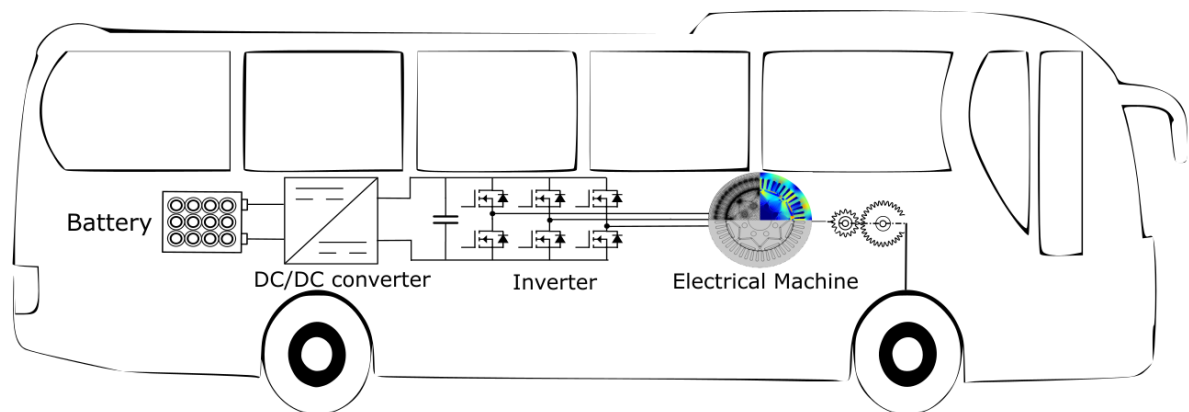


Figure 2.2: Simplified image of the overall powertrain model used in this paper.

## 2.2. Electrical machine

An electrical machine is needed for the powertrain to convert electrical energy to mechanical energy, which must be done the other way around when regenerative braking is considered. There are two commonly used electrical machines for electric vehicles in commercialized applications and also research studies[27]:

1. Permanent magnet synchronous machine (PMSM)
2. Induction machine (IM)

Depending on the usage of the vehicle, the IM has advantages over the PMSM, the same goes for the PMSM. The electric bus will probably mostly ride within the city, thus meaning that it will have a low-speed region.

The PMSM will be used in this paper as the electrical machine for the powertrain. The PMSM has higher efficiency at low speeds compared to IM, which results in better battery utilization and a larger driving range [27]. An electric bus within the city will usually operate at lower speed values. The advantage mentioned makes this machine preferable compared to the IM.

## 2.3. Battery

### 2.3.1. Battery model

Different battery models are available in literature while building a model for an electric bus. This paper will use an equivalent circuit model to model the battery. The dual polarization (DP) model has the best dynamic performance and SOC estimation compared to other electric circuit battery models [24] [25] [42] and is thus chosen for the battery design. This is backed by the Hybrid Pulse Power Characterization (HPPC) test, Dynamic Stress Test (DST), and the FUDS test with multiple amounts of RC networks, which resulted in showing that two RC networks are the best amount for electric circuit battery models [25]. The DP model is shown in figure 2.3.

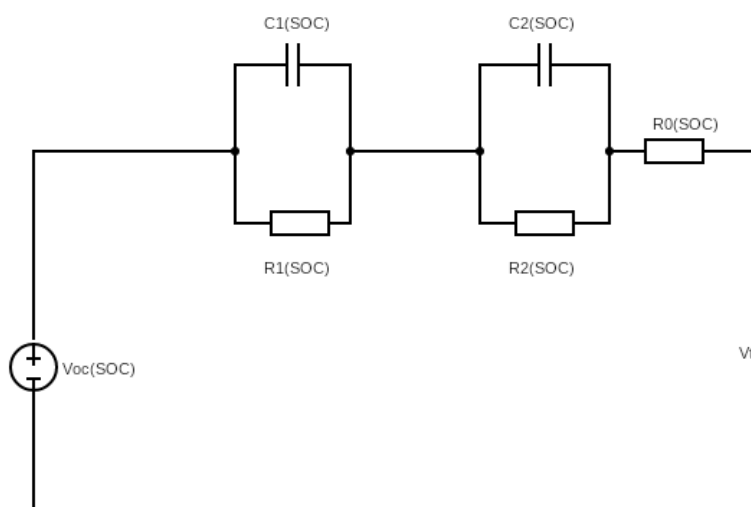


Figure 2.3: The DP model.

### 2.3.2. Parameter identification

The parameters from the DP model, which can be seen in figure 2.3, are determined by doing tests on real-life batteries. One of those tests is the standard pulsed discharge test on the Li-ion NMC cell, Sanyo-Panasonic NCR18650GA in paper [36]. This test is based on discharge pulses. The battery cell is discharged until three percent of SOC is removed. The discharge phase is followed by a relaxation period of 10 minutes [36]. The result of this test can be seen in figure 2.4, which represents one particular SOC value. This pulse is repeated from zero SOC to 100 SOC with a stepsize of 3 SOC.

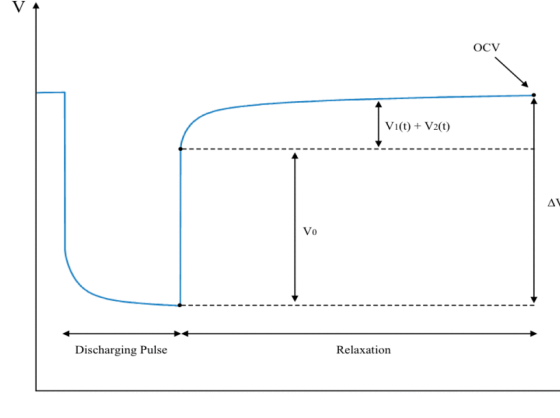


Figure 2.4: Image of the discharge pulses [13].

### Open circuit voltage determination

Figure 2.4 shows that the open circuit voltage (OCV) is obtained by looking at the end of the relaxation phase for a specific SOC [13].

### $R_0$ determination:

The resistance  $R_0$ , from figure 2.3(c) is dependent on the SOC of the battery and can be determined at either the beginning of the discharge pulse or the relaxation period. It is obtained from the straight vertical line part [36][13] which can be seen in figure 2.4. The voltage difference of those parts must be taken and then it must be divided by the current pulse value to determine the resistance. The equations used to determine the resistance are given, by equations 2.1 and 2.2 [36]. The average of the values obtained from the equations is taken as the final value of  $R_0$

$$R_{0\_disch} = \frac{V_{begin\_disch} - V_{end\_disch}}{I_B} \quad (2.1)$$

$$R_{0\_relax} = \frac{V_{begin\_relax} - V_{end\_relax}}{I_B} \quad (2.2)$$

### Time constants determination:

The parameters of the two RC branches of the DP model can be estimated by the time constant and coefficient pairs  $(c_1, \tau_1), (c_2, \tau_2)$  [36]. Equation 2.3 is used to doing the discharge and relaxation transient data analysis to find the time constants and the coefficients. This equation is based on the nonlinear least-squares curve fitting algorithm *Isqnonlin*, with predetermined boundaries, which is available in Matlab [36]. The curve fitting is applied at the non-linear parts of the discharging pulse and relaxation part from figure 2.4.

$$V(t) = c_1(1 - e^{-\frac{t}{\tau_1}}) + c_2(1 - e^{-\frac{t}{\tau_2}}) \quad (2.3)$$

### RC parameter determination:

The parameters  $(c_1, \tau_1)$ , which are introduced previously, are used to determine  $R_1$  for the relaxation transient with the following equation [36]:

$$R_1 = \frac{c_1}{(1 - e^{-\frac{t^*}{\tau_1}})I_B(t^*)} \quad (2.4)$$

Where:

$t^*$  : The time refers to the final condition ( $t = t^*$ ) of the previous discharge transient.

The parameters  $(c_2, \tau_2)$ , which are introduced previously, are used to determine  $R_2$  for the relaxation

transient with the following equation[36]:

$$R_2 = \frac{c_2}{(1 - e^{-\frac{t^*}{\tau_2}})I_B(t^*)} \quad (2.5)$$

The formulas for the discharge transient used to determine  $R_1$  and  $R_2$  are given by [36]:

$$R_1 = \frac{c_1}{I_B(t^*)} \quad (2.6)$$

$$R_2 = \frac{c_2}{I_B(t^*)} \quad (2.7)$$

Where:

$(c_1, c_2)$  : Represents the voltage across the two capacitors at the end of the discharge transient.

The values of  $C_1$  and  $C_2$  for both relaxation and discharge transient are calculated by[36]:

$$C_1 = \frac{\tau_1}{R_1} \quad (2.8)$$

$$C_2 = \frac{\tau_2}{R_2} \quad (2.9)$$

The RC parameters obtained are for relaxation and discharge transient at every SOC breakpoint of the single discharge test. Only one value is needed for each parameter. The average is taken of the relaxing and discharge transient values. This approach increases the model accuracy while reducing the impact of measurement errors[36].

According to paper [36], the methodology described results in an average error of 3.2mV which is 0.09% of the nominal cell voltage(3.6V) when compared with real data in a pulsed discharge. The model results in an average error of 4.4 mV.

The battery parameters are given below:

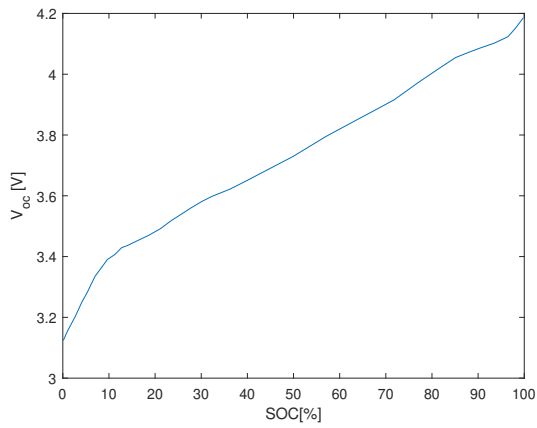


Figure 2.5: Open circuit voltage ( $V_{oc}$ ) vs SOC plot

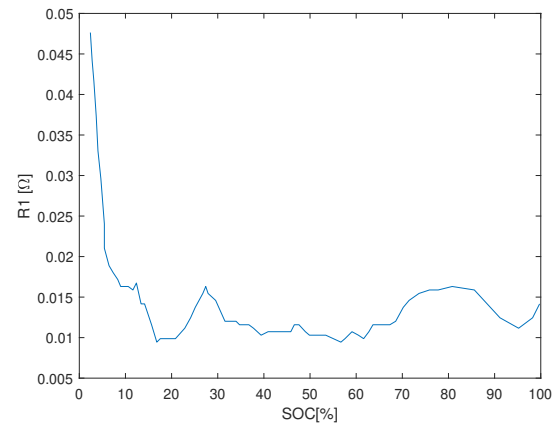


Figure 2.6: Resistance  $R_1$  vs SOC plot

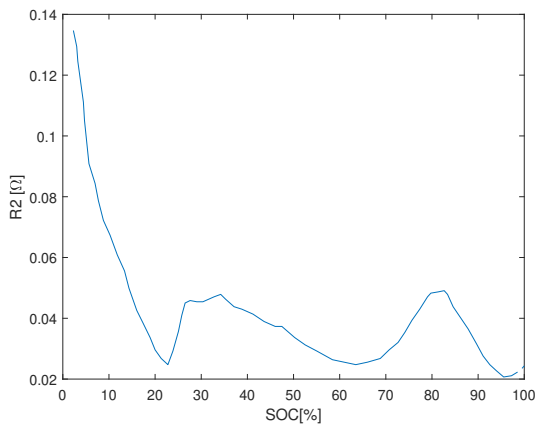


Figure 2.7: Resistance  $R_2$  vs SOC plot

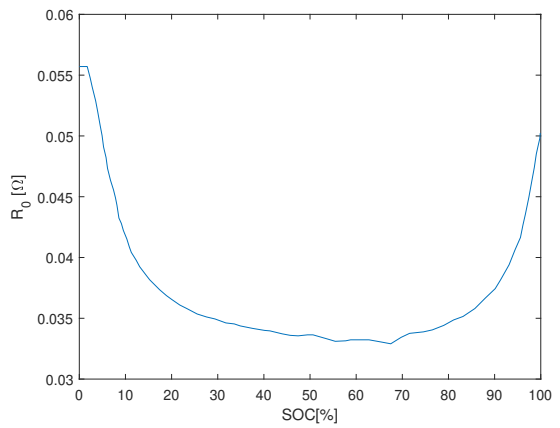


Figure 2.8: Resistance  $R_0$  vs SOC plot

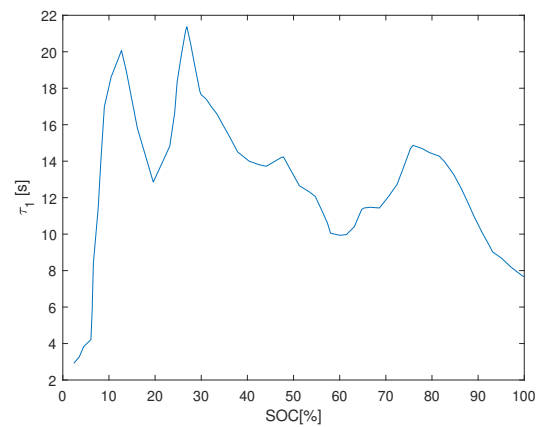


Figure 2.9: Resistance  $\tau_1$  vs SOC plot

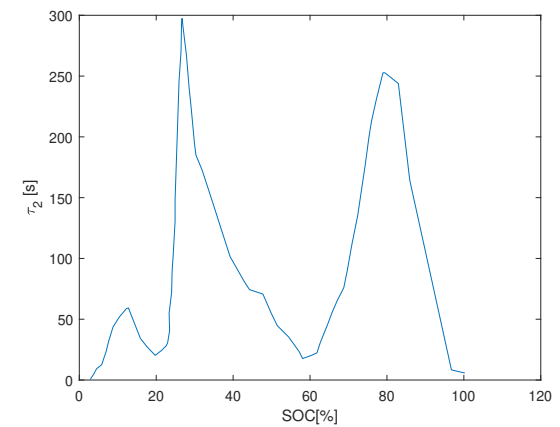


Figure 2.10: Resistance  $\tau_2$  vs SOC plot

# 3

## Bus Characteristics

### 3.1. Bus dynamics

This chapter will discuss the movement behavior of the electric bus. This behavior is determined by the forces acting on the electric bus that provides resistance against the moving bus and by the tractive effort ( $F_t$ ) produced by the powertrain. Equation 3.1 showcases this by Newton's second law to express the vehicle acceleration[18]. Afterward, parameters used for the bus model will be presented.

$$\frac{dV}{dt} = \frac{\sum F_t - \sum F_r}{M} \quad (3.1)$$

$\sum F_r$ : The total resistance.

M: Total mass of the vehicle.

### 3.2. Vehicle Resistance

This section will discuss the rolling resistance force that is indicated with rolling resistance torques  $T_{rf}$  and  $T_{rr}$  in figure 3.1, aerodynamic drag ( $F_w$ ) and hill climbing resistance (the term with  $Mg \sin(\alpha)$ ) in figure 3.1

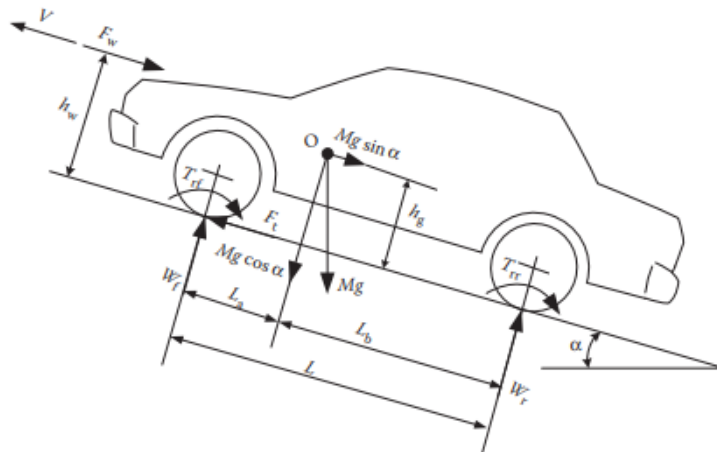


Figure 3.1: Resistive forces acting on an uphill moving vehicle [18].

#### 3.2.1. Rolling Resistance

The rolling resistance of the tires on hard surfaces is caused by hysteresis in the tire materials due to deformation of the tires and/or the surface the vehicle moves on[18]. This force opposes the vehicle's motion. The rolling resistance force  $F_f$  is given by[18]:

$$F_f = f_r M g \cos(\alpha) \quad (3.2)$$

Where:

$f_r$ : Rolling resistance coefficient.

$\alpha$ : Road angle (gradient).

### 3.2.2. Aerodynamic Drag

The vehicle traveling in through air experiences a resisting force against its motion. This is Aerodynamic drag and is due to shape drag and skin friction[18]. Shape drag is caused by the forward motion of the vehicle that pushes the air to the front of the vehicle [18]. The air in front of the vehicle cannot move out of the way instantaneously and the air behind can not instantaneously fill the space left behind, thus creating a force that pushes the car opposite of the motion and pulls the car backwards[18]. The Aerodynamic drag is given[18]:

$$F_w = 0.5 \rho A_f C_D (V - V_w)^2 \quad (3.3)$$

$C_D$ : Aerodynamic drag coefficient.

$V_w$ : Wind speed in the vehicle direction.

$V$ : Vehicle speed.

$A_f$ : Vehicle frontal area.

$\rho$ : Air density.

### 3.2.3. Grading Resistance

The gradient resistance occurs when the vehicle goes uphill or downhill. The gradient force which opposes the vehicle motion is given by[18]:

$$F_g = M g \sin(\alpha) \quad (3.4)$$

## 3.3. Battery parameters

The battery cell used in this paper is the Sanyo NCR18650GA 3350mAh Li-ion cell [38]. Table 3.1 shows the details of the specific cell. The cells are placed in series and in parallel to design the battery of the electric bus. Based on paper [6], in which battery sizing research is performed, the battery capacity is 320kWh. The battery cell capacity is converted to Wh to determine how many cells are needed to get a battery capacity of 320kWh. This is done by multiplying the capacity with the rated voltage that results in 12.06Wh. Approximately 26534 battery cells are needed to have 320kWh of battery capacity.

The battery open circuit voltage ranges between 600V and 800V. This is the current state of the art for electric busses.[4]. The battery capacity needs to be restricted to 80% of its nominal capacity [21]. Thus operating SOC range for the battery is taken to be between 10% SOC - 90% SOC. The battery cells must be placed in series to meet the open circuit voltage range of the battery. Figure 2.5 shows the  $V_{oc}$  of a cell at 10% which is 3.4V while at 90% SOC it is 4.09V. The series cells are obtained by dividing 600V by 3.4V. This results in approximately 177 cells. The total cells needed are described by:  $n_{total} = n_{series} n_{parallel}$ . Solving for the parallel cells results in approximately 150. The series and parallel cells needed to be rounded to whole numbers, which causes the total cell numbers to change. Thus the final total cells needed are equal to  $177 * 150 = 26550$ .

Table 3.1: Parameters of the Sanyo NCR18650GA cell used in this paper.

Battery cell parameter	
Capacity	3350mAh
Rated Voltage:	3.6-3.7V
Cell Weight	47.4g
$n_{series}$	177
$n_{parallel}$	150

### 3.4. Bus Dimensions

This section will provide the dimensions of the bus used in this. The dimension includes the length, front area, aerodynamic drag coefficient, rolling resistance coefficient, weight, and wheel radius. Paper [22] is used to determine the length, front area, aerodynamic drag coefficient, and wheel radius.

The bus weight is determined by the summation of the bus curb weight, the passenger amount in the bus, and the battery weight. A 12m bus has a maximum number of 85 passengers [22]. The average weight of a passenger is taken to be 68kg [5], this results in a total passenger mass of 5780kg. The battery mass is determined by taking the mass of a single battery cell and multiplying it by the total amount of cells needed for the battery. The battery mass is 1258.5kg. The average gross weight of multiple 12m city buses commercially used in Europe equals 18537 kg [22]. This means that the curb weight of the bus is approximately 11500 kg in this paper. This is within the range values for curb weights provided in paper [22] and is similar to the curb weight used in paper [5]. The bus weight taken in this paper is thus an accurate representation of a 12m electric bus weight. The curb weight is needed to determine the bus weight when the battery size becomes possibly smaller due to opportunity charging. The battery size can be affected when opportunity charging is implemented, thus changing the gross weight of the bus. All the values used can be seen in table 3.2.

Table 3.2: The bus dimensions chosen are determined by analyzing the most frequently used bus dimensions[22].

Bus Dimensions:	
Length	12 m
$A_f$	7.9 m <sup>2</sup>
$C_D$	0.75
Wheel Radius	0.4783m
$M_{bus}$	18537 kg

The rolling coefficient  $f_r$  is given by equation 3.2. This coefficient is different for varying speeds. This can be seen in figure 3.2. Based on experimental results, many empirical formulas are proposed for calculating rolling resistance on a hard surface [18]. In vehicle performance calculations, it is sufficient to estimate the rolling resistance as a linear function of speed [18]. The rolling coefficient,  $f_r$ , is determined by equation 3.5, which predicts the coefficient with acceptable accuracy for speeds up to 128 km/h[18]. This equation is used for the most common range for inflation pressure for passenger cars on concrete roads [18].

$$f_r = 0.01(1 + \frac{V}{160}) \quad (3.5)$$

V: The vehicle speed in km/h

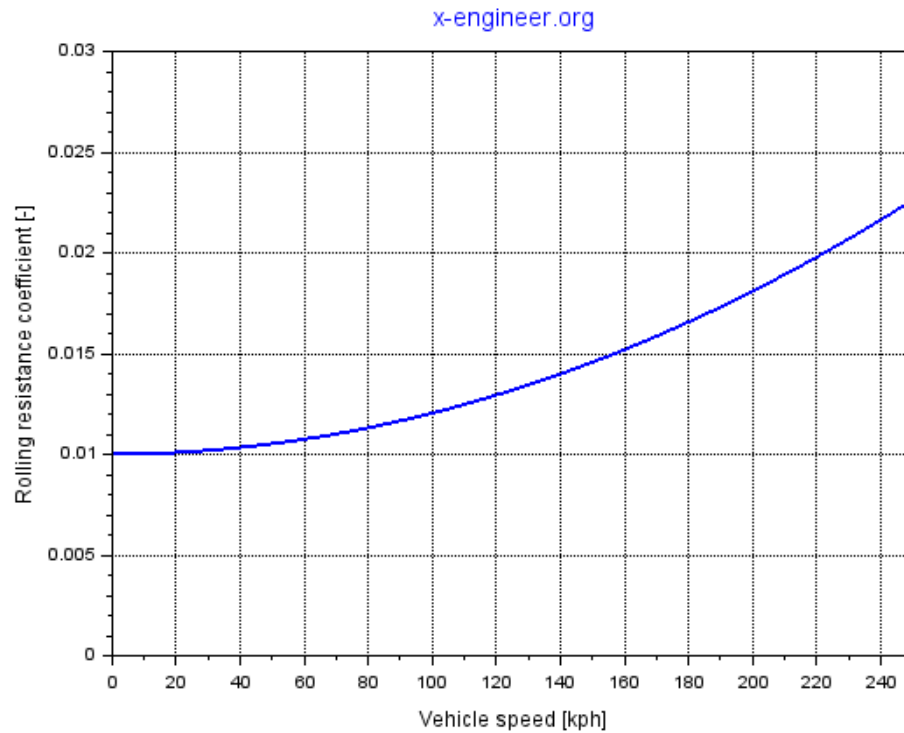


Figure 3.2: Plot of a rolling resistance coefficient vs vehicle speed [1].

## 3.5. Bus Performance

### 3.5.1. Top speed

The maximum speed of the wheel is chosen to be 80km/h. This is the average top speed of several commercial battery electric city buses shown on paper [22]. This is a suitable speed since the bus will probably have a driving speed below or equal to 50km/h within a city.

### 3.5.2. Road angle

The grading resistance and the rolling resistance are dependent on the road angle. This can be seen from equations 3.2 and 3.4. The road is chosen to be flat in this paper, which means that the grading resistance has a value of 0 N. The first reason for this is the usually flat terrain of the Netherlands. The driving cycle data are from Arnhem, a city in the Netherlands. The second reason is that the road angle is not provided in the driving cycle data used in this paper.

### 3.5.3. Acceleration and Deceleration

The maximum acceleration for the bus is chosen by considering the comfort of the passengers. The maximum acceleration to keep passengers comfortable is often limited to around 1.5-2  $m/s^2$  [22]. This paper will use 1.5  $m/s^2$  as acceleration, which is eventually chosen by paper [22]. The acceleration is used to do calculations needed for the EM parameters.

## 3.6. Gear ratio and EM parameters

This section will state the values used for the EM design. This section will also present the gear ratio used.

### 3.6.1. Gear

The gear ratio is determined by using the maximum wheel and EM speed. The gear ratio is determined by equation 3.6. The efficiency of the gearbox is 97%. The maximum machine speed is 11000 rpm [22]. The gear ratio will then be 24.7907.

$$k_{gear} = \frac{\omega_{em,max}}{\omega_{wheel}} \quad (3.6)$$

### 3.6.2. EM parameters and inverter efficiency

The vehicle resistance forces given in section 3.2 will be used to determine the rated torque needed for the PMSM. The rated torque is given by:

$$T_{max} = \frac{r_{wheel}(Ma + F_f + F_w + F_g)}{k_{gear}\eta_g} \quad (3.7)$$

The rated torque is calculated to be 642.48Nm. The rolling coefficient for this calculation is assumed to be 0.015, which is the rolling coefficient value when the 80 km/h speed value is used in equation 3.5. The rated speed is needed to determine the maximum power of the EM and to model the machine torque properly. The maximum power is taken from paper [22] and equals 250kW. This value is the average of the most frequently used maximum machine powers. The rated speed is determined by solving the following equation:

$$P_{max} = T_{max}\omega_{rated} \quad (3.8)$$

The PMSM is a high-efficiency electrical machine that falls within the IE5 premium class efficiency [15]. The efficiency values vary between 92% to 97% [15]. This paper will assume the average of this range, which is 94.5 % since this paper does not delve into loss calculations of the PMSM.

The efficiency of the 3-phase DC-AC inverter is 98%[23]. The table below shows all parameters mentioned in this section.

Table 3.3: Parameters used for modeling the PMSM, gears, and inverter

EM parameters:	
$T_{max}$	644.3 Nm
$n_{max}$	11000 rpm
$n_{rated}$	3705 rpm
$P_{max}$	250 kW
Gearbox efficiency	97%
PMSM efficiency	94.5%
Inverter efficiency	98%

## 3.7. Auxiliary and HVAC

The auxiliary data in this report is taken from paper [16].

The auxiliaries are predominately the heating, ventilation, and air conditioning (HVAC) load plus other loads like onboard lights, motors, screens, control systems, and more [16]. The auxiliary is thus represented by:

$$P_{aux} = P_{HVAC} + P_{base} \quad (3.9)$$

The HVAC requirement is calculated by the thermodynamic heat exchange model between the trolleybus and the environment [16]. More detail about the calculation can be found on paper [16]. The Arnhem bus types, on which the driving cycles in this paper are based, are controlled with a duty cycle ( $t_{cycle}$ ), the on-time ( $t_{on}$ ) of the HVAC for each period is dictated by the average HVAC power requirement of the bus during a cycle [16].  $t_{on}$  is given by [16]:

$$t_{on} = t_{cycle} \frac{\overline{P_{HVAC}}}{P_{rated}} \quad (3.10)$$

$\overline{P_{HVAC}}$ : The average power requirement within a duty cycle.

$P_{rated}$ : The nominal HVAC power.



# 4

## Simulation of electric powertrain of electric buses

This chapter will discuss the simulation models used in this paper. The first model discussed is the vehicle model, which follows the driving cycle and computes the battery's power to deliver or take. Afterwards, the battery model is discussed from which the SOC, terminal battery pack power and terminal battery pack energy are calculated.

### 4.1. Vehicle model

This section will describe the vehicle model implemented in this report. The model is shown in figure 4.1.

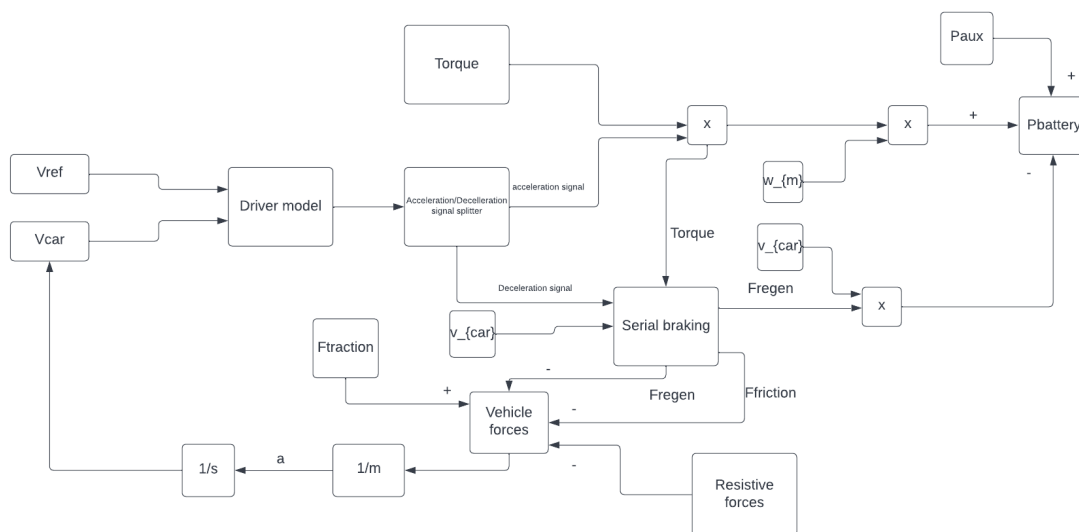


Figure 4.1: The total vehicle model with the driver model, serial braking model, and vehicle dynamic.

#### 4.1.1. Driver model

The driver model implemented in this report aims to reduce the difference between the reference speed the electric bus needs to follow and the actual bus speed,  $\Delta V$ . The sign of  $\Delta V$  decides whether the driver is accelerating or using the brake [32].

$\Delta V$  is sent as input to the PI controller. This controller is represented with equation 4.1. The proportional gain P and Integral gain I are tuned until a minimum value of  $\Delta V$ . The P and I values also

need to be tuned to keep the output of the PI controller oscillation free. The output of the PI controller is then fed to a saturation block to limit the pedal signals at a range of -100 and 100. This range represents the percentage of the pedal input applied [2]. The range is normalized to -1 and 1, which is done to use range as input for forward movement or braking model. The negative values indicate braking behavior by pressing the braking pedal [32]. The positive values represent acceleration by pressing the accelerator pedal. [32].

$$PI(s) = P + I \frac{1}{s} \quad (4.1)$$

Where:

P: Proportional gain.

I: Integral gain.

#### 4.1.2. Forward movement

The output of the PI controller ranges between 0 to 1. This output is used for the forward movement. The PI controller output for forward movement is denoted as  $D_a$ . The torque demanded is obtained by multiplying  $D_a$  with the maximum machine torque. Equation 4.2 shows the demanded torque.

$$T_{Dem} = T_{max} D_a \quad (4.2)$$

The power needed from the machine to move the vehicle forward is obtained by multiplying  $T_{dem}$  with the angular speed of the machine [14]. The value for rated torque depends on whether the rated speed is exceeded. This can be seen in figure 4.2. The flux weakening method is used to increase the speed of the machine beyond the rated speed. The speed range from rated speed to maximum speed is within the constant power region.  $T_{max}$  equals  $T_{rated}$  in the constant torque region.  $T_{max}$  equals to  $\frac{P_{max}}{\omega_m}$  in the constant power region. The torque and speed characteristics of the machine become valid for braking when they are mirrored with the x-axis. This is why the  $T_{max}$  is also used in the braking model.

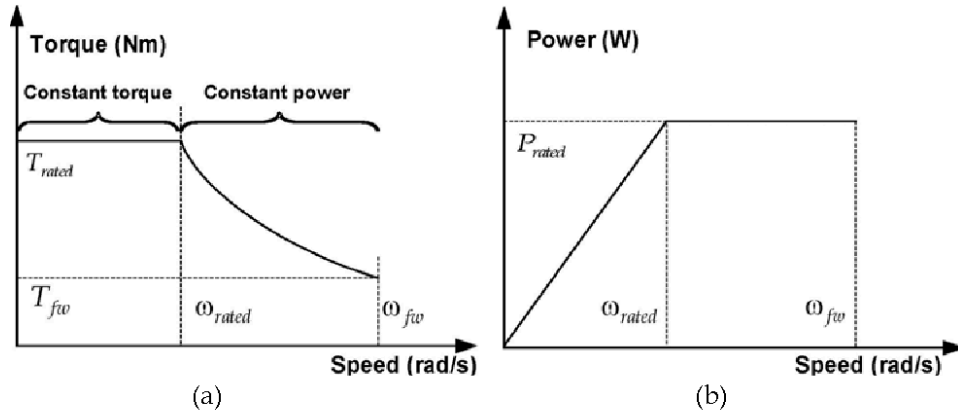


Figure 4.2: a) Torque speed curve of the PMSM. b) Power speed curve of the PMSM [12].

#### 4.1.3. Braking strategy model

The output of the PI control going from -1 to 0 is sent to the braking strategy model and is noted as  $D_b$ . The maximum braking force  $F_{br\_max}$  needs to be determined.  $F_{br\_max}$  depends on the normal load acting on the bus and the adhesion between the tires and the road and is expressed as follows [32][2],

$$F_{br\_max} = \varphi M_{bus} g \quad (4.3)$$

$\varphi$ : Adhesion coefficient between the tires and the road, which has typical values around 0.8 on dry or wet asphalt and concrete surfaces [32].

$g$ : The acceleration due to gravity in  $m/s^2$

The two braking strategies that are typically used to implement brake blending are serial and parallel braking [2]. Parallel braking distributes the brake force uniformly distributed between friction brakes

and regenerative brakes [2]. Series braking first applies regenerative braking. Frictional brakes are used additionally only if regenerative braking is not enough to brake the vehicle [2].

The serial braking strategy is used in this paper because this strategy can increase fuel efficiency by 15-30 % [2]. This results in maximum utilization of the regenerative brakes [2]. The implementation of the serial regenerative braking strategy can be seen in figure 4.3.

The braking strategy starts by taking the maximum braking torque obtained by multiplying equation 4.3 with the wheel radius. Afterwards, the SOC is checked. The upper limit for the SOC is 90%. This percentage indicated that the battery is full. Thus all the braking will be frictional.

If the SOC is less than 90% then it is checked whether the demanded torque for braking is equal to or less than the maximum machine torque. If this is the case then braking will be fully regenerative, otherwise, a check is performed on whether 70% of the braking torque is smaller or equal to the regenerative torque. If this condition is valid then 30% of the braking torque is frictional while 70% is regenerative braking. The 30:70 ratio assumption is taken from paper [2]. The maximum machine torque will be used for regenerative braking while additional braking torque demand will be covered with frictional brakes when 70% braking torque is larger than the regenerative torque

An additional condition to the braking strategy is that speeds less than 5km/h will use frictional braking instead of regenerative braking. The electromotive force generated is low at a low speed. This leads to charging cells at high currents and low voltages [2]. Secondly, the charging and discharging cycles are very short at low speeds. This leads to micro cycling at the battery due to constant directional change of high currents. This affects the lifetime of the battery pack[2].

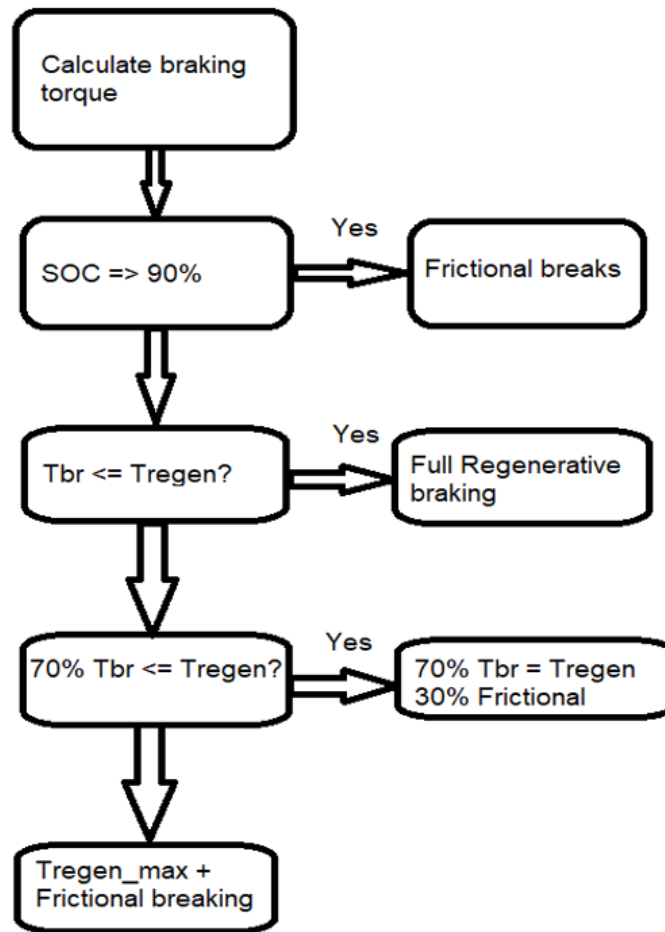


Figure 4.3: Serial braking strategy flowchart.

#### 4.1.4. Vehicle speed

The vehicle speed is derived in a couple of steps. First, the traction force of the machine at the wheels is determined by using the equation 4.4. The resistive forces oppose the traction force so they are subtracted from the traction force together with the braking force if the brakes are used. This is shown in equation 4.5.

$$F_t = T_{machine} \frac{k_{gear}}{r_{wheel}} \eta_g \quad (4.4)$$

$$Ma = F_t - \sum F_r - F_{break} \quad (4.5)$$

Equation 4.5 is then solved to determine the acceleration. The acceleration is then fed into an integrator block in Simulink, with an initial condition of 0 m/s, to find the vehicle speed.

#### 4.1.5. Battery input power

The signal send to the battery as input is the sum of the traction power of the machine, the regenerative braking power, and the auxiliary power demand. The traction power and the auxiliary power are summed up while the regenerative braking power is subtracted to determine the power demand. Positive power demand means that the battery needs to discharge. A negative power demand means that the battery needs to be charged. The required traction power is calculated by multiplying the positive torque output of the machine by its mechanical speed. The PMSM and the inverter have losses that need to be included in the power demand. Equation 4.6 gives the power demand for the traction force.

$$P_{pmsm} = \frac{T\omega_m}{\eta_{pmsm}\eta_{inverter}} \quad (4.6)$$

The power recovered from regenerative braking is calculated by taking the output from the braking strategy algorithm. The torque output is the wheel torque, and it is converted into force, which is then multiplied by the vehicle speed to get the power. The losses from the machine and the inverter need to be included. The power recovered by braking is given by the equation below.

$$P_{regen} = \left( \frac{T_{regen}k_{gear}\eta_{gear}}{r_{wheel}}v_{car} \right) \eta_{pmsm}\eta_{inverter} \quad (4.7)$$

The charging and discharging efficiency of Li-ion battery packs is 95% [32]. The battery charging due to regenerative braking and the discharging demand due to the traction effort and auxiliary are given by the following equations:

$$P_{bat,charge,input} = P_{regen}\eta_{charge} \quad (4.8)$$

$$P_{bat,discharge,input} = \frac{P_{pmsm} + P_{aux}}{\eta_{discharge}} \quad (4.9)$$

## 4.2. Battery model

The battery model is made with the parameters from section 2.3.

### 4.2.1. Single cell current demand

The current demand of one cell is derived by using the power input described in section 4.1.5 and equation 4.10 [32]. The  $P_{cell,dem}$  is derived by taking the power input. The power input is divided by the total amount of cells used in the battery. The current demand is positive when power is needed from the battery, while it is negative when the battery is charged.

$$I_{cell,dem} = \frac{V_{oc} - \sqrt{V_{oc}^2 - 4R_0P_{cell,dem}}}{2R_0} \quad (4.10)$$

The battery resistance and the open circuit voltage in equation 4.10 dependent on the SOC. Thus the battery SOC is updated at each time step using the current integration method known as Coulomb counting [32]. The equation for Coulomb counting is given below at equation 4.11.

$$SOC = SOC_0 - 100 \int \frac{I_{cell,dem}}{3600C_{cell}} dt \quad (4.11)$$

Where:

$SOC_0$ : Initial battery state of charge in %.

$C_{cell}$ : The capacity of a single cell in Ah.

### 4.2.2. DP model

The DP model introduced in section 2.3 is modeled using the model given in paper [36]. The model can be seen in figure 4.4. This model calculates the battery terminal voltage by subtracting the voltages across the  $R_0$  resistance and the RC networks from  $V_{oc}$ , which is shown in equation 4.12 [36]. Lookup tables are used to represent the cell values since the RC networks together with the  $V_{oc}$  and  $R_0$  are all dependent on SOC. The SOC calculated from equation 4.11 is fed into these tables to determine the right value at the specific SOC.

$$V_B = V_{oc}(t) - (R_0I_{cell,dem}) - R_1I_{cell,dem}(1 - e^{-\frac{t}{\tau_1}}) - R_2I_{cell,dem}(1 - e^{-\frac{t}{\tau_2}}) \quad (4.12)$$

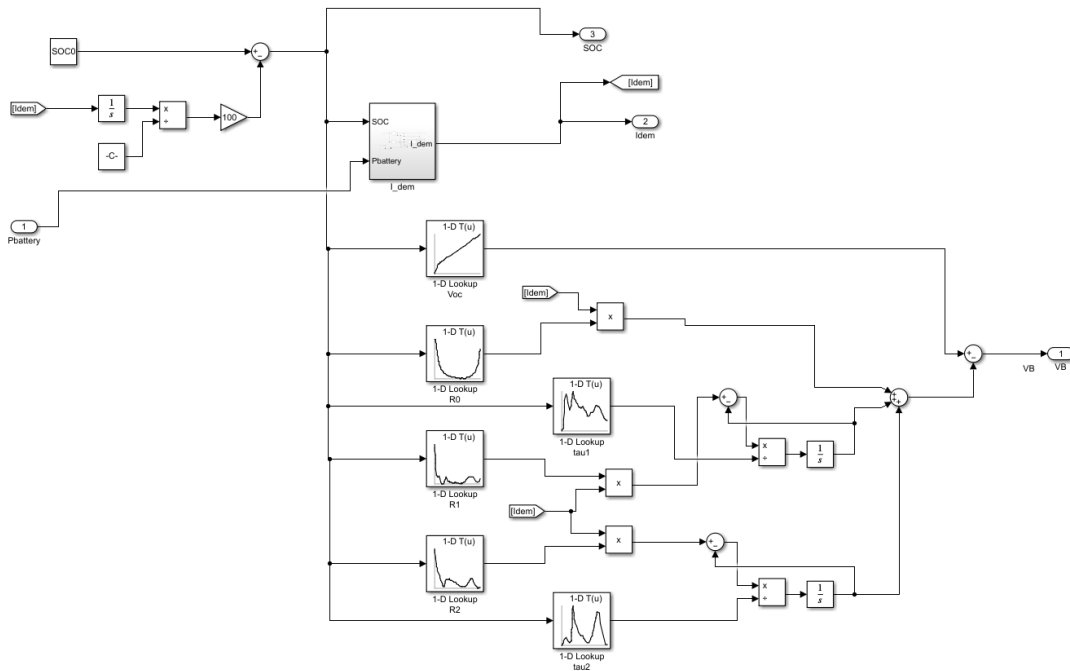


Figure 4.4: The DP model together with equations 4.10 and 4.11 modelled in MATLAB/Simulink.

### 4.2.3. Output of battery model

The output of the DP model is the terminal battery pack voltage, the total battery pack current, and the SOC. The terminal battery pack voltage and the total battery pack current are multiplied by the number of cells in series and parallel. This can be seen in equations 4.13 and 4.14 [32]. The battery voltage and current are multiplied to find the terminal battery pack power in [W]. The power is fed into an integrator block in MATLAB/Simulink. The output of the integrator block is divided by 3600 to determine the terminal battery pack energy [Wh][32]. This is shown in figure 4.5. The SOC is used in the braking strategy model and at the opportunity charging case implementations, which are discussed in the proceeding chapters.

$$V_{Bat-pack} = V_{cell}N_{cells,series} \tag{4.13}$$

$$I_{Bat-pack} = I_{cell}N_{cells,parallel} \tag{4.14}$$

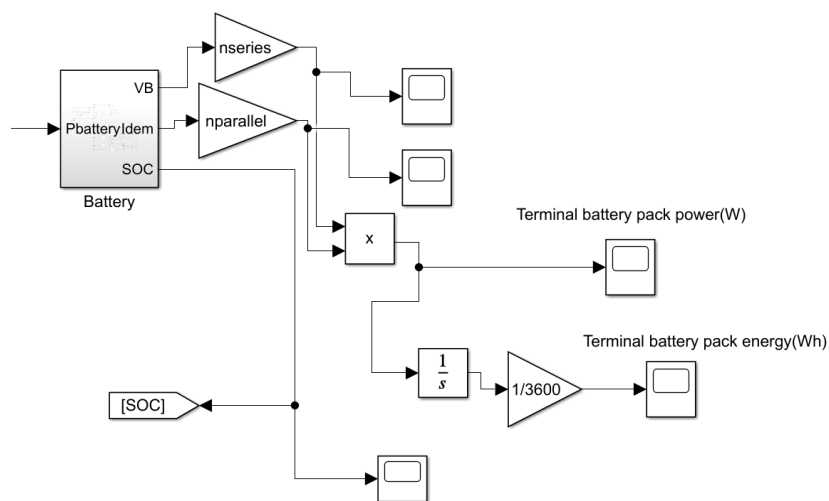


Figure 4.5: The battery output modeled in MATLAB/Simulink.

# 5

## Opportunity Charging

### 5.1. Inductive charger

#### 5.1.1. Wireless charger overview

The charger that is used in this paper is a wireless inductive charger at bus stops. This means that the bus needs a wireless charging system instead of a plug-in charger. Both charger types are shown in figure 5.1. The figure shows that fewer components are placed within the bus when wireless charging is used, while an inductive charging pad is added to the bus to make wireless charging possible.

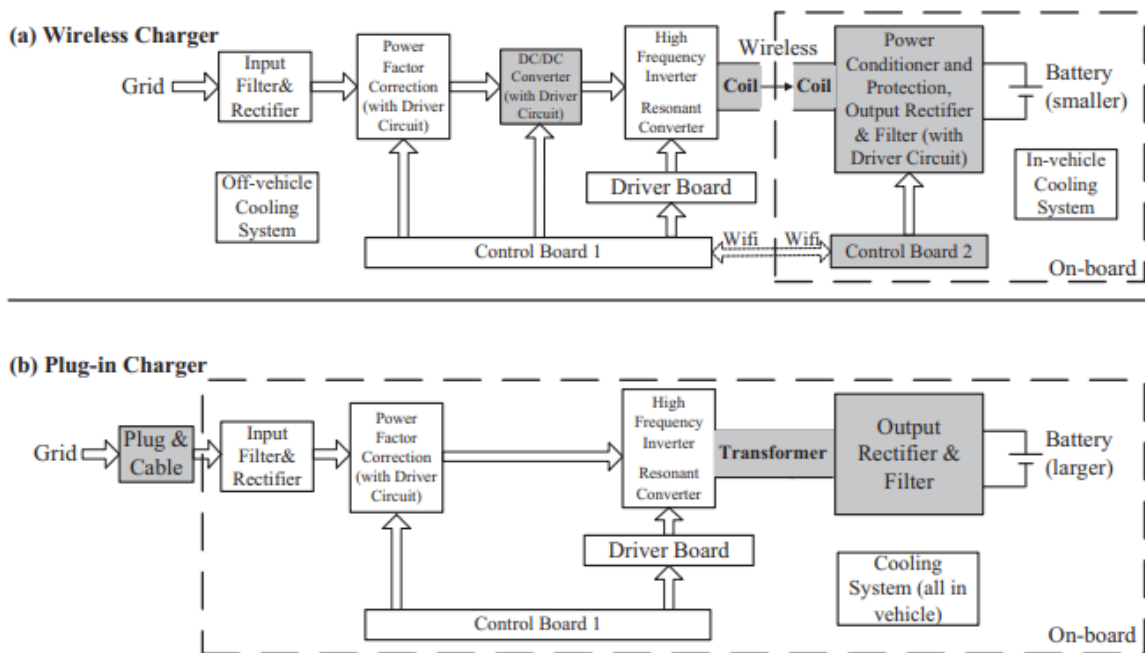


Figure 5.1: Comparison of the wireless charger (a) and plug-in charger (b) based on a 6kW wireless charger from Professor Chris Mi's laboratory at the University of Michigan, Dearborn [7].

Fewer components within the bus could mean that the weight of the bus is different when an opportunity charger is used. This paper assumes that the bus weight given in Chapter 3 is from a plug-in charged electric bus. The weight comparison is done with the 6kW wireless charger from Professor Chris Mi's laboratory at the University of Michigan, Dearborn. Paper [7] provides the weight of each component shown in figure 5.1. The components onboard for the wireless charger and the plug-in charger are compared. It can be seen that the wireless charger of 6kW weighs 11.4kg while the plug-in charger weighs 14.8184kg. However, the power transmitted in this paper is not specifically 6kW. Multiple sets

of the 6kW charger are needed if larger power values are used [7]. The material burden is scaled up proportionally when multiple sets are needed [7]. The new weight of the bus is determined by determining how many sets of 6kW chargers are needed to realize the specific power rating. Different charger values larger than 6kW could have been used. 6kW chargers are chosen because paper [7] gives a detailed list of the component weights. The new bus weight is then calculated by taking the difference in the weight of the wireless and plug-in chargers. The calculation of the wirelessly charged electric bus is shown in equation 5.1.

$$M_{bus,opp} = M_{bus,plug-in} - n_{sets}(M_{plug-in,charger} - M_{opp}) \quad (5.1)$$

$M_{bus,plug-in}$ : The bus weight given in chapter 3.

$n_{sets}$ : The amount of 6kW charger sets needed for a power rating.

$M_{plug-in,charger} - M_{opp}$ : The weight difference between the plug-in charger and the opportunity charger.

### 5.1.2. System Efficiency

Inductive power transfer (IPT) systems have been developed over the last decade, with prototypes ranging from 2kW to 200kW with overall efficiencies from AC to DC battery ranging from 80 to 95% [44]. The information needed for this paper is the power supplied together with the whole system's efficiency. Table 5.1 shows commercial EV stationary inductive chargers with their sources.

Table 5.1: IPT producing companies with the achieved efficiencies at certain power rating

Power	Efficiency	Company	Source
200 kW	94%	Inductev	[33], [11]
100 kW	92%	IPT	[43]
60 kW	>90%	IPT	[9]
50 kW	90%	INTIS	[26],[43]
<50 kW	93 - 90%	WAVE IPT,Electreon,Plugless Power,Lumen Freedom, Witricity	[9],[43]

A power rating that is not in the table 5.1 will use the efficiency of 92% as the opportunity charger efficiency which defines the efficiency from grid to battery. This efficiency is chosen because most wireless charging devices will operate at approximately 92% with a difference of  $\pm 2\%$  [19], which is also in accordance with table 5.1.

## 5.2. Different opportunity charging case implementations

This section will discuss the different situations considered when opportunity charging is used at bus stops. The goal of the opportunity chargers is to make a single bus capable of operating a whole day while only being charged by the opportunity charger.

### 5.2.1. Opportunity charging at every stop

The situation discussed in this subsection looks at the case when every bus stop in a certain driving cycle has an opportunity charger installed. The parameters changed in this case are the opportunity charger power rating values between 200kW and 100kW and the time spent on the bus stops will go from one minute to 30 seconds.

The assumptions made in the case are:

- The starting and final destination will not have an opportunity charger.
- The bus will not be charged other than at the stops.
- The waiting time at every stop is the same.
- The bus will have to operate at its maximum passenger capacity.
- The battery is at 90% SOC at the start.

- Standstill duration longer than or equal to 15 seconds, in the driving cycles, are considered stops. Otherwise, the standstill is assumed to be due to regular traffic and traffic lights
- A route which is, for example, represented with grid sections numbers 12-24-15-24-12 (more detail about this is given in section 1.2), is assumed to have a substation/final destination at 15 when the standstill duration is larger than 60 seconds, thus no charger is placed there.

This situation will provide the smallest possible battery size for a specific driving cycle.

### 5.2.2. Minimum amount of stops needed

This situation will look at the minimum stop amount needed to make the bus operate the whole day with only opportunity charging. This case will use different power ratings and waiting times for the chargers. The waiting times at the chargers span from one minute to thirty seconds. The overview of the algorithm used can be seen in figure 5.2. The start time of the stops of a driving cycle is determined before the algorithm is used. This is done to determine the location of the bus stop at a specific driving cycle. This makes the removal/addition of bus stops, which differs for each driving cycle, easier. After doing this, the algorithm in figure 5.2 is used.

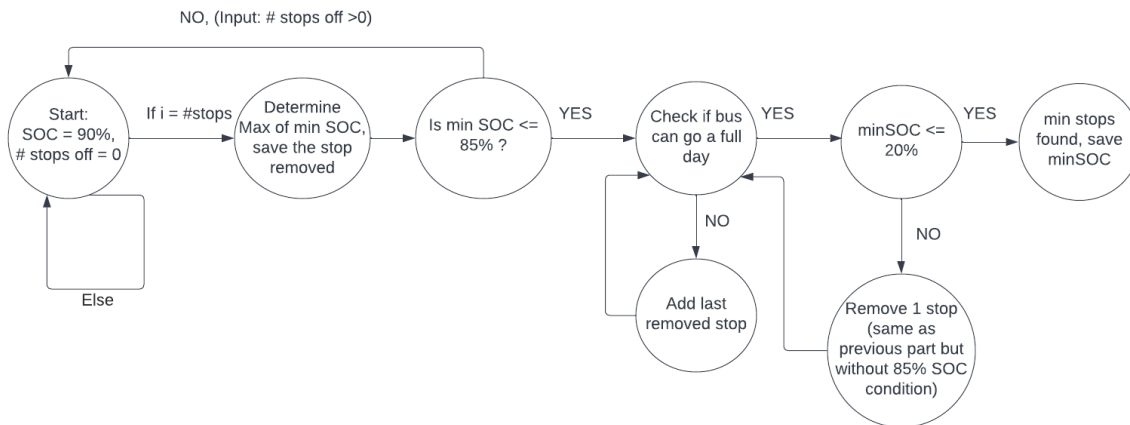


Figure 5.2: Diagram of the system that determines the minimum amounts of stops needed for a full daily operation of the bus

The algorithm starts with a full battery and with opportunity chargers at every stop. Each stop in the driving cycle is turned off one by one. The minimum SOC after a full trip is stored for each bus stop tested. The maximum value of the different minimum SOC values stored is detected. The bus stop with the largest minimum SOC is removed since it is the least useful bus stop. This process is repeated till the minimum SOC is less than or equal to 85% SOC. The bus stops that are turned off are not checked again, which increases the algorithm speed.

A check is performed when the minimum SOC is less than or equal to 75%. This is done to determine if the amount of bus stops removed is too much or if further bus stop removal is needed. The check is done by looking at whether the bus can make a full day's trip. The most recently removed stop is added back if a full daily trip is impossible. Afterwards, the check is repeated. A check is done on whether the minimum SOC is less or equal to 20% if the bus can travel a full day. This check is done since it could be the case that the stop amounts equipped with a charger are too much. One stop is removed if the stops with opportunity chargers are more than needed. The removal of the bus stops is done by looking at which bus stop removal results in the maximum amount of minimum SOC, just like the stop removal method mentioned earlier. The minimum amount of stops is found when the minimum SOC is less than or equal to 20%. The minimum SOC and the bus stop with inactive chargers are saved. They are later used to perform the battery sizing described in section 5.3.

### 5.3. Battery sizing

The initially used battery of 320kWh could be oversized when opportunity charging is implemented. The bus will get extra electricity while waiting at the bus stops. This could potentially reduce the need for electricity storage. The battery downsizing need is checked by looking at the minimum SOC after a trip with the bus. The parallel cell amount of the battery is increased by one if the minimum SOC is between the range of 20-10% when the bus is unable to travel for a full day. New battery size is determined by the difference between the minimum SOC and the minimum SOC after a full day. This is shown in equation 5.2. The minimum SOC is checked. The new amount of parallel cells in the battery is determined afterwards. The battery sizing is stopped when the minimum SOC is below 15% after the bus is done for the day. New battery size is calculated with equation 5.3.

$$SOC_{left} = SOC_{min} - 10\% \quad (5.2)$$

$SOC_{left}$ : The amount of SOC that is left in excess.  
 $SOC_{min}$ : The minimum SOC after a full-day trip.

$$E_{battery,new} = E_{battery} \left(1 - \frac{SOC_{left}}{100}\right) \quad (5.3)$$

The battery cells in series should not be changed to maintain the open circuit voltage range mentioned in section 3.3. The only option is to change the cells which are placed in parallel. The new amounts of parallel cells needed are determined by dividing the total amounts of cells by the cells placed in series. The number of parallel cells is then rounded up if the number is fractional since there can only be whole amounts of cells.

The last step is to repeat the previous steps until the minimum amount of parallel cells is found. This is necessary because the mass of the battery is changed when it is downsized. This affects the resistive forces which in turn affects the energy consumption of the bus. A difference in energy consumption means that the SOC of the battery is also affected. The minimum amount of parallel cells  $n_{parallel}$  is found if the  $n_{parallel} = n_{parallel,new}$ . This indicates that the minimum amount of cells possible is found. This additional condition is set since there could be a possibility that the minimum SOC is above the range of 15-10% SOC while the battery cannot be downsized further. If this condition is true then the algorithm is stopped and the battery size is determined by equation 5.3. The whole process of battery sizing is repeated when the additional condition is not met. All these steps can also be seen visually in figure 5.3.

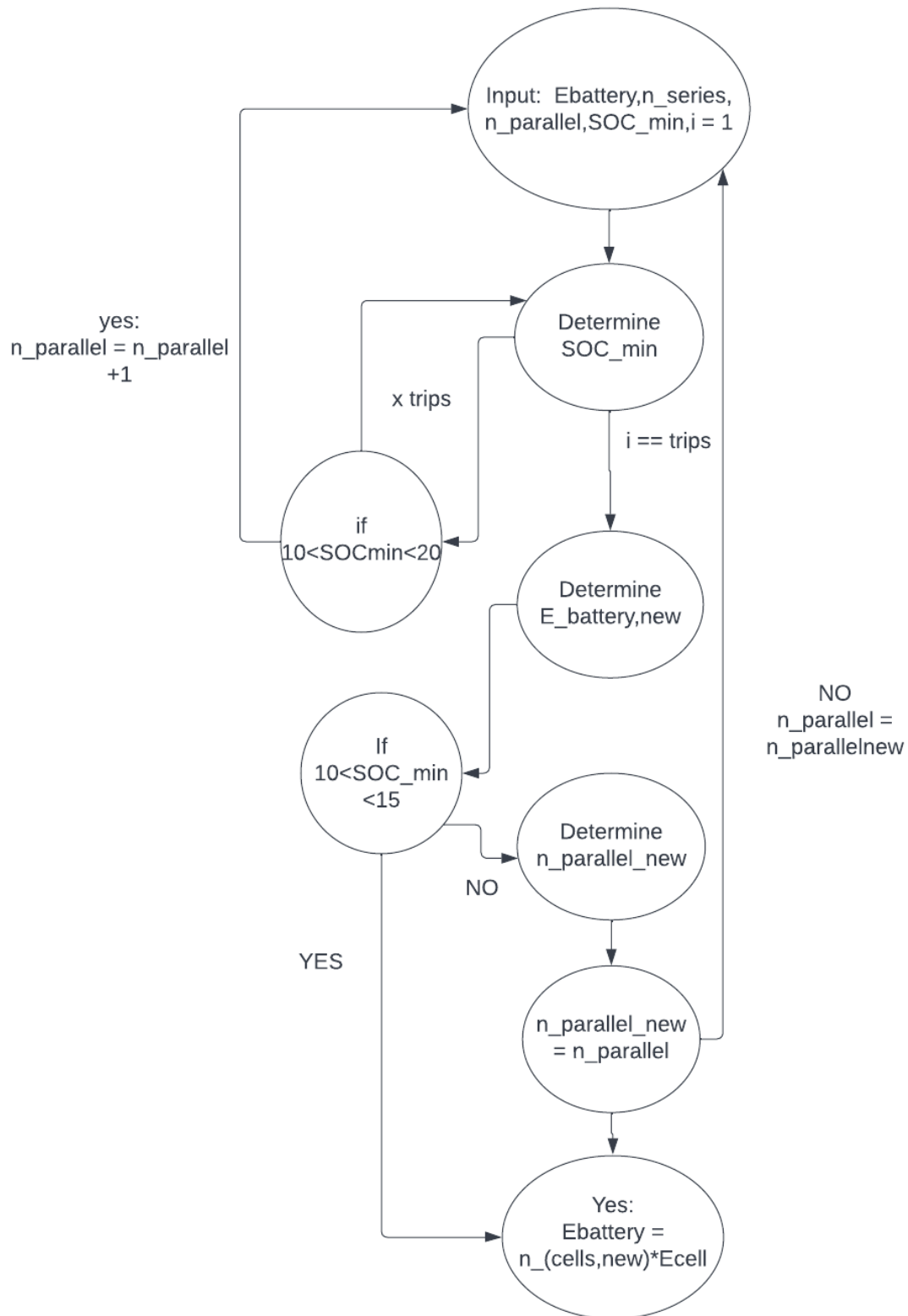


Figure 5.3: Diagram of the battery sizing progress

## 5.4. Charging model

The opportunity charging model implemented in this paper is shown in figure 5.4. The input of the model is the SOC of the battery. The output is the power delivered at a specific time in the simulation. Figure 5.5 shows the charging model in more detail. The subsections in this section will explain what each part does.

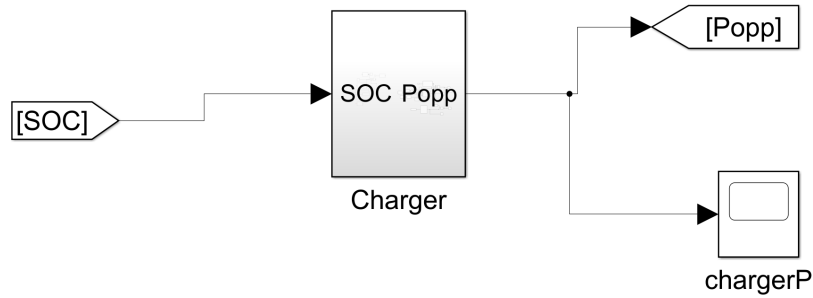


Figure 5.4: The overview of the opportunity charger model in MATLAB/Simulink.

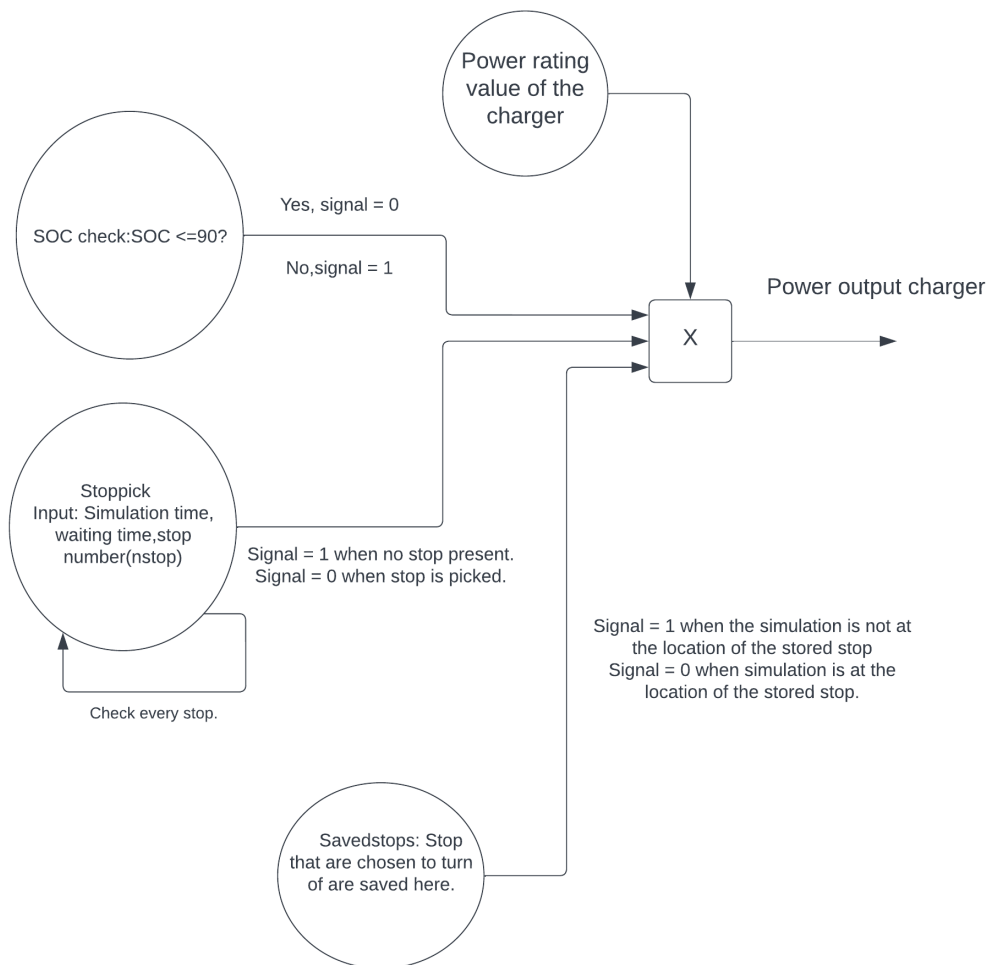


Figure 5.5: Opportunity charger model diagram.

### 5.4.1. SOC check

The opportunity chargers will deliver a certain amount of power to the bus battery. This power is computed by equation 5.4. The battery has an upper limit of the SOC percentage that it can not exceed. The SOC check looks if the SOC is below this upper limit. A signal value of one is sent when the SOC is lower than the upper limit. Otherwise, a signal with the value of zero is sent. This will turn the charger off. This signal will make the charger output zero since the signals coming from the subsystems are multiplied by the power rating of the charger.

$$P_{opp,in} = P_{opp}\eta_{opp} \quad (5.4)$$

$\eta_{opp}$ : The overall efficiency of the opportunity charger.

### 5.4.2. Stoppick

All the chargers at the stops are initially turned on. The charger model will alternately turn off chargers at the bus stops. This will be repeated until the minimum amount of chargers at the bus stops is left on to make the bus operate a full day. The Stoppick subpart in figure 5.5 picks one stop to turn off from every bus stop in the driving cycle. The inputs of Stoppick are the simulation time, the times at which stops are present, the waiting time at the bus stop, and a signal which turns the Stoppick subpart on or off.

The Stoppick sub-model turns every stop off, one at a time while leaving the other bus stops on. The sub-model starts at the first stop, which is turned off. The other bus stops are left open and the minimum SOC of the battery after a daily trip is stored. This procedure is repeated at every bus stop. The sub-model sends a zero signal, with the same duration as the stop waiting time. This zero signal makes the charger output 0 W when a bus stop is turned off. A signal value of one is sent otherwise. The bus stop that is the least effective is stored and kept off. This is done after the Stoppick sub-model is done after checking the last bus stop. The stored bus stops that need to be kept off, are also sent to Stoppick. This saves computation time since double-checking a bus stop is unnecessary.

### 5.4.3. Savedstops

The Savedstops sub-model takes the stored results from Stoppick and puts them out. This sub-model makes turning multiple chargers off at the same time possible. This sub-model sends a signal value of zero for the stops that need to stay off. Otherwise, a signal value of one is sent.



# 6

## PV system for opportunity charging

Opportunity chargers need an energy source to enable their use. The energy source could be the electricity grid. The possibility of grid congestion is present since high-rated power values are needed for the opportunity chargers. This chapter will discuss the photovoltaic (PV) system implemented for opportunity charging.

### 6.1. PV power output model

The PV model used in this paper is a per-second simulation of the energy output of the solar panels [17]. The model takes into the solar altitude ( $a_s$ ), solar azimuth ( $A_s$ ), global horizontal irradiance (GHI), diffuse horizontal irradiance, ambient temperature, ground temperature wind speed, cloud shading into account [17]. It is assumed that the module placement causes that panel-on-panel shading not present [17].

The global irradiance ( $G_m$ ) is calculated by the sum of the direct, diffuse, and reflected irradiances. The detailed equations for these terms are described in [40].

The PV module data sheet provided by the manufacturer shows the efficiency deviation of the solar module from the standard testing conditions (STC) due to the solar cell temperature. Quantifying irradiance variation effect on the solar module performance is less straightforward [17]. The overall module efficiency that accounts for the temperature and irradiance influence can be approximated by [17]:

$$\eta(T_M, G_M) = \eta(25^\circ C, G_M)[1 + \kappa(T_M - 25^\circ C)] \quad (6.1)$$

$T_M$ : The module temperature.

The first term represents the effect of irradiance and the second that of temperature with  $\eta$  computed as [17]:

$$\eta = \frac{1}{\eta(STC)} \frac{\partial \eta}{\partial T} \quad (6.2)$$

The selected PV module in this model is the 'AstroSemi 365W' mon-crystalline panels from Astronergy. The PV modules have a rated power of 365 Wp and an efficiency of 19.7% at STC. The model described in this section has a PV power output which is shown in figure 6.1. From this figure, it can be seen that the area of the PV module is needed to have the power output of one module. The module area is 1.85  $m^2$ . This value is obtained from the module datasheet.

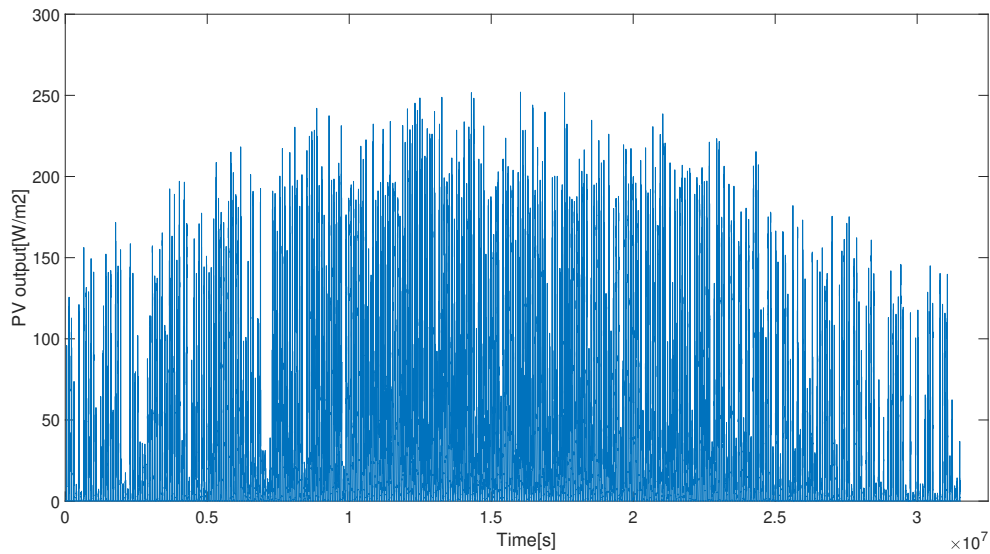


Figure 6.1: Output of the PV model

## 6.2. PV system placement and assumptions

### 6.2.1. PV module placement

The module placement is aimed to be placed on the roof of the bus stops. Bus stop booth measurements in the Netherlands are 1.5 to 2.330 meters wide, while the length could go from 3.9 to 4.5 meters [3]. Thus the booth top has some space to place PV modules. The total area used for stops has a long range between 12 to 22 meters [20]. This means that there is a possibility to increase the length of the bus stop booth if needed or to place modules near the bus booth. 12 meters is taken as the maximum possible length of the bus stop booth. The minimum length of the bus stop area is chosen as the length. This is done since no data is available about the bus stop areas. The lower length range is chosen to increase the chance of making the PV module placement on stops more realistic and possible.

### 6.2.2. Assumptions

There are a couple of possibilities for placing and using the PV modules to try to power the opportunity chargers:

1. Only use PV modules as the source and only use the stop that has the opportunity charger.
2. Use a mixture of the grid and PV modules to power the opportunity charger.

The daily bus operation will test PV energy as a charger supply. The PV system will be scaled by keeping congestion in mind. Congestion of the grid could happen when the grid needs to deliver or take too much energy. The module amount is chosen to supply the charger demand of the day with the best PV input. The modules are scaled to have a similar or equal PV battery SOC at the end and start of the day. This prevents or reduces the overproduction of solar energy that could cause grid congestion. The worst day of the year, the day with the least power produced by the PV modules, is taken to size the battery since the battery is needed most on this day. The size determined here will be sufficient for every other day of the year.

## 6.3. Simulation Model

The simulation model to implement the PV addition on bus stops is implemented in Simulink. The PV simulation model inputs are the output of the PV model described in section 6.1, the power rating of the opportunity charger, the charging time, and the SOC of the battery used for the PV system. The power demand from the opportunity charger is given by equation 6.3. The charger power demand is divided by the discharge efficiency of the battery to account for the losses created while energy is

taken out from the battery. The PV charging power is given at the equation 6.4, where the battery losses are included with the PV model output. The PV simulation model uses the SOC of the PV battery to determine whether the PV system can provide the charging power rating. The PV battery does not discharge when its charge is low, instead, it uses the PV system or the grid to charge itself. PV battery stops discharging when the SOC is less than 20%. When this is not the case, it is assumed that the battery can meet the opportunity charger power demand. The simulation model inputs are then used for the battery model described in section 4.2.2.

$$P_{PV,discharge} = \frac{P_{charger}}{\eta_{discharge}} \quad (6.3)$$

$$P_{PV,charge} = \eta_{charge} P_{PVmodelout} \quad (6.4)$$

The PV simulation model is made with the following assumptions:

- The input and output of the PV system are the same for the whole operational day of the electric bus.
- The only difference in discharge at different stops is the moment in time that it happens.
- When a battery at one of the stops is empty, all the other stops have empty batteries.
- The PV battery is at 80% SOC at the start of the simulation.

The assumptions are not 100% accurate. The discharge of the PV battery and the supply of energy to the bus is dependent on the SOC of the bus battery. The battery is not discharged when the bus battery is full. There is a possibility that there is a difference in the SOC value of the bus battery at different stops. The charger will not supply when the SOC of the bus battery is at its maximum value. Another inaccuracy that the assumptions have is the negligence of the fact that at the beginning of each day, the PV input obtained is smaller than in the afternoon. Close to the evening, it is again less than in the afternoon. The position of the bus stop and where the bus is at a specific time cause a difference in the SOC of the PV battery due to the difference in PV input during the day. The first stop at the driving cycle, which is at the start of the day when the bus drives the first cycle. The PV battery at the first stop will have less SOC compared to the last bus stop of the driving cycle when a bus arrives. However, these differences are assumed to be small and negligible. The battery is assumed to be full at the start of the day, ensuring that the opportunity charger power demand will be met at the start.

The simulation model will only focus on one stop. Every single bus stop in the driving cycle is turned off when one of the PV batteries at a bus stop is empty.

## 6.4. Energy-Neutrality Ratio

The Energy-Neutrality Ratio ( $\zeta$ ), shown in the equation 6.5 [17], shows the rate at which the PV system can supply the energy demand. If the PV system can meet the entire load, then  $\zeta = 1$  [17].  $\zeta$  below 1 means that the PV system can not supply the load demand alone. Exceeding the value of 1 means that the PV system supplies more than there is demand. The Energy-Neutrality ratio indicates the percentage that the PV system can cover the demand needed.

$$\zeta \triangleq \frac{\int_{year} P_{PV} dt}{\int_{year} P_{load} dt} \quad (6.5)$$



# 7

## Results & Discussion

### 7.1. Opportunity charging at every stop

This section shows the results in figures 7.1-7.4 of the battery sizes when every stop has an opportunity charger with a specific charging time. The simulation is performed with the assumptions stated in section 5.2.1 for the different driving cycles introduced in section 1.2. Every stop in a driving cycle has a charger that will be operational. The power ratings analyzed vary from 100kW to 200kW. The lowest value chosen is 100kW because lower power ratings are insufficient to make the bus operate nonstop for a full day when only opportunity charging is applied. The waiting time varies from 30 seconds to 1 minute. The charging times are kept below or equal to 1 minute. This prevents long waiting times for the passengers. These charging times extend the waiting time at stops by 10 to 30 seconds compared with a regular waiting time at stops. Three to five stops at every driving cycle used has longer waiting times at stops than the usual 20 seconds.

Figure 7.1 shows the result of the 200kW charger for different waiting times. These results are obtained from the driving cycles introduced in this paper. The battery size values have a downward trend when the waiting time is increased. The battery value range is smaller when the waiting time is increased. Table 7.1 shows the average battery value obtained from the result shown in figure 7.1. The average battery size is below 100 kWh for waiting times longer than 40 seconds. The waiting time of 60 seconds shows that all the battery sizes are below 100kWh. The smallest average battery size of 51 kWh is shown at 60 seconds of waiting time. The difference between the average battery sizes becomes larger when the waiting time becomes longer.

Table 7.1: The average battery values at a specific waiting time when a 200 kW charger is used.

Waiting times:	30 sec	40 sec	50 sec	60 sec
Average battery size:	177.18 kWh	92.58 kWh	62.44 kWh	51.5 kWh

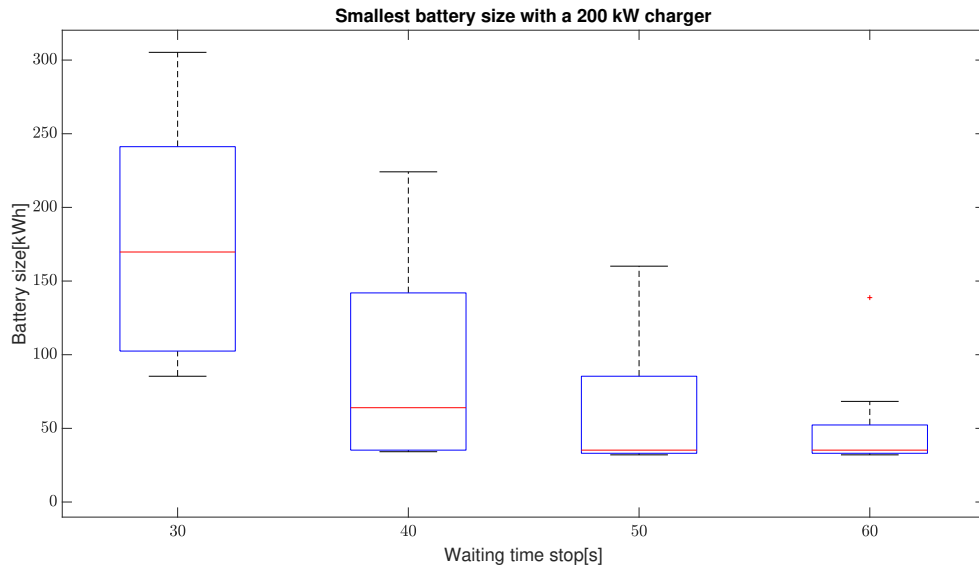


Figure 7.1: The smallest battery sizes at 200kW charger power rating and stop waiting times result obtained from the different driving cycles.

Figure 7.2 shows the result of the 150 kW charger for different waiting times obtained from the different driving cycles. The battery size at 30 seconds is ranging from 305 kWh to approximately 240 kWh ranges. Battery sizes show a downward trend while the waiting time is longer. Table 7.2 shows the average values obtained from the results shown in figure 7.2. The difference between the average battery sizes is somewhat similar when the waiting time becomes longer by 10 seconds. The average values at 150 kW are approximately two times larger than the 200 kW charger results. The only exception is the waiting time of 30 seconds, at which the difference is less than two times the battery size.

Table 7.2: The average battery values at a specific waiting time when a 150 kW charger is used.

Waiting times:	30 sec	40 sec	50 sec	60 sec
Average battery size:	267.91 kWh	204.92 kWh	153.16 kWh	100.86 kWh



Figure 7.2: Driving cycles with the smallest battery sizes at 150kW charger power rating and stop waiting times result obtained from the different driving cycles.

Figure 7.3 shows the result of the 125 kW charger for different waiting times. The waiting time of 30 seconds is almost impractical for the 125 kW charger. Only one driving cycle can have a waiting time of 30 seconds with this charger power rating. The battery size trend is going down while the waiting time of the stops is lessened, like the power ratings previously mentioned. Battery sizes are starting to exceed the value of 100 kWh more often at 60 seconds of waiting time. The average battery sizes are given in table 7.3.

Table 7.3: The average battery values at a specific waiting time when a 125 kW charger is used.

Waiting times:	30 sec	40 sec	50 sec	60 sec
Average battery size:	320 kWh	270.52 kWh	190.34 kWh	141.8 kWh

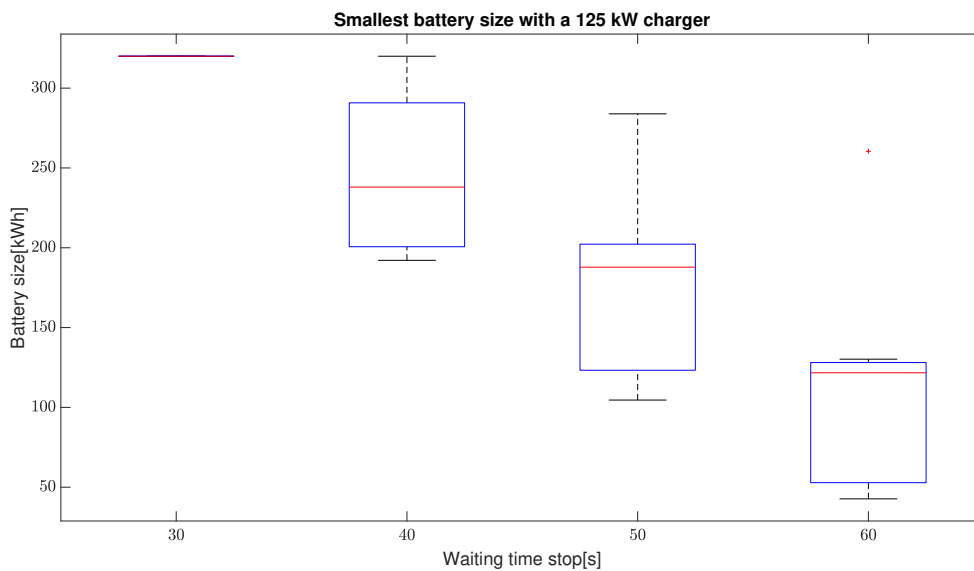


Figure 7.3: Driving cycles with the smallest battery sizes at 125kW charger power rating and stop waiting times result obtained from the different driving cycles.

Figure 7.4 shows the result of the 100 kW charger for different waiting times obtained from the driving cycles. The waiting times of less than 50 seconds are too short for the 100 kW charger. The battery size trend is going down while the waiting time of the stops is lessened, like the other power rating values mentioned. The smallest values exceed the value of 100 kWh by a large margin. Thus the battery sizes become significantly larger at this power rating, while also having a longer charging time at stops.

Table 7.4: The average battery values at a specific waiting time when a 100 kW charger is used.

Waiting times:	50 sec	60 sec
Average battery size:	277.08 kWh	206.36 kWh

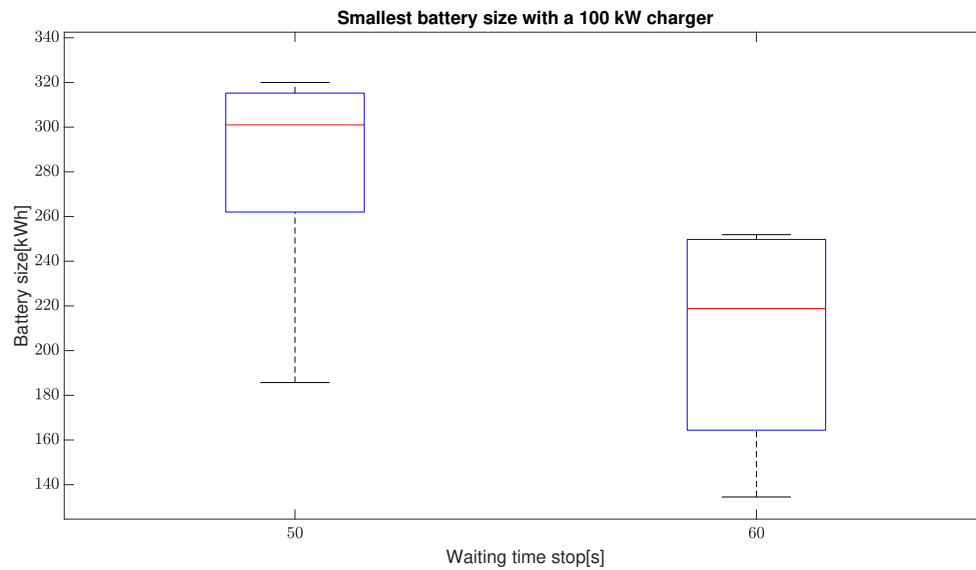


Figure 7.4: Driving cycles with the smallest battery sizes at 100kW charger power rating and stop waiting times result obtained from the different driving cycles.

## 7.2. Discussion of the minimum battery size

The battery sizes become smaller when the waiting time is increased for all charger power ratings. This is required and logical since a longer charging time means less need for a large battery. This is logical since the battery is charged constantly within the driving cycle due to opportunity charging, making more energy storage unnecessary. The battery size is affected by different driving cycles. The driving cycle speed, braking behavior, stop placement, and stop amounts are all factors that cause different results for different driving cycles.

It can be seen that the smallest battery sizes are at the 200 kW charger. 200 kW and 150 kW have battery sizes that are mostly below 100 kWh when looking at the waiting time of 60 seconds. The values at 200 kW with a waiting time of 60 seconds have the smallest battery values. The battery value range at the 200 kW charger with 60 seconds of waiting time seems like the smallest possible for an electric bus with the opportunity chargers. The average value of the battery at 60 seconds waiting time for a 200 kW charger is 51.5 kWh.

The difference between battery sizes for 200 kW and 150 kW chargers at 60 seconds is the lowest when both ratings are compared. The 100 kW charger shows the largest battery sizes of all the power ratings. These results show that the 200 kW charger is preferred when the battery must be as small as possible.

## 7.3. Results of the minimum amount of stops

### 7.3.1. Minimum stops at 200kW

The charger amounts at stops have a downward trend when the waiting time is increased, which is expected since charging the battery longer means less need for additional chargers. The percentage of stops with chargers needed most of the time is approximately between 80 and 60 percent of the total bus stops available. At 40 seconds of waiting time, this percentage range goes down to 60 to 50 percent of the total available stops. The stop percentage used ranges from approximately 55 to 40 percent for most of the 50 seconds waiting time cases. For 60 seconds the percentage range of used stops spans from 45 to 35 percent. The percentage difference is larger between the waiting time of 30 seconds and 40 seconds compared to other waiting times.

Figure 7.5 shows the battery sizes at the minimum number of stops. The battery sizes are not signifi-

cantly reduced compared to the original 320 kWh battery. This is because the minimum stop amount is determined to provide enough charge to finish the daily trip. The battery sizes will become smaller when additional stops are added to the minimum amount of bus stops used. The median of the battery sizes shows a drop after the waiting time of 40 seconds.

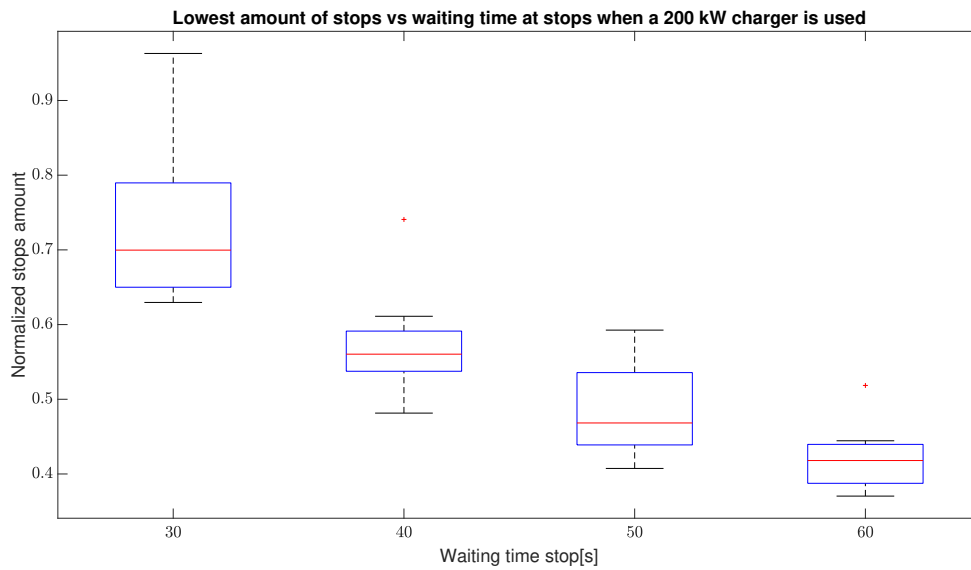


Figure 7.5: Driving cycles with the lowest amount of stops at 200kW charger power rating and stop waiting times obtained from different driving cycles.

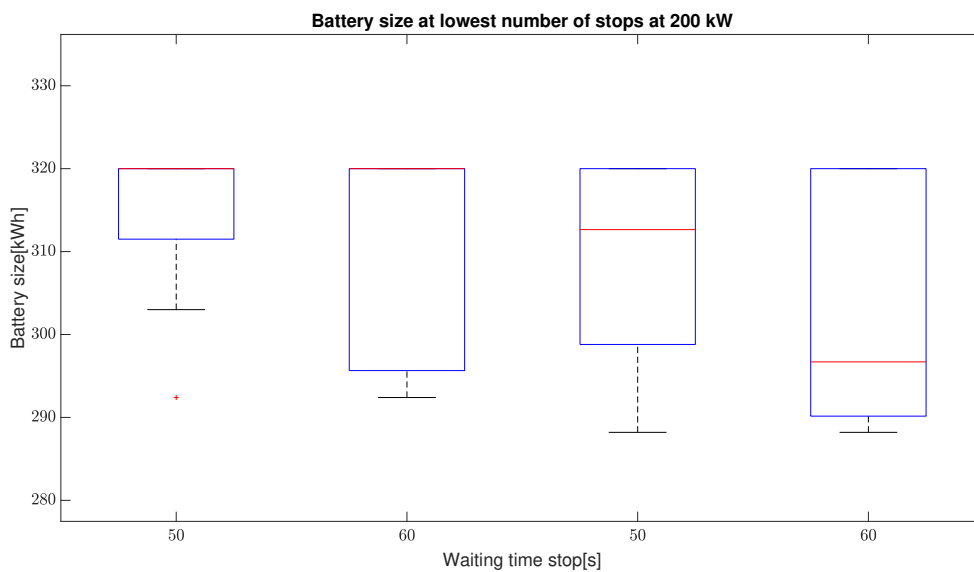


Figure 7.6: The battery size for driving cycles with the lowest number of stops is used at 200kW charger power rating and stop waiting times obtained from different driving cycles.

### 7.3.2. Minimum stops at 150kW

The charger number at stops has a downward trend when the waiting time is increased. The percentage of used bus stops at 30 seconds of waiting time is mostly between 95 and 85. The percentage range for most of the driving cycles for 50 seconds of waiting is between 75 and 65 percent of stops that need chargers. For 40 seconds the percentage range is usually between approximately 70 to 60 percent. The used bus stops span usually from 57 to 52 percent. The measurements show again that the difference

between 30 to 40 seconds of waiting time is the largest compared to other waiting time differences. The battery sizes are not reduced a lot when minimum stops are used. The battery sizes are between 320 kWh and 300 kWh most of the time. The exception to this is the 60 seconds waiting time, which reaches below 300 kWh.

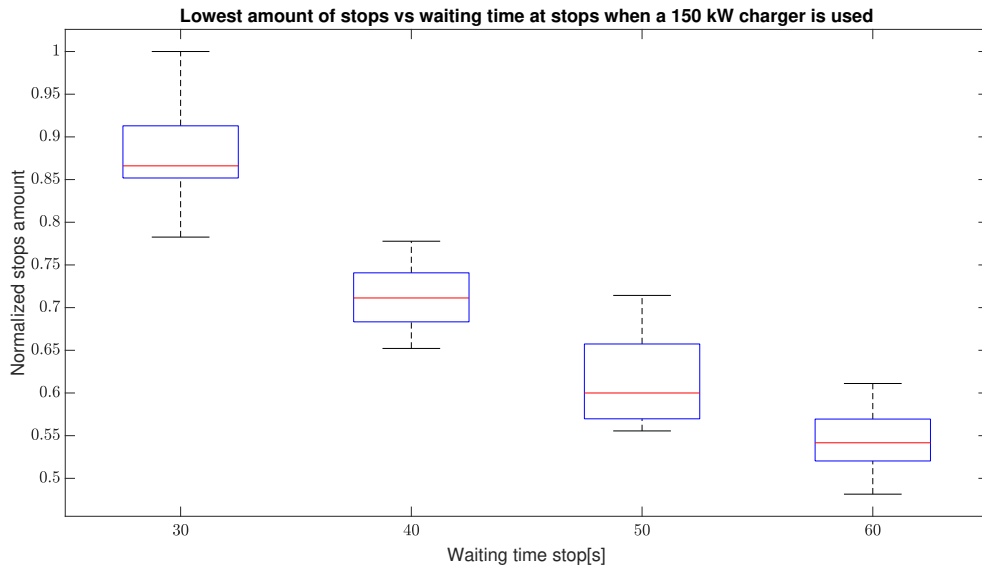


Figure 7.7: Driving cycles with the lowest amount of stops at 150kW charger power rating and stop waiting times for different driving cycles.

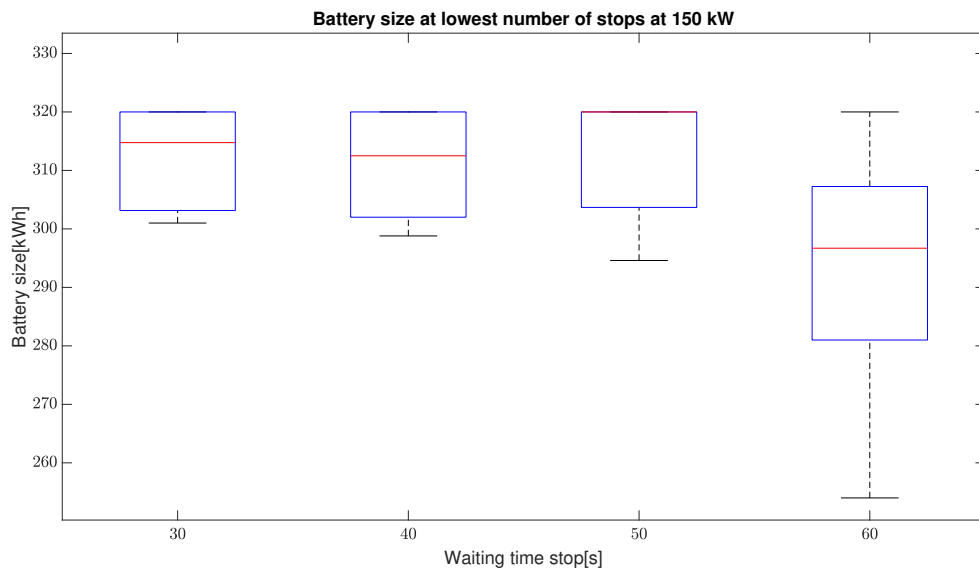


Figure 7.8: The battery size when driving cycles with the lowest amount of stops is used at 150kW charger power rating and stop waiting times.

### 7.3.3. Minimum stops at 125kW

Like the previously discussed power ratings, the charger amounts at the stops have a downward trend. 30 seconds seems a far stretch for 125 kW. Only one cycle can handle this waiting time with this power rating. This driving cycle needs to use all the stops available. The percentage range at 40 seconds is usually between 95 and 85 percent. At 50 seconds the stop amount used is between 80 to 70 percent. At 60 seconds, the stop percentage range is usually between 75 percent and 60 percent.

The battery size range for every waiting time is between 320 kWh and approximately 295 kWh.

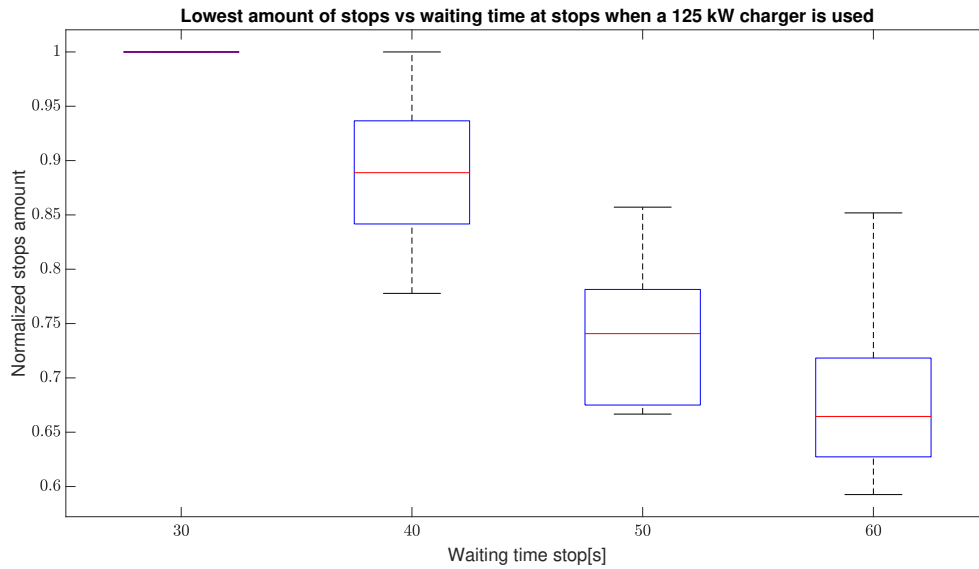


Figure 7.9: Driving cycles with the lowest amount of stops at 125kW charger power rating and stop waiting times.

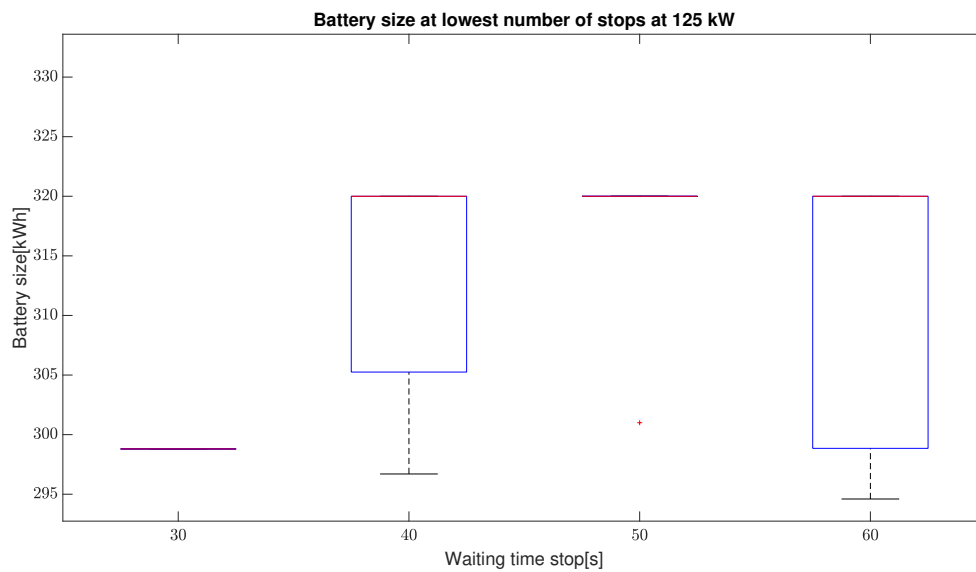


Figure 7.10: The battery size when driving cycles with the lowest amount of stops is used at 125kW charger power rating and stop waiting times.

### 7.3.4. Minimum stops at 100kW

The stops amount percentage compared to all stops ranges from 100 to 83 percent at a waiting time of 50 seconds. At 60 seconds this range drops to between 83 to 70 percent.

The battery size varies between 320 kWh and 295 kWh for every waiting time at the stop and for every driving cycle.

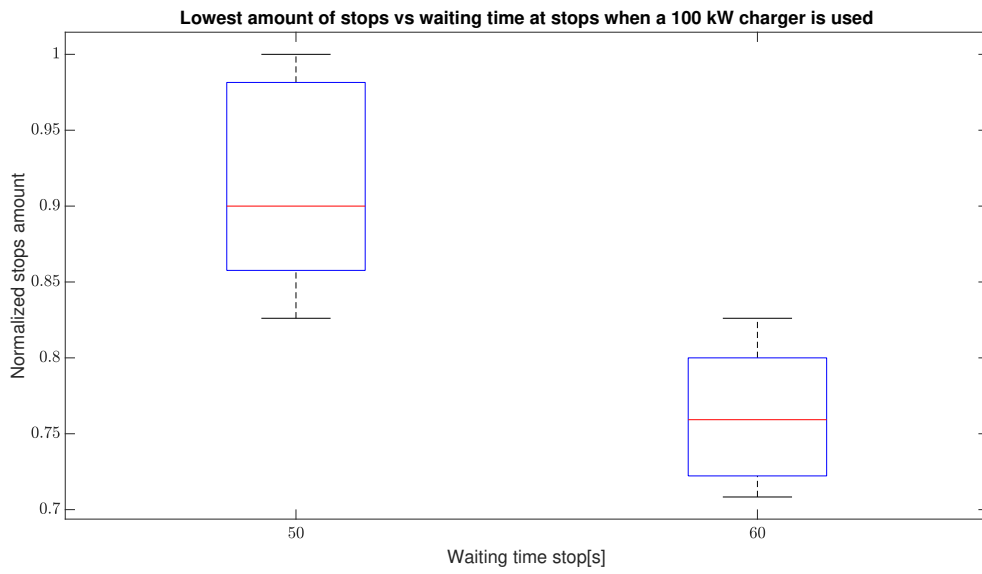


Figure 7.11: Driving cycles with the lowest amount of stops at 100kW charger power rating and stop waiting times.

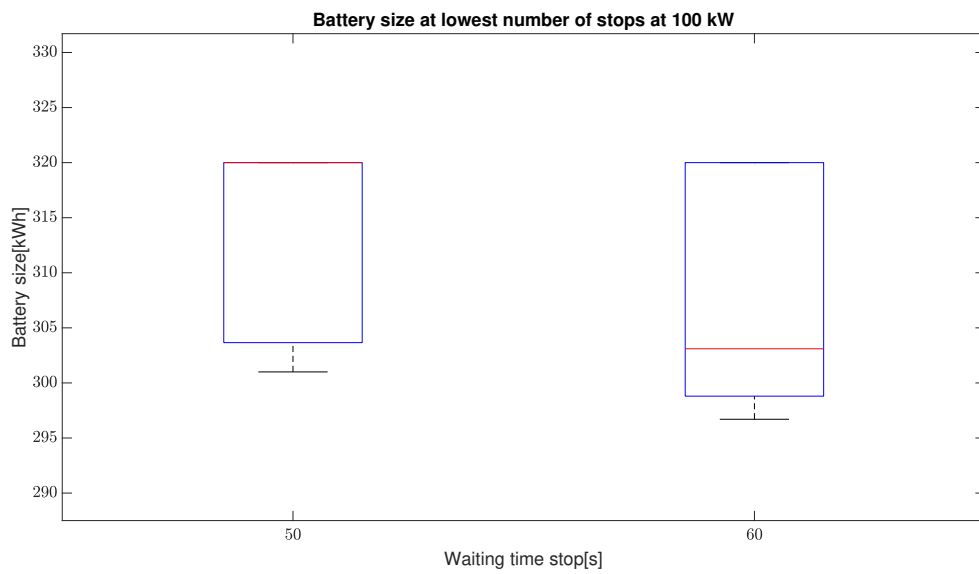


Figure 7.12: The battery size when driving cycles with the lowest amount of stops is used at 100kW charger power rating and stop waiting times.

## 7.4. Discussion of the minimum amount of stops

The minimum amount of bus stops decreases when the waiting time at the bus stop is increased. This is expected since more charge is provided to the battery for a longer waiting time. The amount of bus stops differences between 30 and 40 seconds is larger compared to the difference between the other waiting times for all power ratings.

Lowering the power rating at chargers has more effect on the number of stops needed compared to increasing the waiting time by 10 seconds. The range of normalized bus stops amount goes down between 0.1 and 0.15 when the waiting time is increased, while this difference is between 0.3 and 0.15 when the power rating is increased by 50 kW and 0.2 and 0.15 when the power rating is increased by 25 kW. The difference in stop amounts between 100 kW and 150 kW is larger than the difference between 150 kW and 200 kW.

100 kW seems to be an unreasonable option while looking at the normalized stop amount compared to other power ratings. The waiting time of 50 and 60 seconds results in a high amount of stops. Other power ratings have a lower charger amount for the same waiting time.

The same reasoning for 100 kW can be used for 125 kW when compared to 150 kW and 200 kW. An additional reason against 125 kW is that lower waiting time is more convenient for bus passengers when opportunity charging is used since the waiting time at a stop is lower. Both 150 kW and 200 kW chargers can handle 30 seconds of charging time while for 125 kW chargers, this seems to be hard.

200 kW chargers have the lowest charger amount needed while possibly having the lower battery size at the bus when a minimum amount of chargers are used. This means that the electric bus is lighter and consumes less energy. 150 kW chargers have higher charger amounts and slightly larger battery sizes than the bus. However, less energy is needed per stop for the 150 kW. However, the lack of traffic light position data could mean that some spots considered as stops could be traffic lights, with that in mind, 200 kW could be the safer option to prefer. The 200 kW charger with 30 seconds of waiting time seems to be the best choice for opportunity charging when looking at the results provided for the lowest amount of stops used.

## 7.5. PV Results

### 7.5.1. PV system sizing

The module amount at a stop for different power ratings and waiting times is given in the figures below. The horizontal line represents the maximum number of modules that could fit at a singular bus stop. The module amounts are determined by investigating the day with the most PV power input, while the batteries are sized to withstand the day with the worst. Demand that could not be covered by PV is covered with the grid. Assumptions made in this section cause the grid can deliver power at times when there is no congestion.

#### 200 kW charger module amount and battery size

The 200 kW charger results show that the PV module amount needed at a stop for waiting times of 50 and 60 seconds is usually more than the maximum amount of modules that can fit the bus stop. These results show the situation for a singular bus stop. The results show a need for additional space, other than the stop where the charger is placed for waiting times 50 and 60 seconds. The module amount needed at stops fits at the available area at the bus stops for most of the driving cycles when the waiting time is 30 or 40 seconds.

The battery sizes shown in figure 7.16 are battery sizes per stop that are chosen to withstand the worst day of the year. The battery sizes show a downward trend with the lesser waiting time. The difference between different driving cycles is explained by the number of charges done at a bus stop. More frequent charging means that there is a need for additional energy supply throughout the day, hence the battery size differences at a specific waiting time.

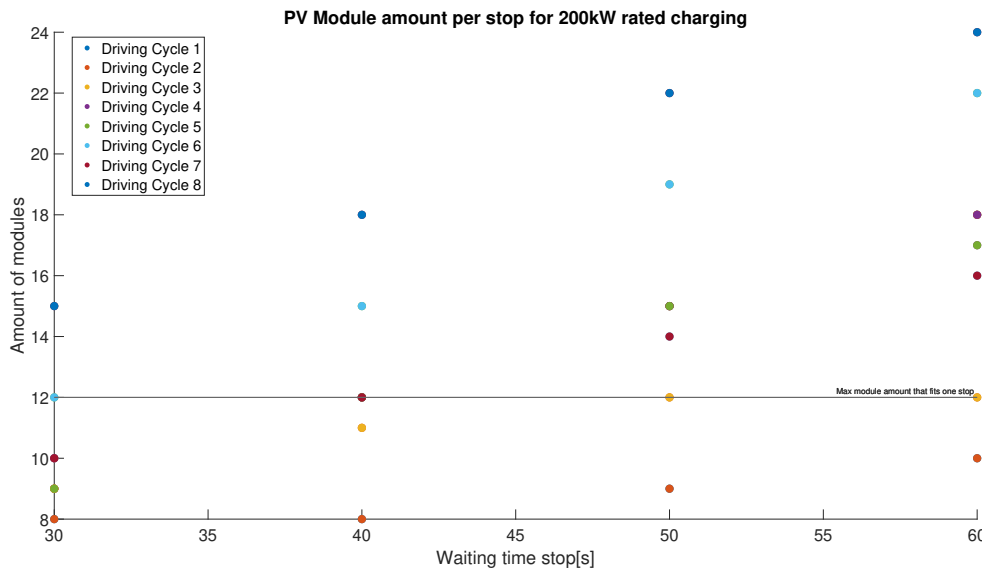


Figure 7.13: The module amount needed per 200 kW charger at one stop to sustain the best day of the year with only PV for the different driving cycles. The line represents the maximum module amount that is placeable at a single stop.

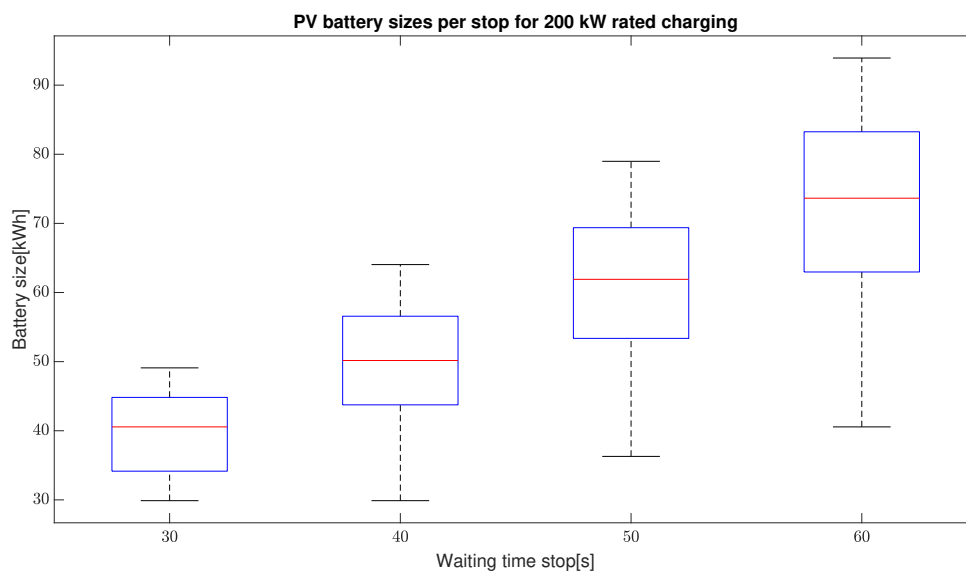


Figure 7.14: The battery sizes needed per stop for different waiting times and a 200 kW charger.

### 150 kW charger module amount and battery size

The 150 kW charger results show that the amount of modules needed exceeds the maximum amount that fits at the bus stop area at a waiting time of 60 seconds. This is the case for a couple of driving cycles. For the other waiting times, other than one driving cycle at 50 seconds, all the modules needed can be fit at a singular bus stop. It could thus be concluded that the maximum amount of modules that fit at a bus stop is sufficient for waiting times equal to or less than 50 seconds.

The battery sizes shown in figure 7.14 are battery sizes per stop which are chosen to withstand the worst day of the year. The battery sizes show a downward trend with the lesser waiting time. The difference between different driving cycles is explained by how many times the bus passes the stop. Since more frequent charging means that more energy supply is needed throughout the day, hence the battery size differences at a specific waiting time.

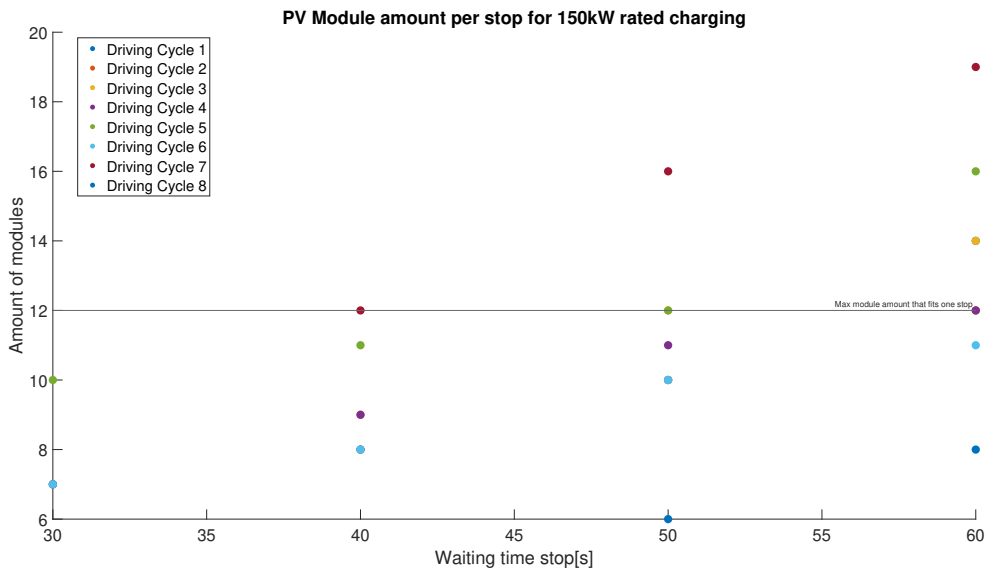


Figure 7.15: The module amount needed per 150 kW charger at one stop to sustain the best day of the year with only PV for the different driving cycles. The line represents the maximum module amount that is placeable at a single stop.

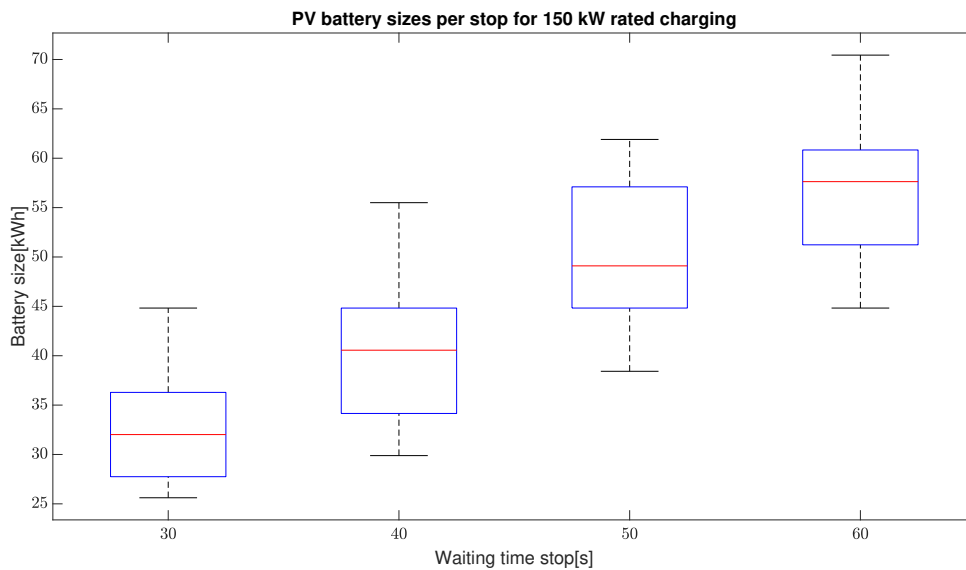


Figure 7.16: The battery sizes needed per stop for different waiting times and a 150 kW charger.

**125 kW charger module amount and battery size**

The 125 kW charger results show that the PV module amount could be fit on a singular stop for almost all the driving cycles. A couple of exemptions can be seen at waiting times of 50 and 60 seconds.

The battery sizes shown in figure 7.18 are battery sizes per stop that are chosen to withstand the worst day of the year. The battery sizes show a downward trend with the lesser waiting time. The difference between different driving cycles is explained by how many times the bus passes the stop. Since more frequent charging means that more energy supply is needed throughout the day, hence the battery size differences at a specific waiting time.

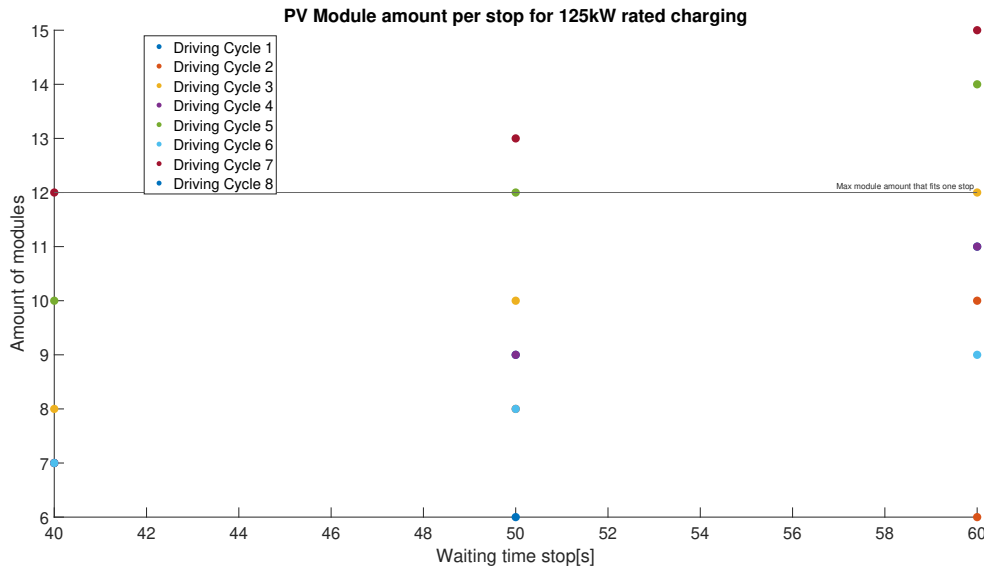


Figure 7.17: The module amount needed per 125 kW charger at one stop to sustain the best day of the year with only PV for the different driving cycles. The line represents the maximum module amount that is placeable at a single stop.

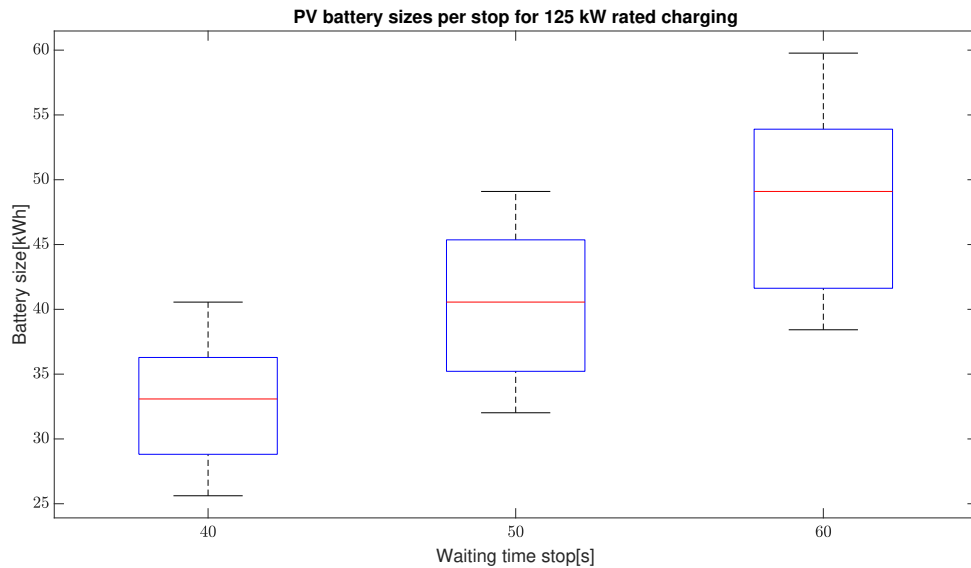


Figure 7.18: The battery sizes needed per stop for different waiting times and a 125 kW charger.

**100 kW charger module amount and battery size**

The 100 kW charger results show that the PV module amount could be fit on a singular stop for all the driving cycles and possible waiting times.

The battery sizes shown in figure 7.16 are battery sizes per stop that are chosen to withstand the worst day of the year. The battery sizes show a downward trend with the lesser waiting time. The difference between different driving cycles is explained by how many times the bus passes the stop. Since more frequent charging means that more energy supply is needed throughout the day, hence the battery size differences at a specific waiting time.

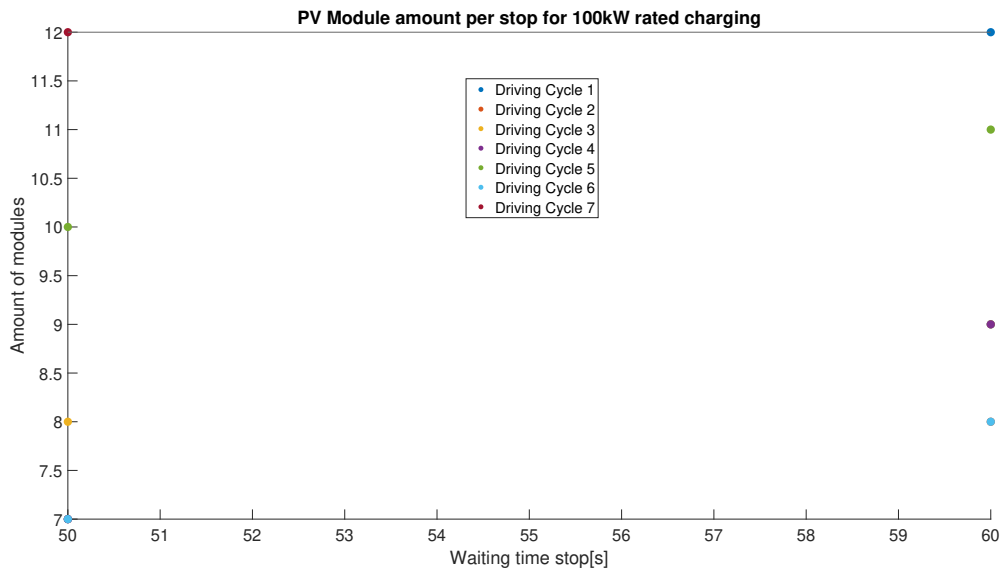


Figure 7.19: The module amount needed per 100 kW charger at one stop to sustain the best day of the year with only PV for the different driving cycles. The line represents the maximum module amount that is placeable at a single stop.

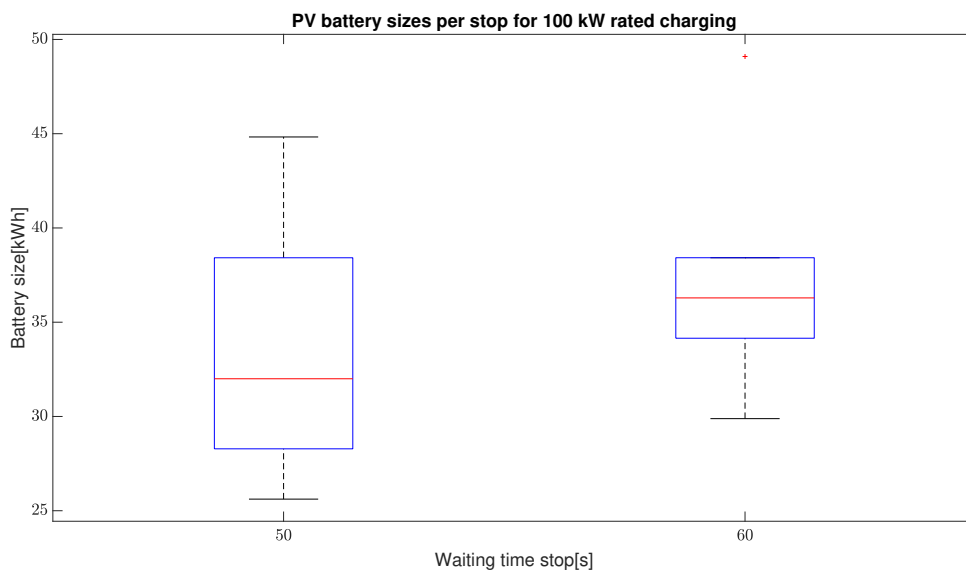


Figure 7.20: The battery sizes needed per stop for different waiting times and a 100 kW charger.

### 7.5.2. Standalone PV system or grid-tied PV system

The possibility of a standalone system can be decided by looking at the Energy-Neutrality Ratio, which is introduced in section 6.4. The power ratings of 200 kW and 150 kW are analyzed and the waiting times are taken at which the maximum amount of modules at stops seems to be possible according to section 7.5.1. The results are shown in figures 7.21 to 7.25. The results indicate that a standalone PV system is incapable of covering the yearly demand at most of the driving cycles. It needs to be kept in mind that seasonal changes in the weather are significant to consider. An example of excess or less energy production of PV compared to the demand is shown in figure 7.26. This figure shows the lacking or excess production of PV energy compared to the charger demand expressed in days in the year. The winter months show a significant need for an additional energy source. It can be seen that even some of the summer days need additional energy other than the PV system. A grid-tied PV system is thus needed for additional energy supply.

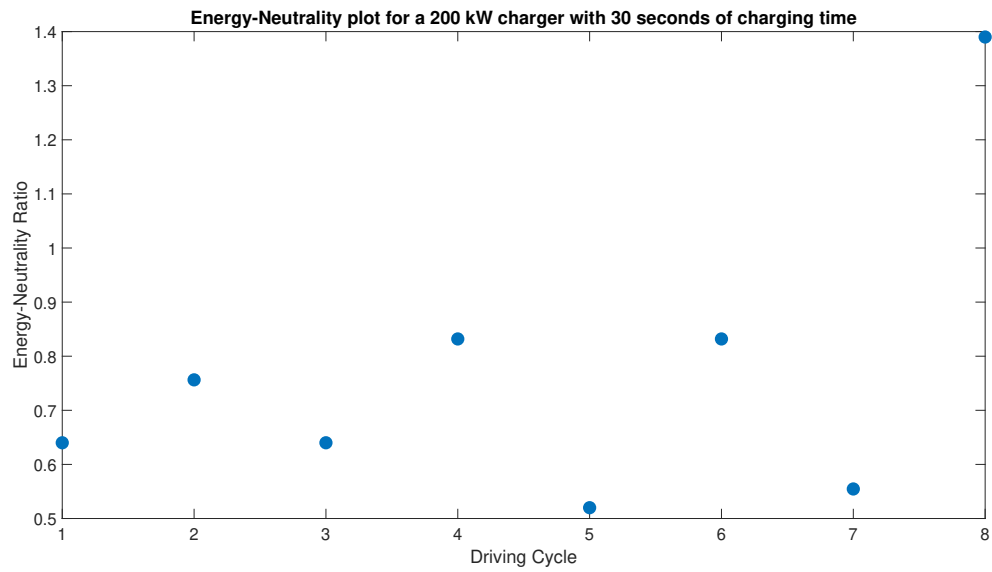


Figure 7.21: The Energy-Neutrality Ratio for each driving cycle for a charger with a 200 kW power rating and 30 seconds of charging when 12 modules are placed on the stop.

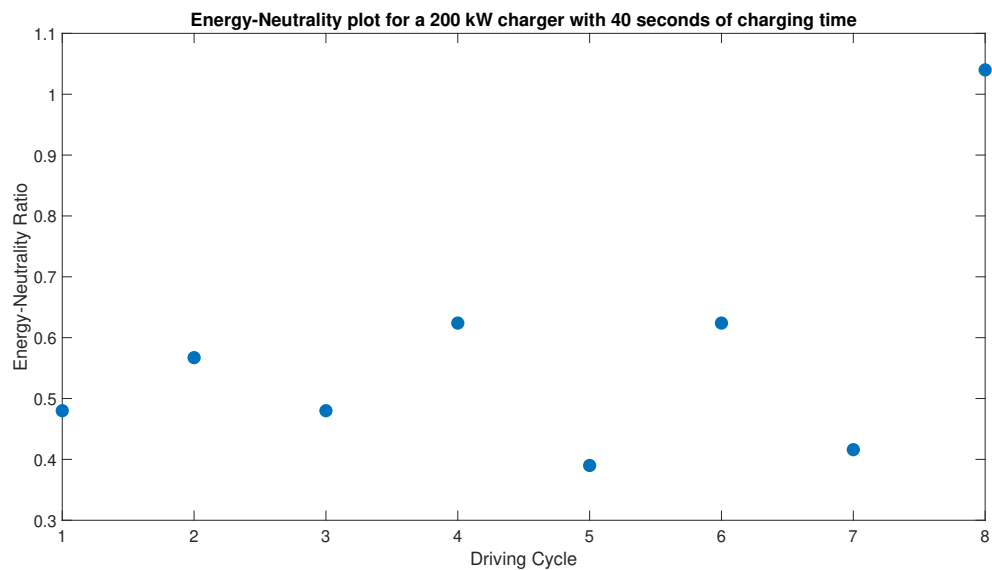


Figure 7.22: The Energy-Neutrality Ratio for each driving cycle for a charger with a 200 kW power rating and 30 seconds of charging when 12 modules are placed on the stop.

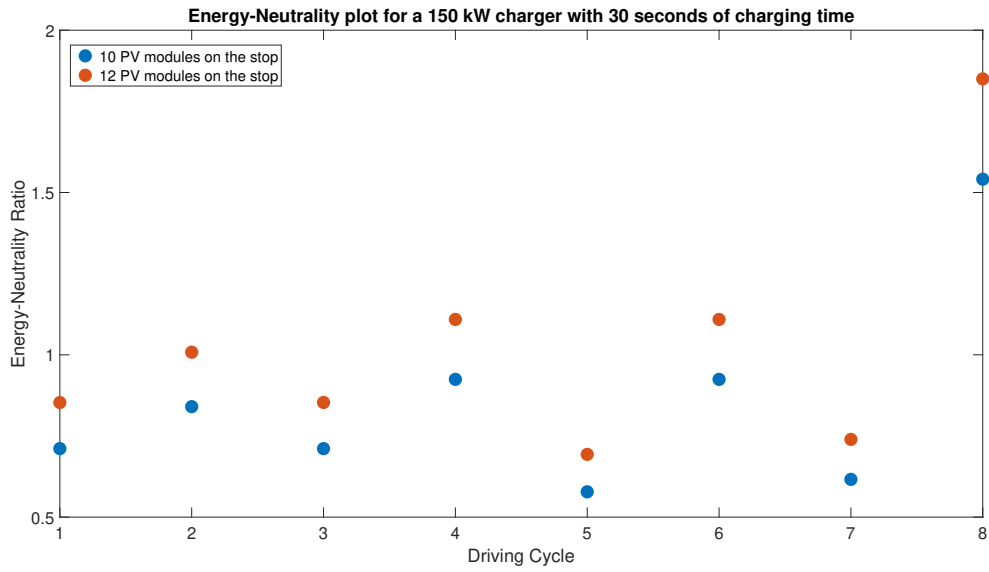


Figure 7.23: The Energy-Neutrality Ratio for each driving cycle for a charger with a 150 kW power rating and 30 seconds of charging when 10 and 12 modules are placed on the stop.

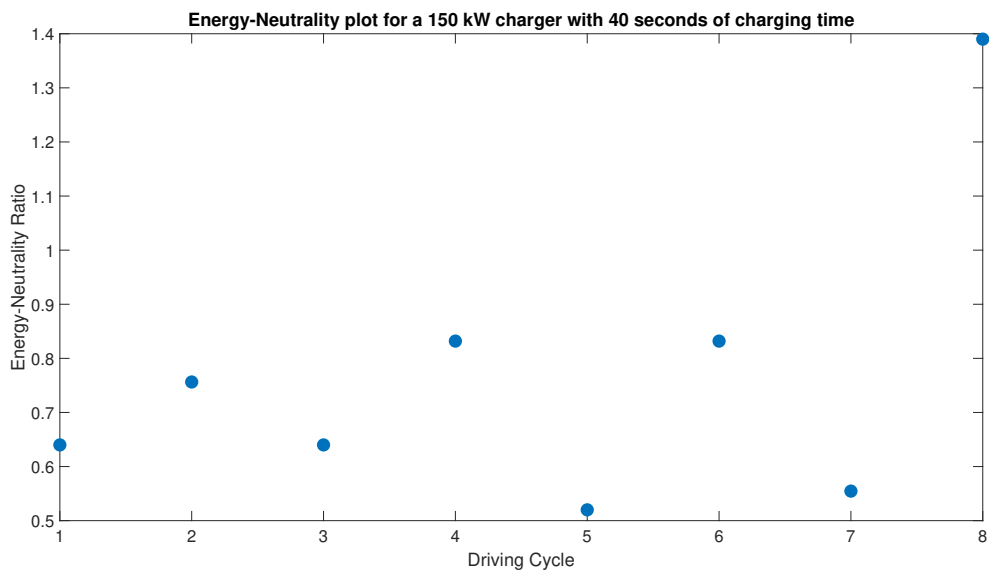


Figure 7.24: The Energy-Neutrality Ratio for each driving cycle for a charger with a 150 kW power rating and 30 seconds of charging when 10 modules are placed on the stop.

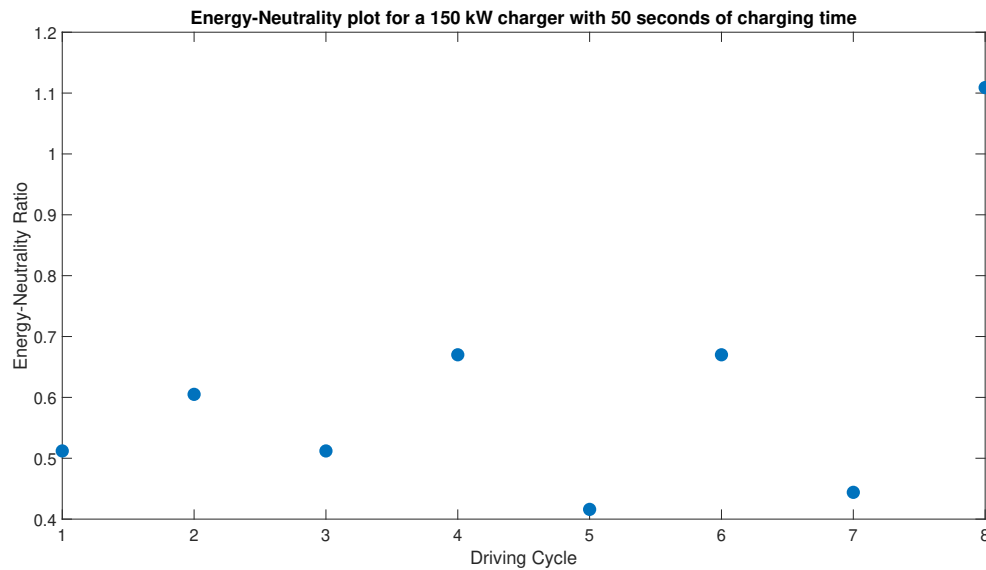


Figure 7.25: The Energy-Neutrality Ratio for each driving cycle for a charger with a 150 kW power rating and 30 seconds of charging when 10 modules are placed on the stop.

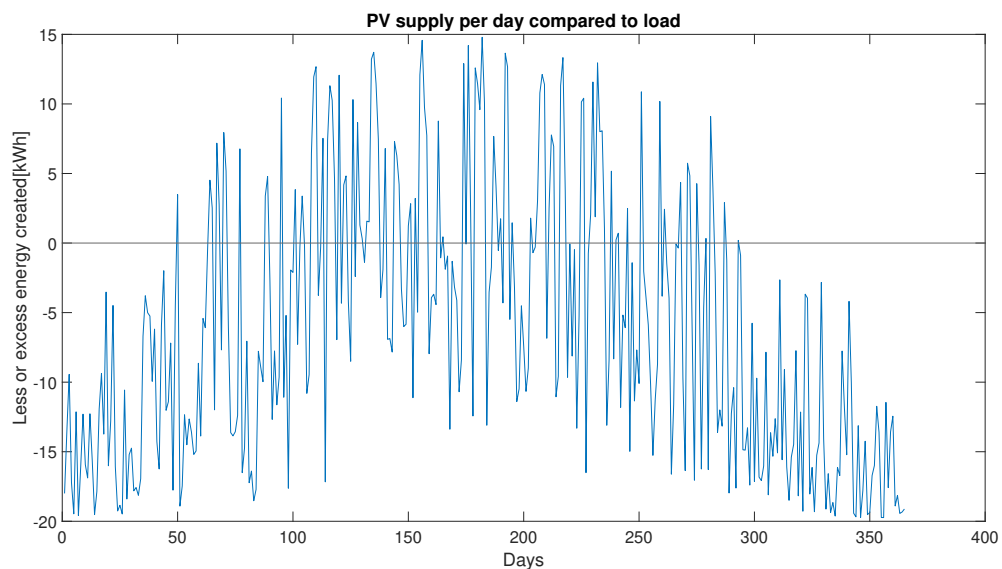


Figure 7.26: The less or excess energy provided by the PV system for a charger of 150 kW that charges 30 seconds with 12 modules used for one of the driving cycles.

## 7.6. PV discussion

This section will discuss the results obtained at PV results. The PV system needs to be a grid-tied PV system, which can be deduced from the Energy-Neutrality Ratio and the lacking energy for the charger demand. The energy demand for the chargers is not always met by the PV system. This is especially the case at months outside the summer. The grid-tied PV system will have a backup battery to store the PV energy that is generated by the PV system in the battery. This will result in the reduction of the grid dependency of the PV system.

The grid-connected PV system assumptions are made to reduce the possibility of grid congestion as much as possible. The system battery and PV modules are scaled to make the chargers operational

during bus operating times. The battery can store energy at times when the demand on the grid is not a lot. The battery is thus storage for energy, which could be used to store energy delivered by the grid when congestion can be avoided.

The results show that for a 200 kW charger, only 30 second waiting time results in PV modules that fit at the stop area. There is only one outlying driving cycle. The excess modules needed at other waiting times need to be placed somewhere else for at least half of the driving cycles. The placement could be on other stops or nearby the bus stop depending on the area available at a specific stop neighborhood.

The results of the 150 kW charger show that for waiting times of 30 seconds, 40 seconds, and 50 seconds, the PV module's amount is sufficient to meet the demand at the best PV day without the grid. 125 kW and 100 kW chargers do not need more modules than the maximum number of modules placed on stops.

200 kW and 150 kW chargers that charge for 30 seconds seem to be the more attractive options for opportunity charging. This is because quick charging is more convenient for passengers. Also, the module amounts needed to power the best day of the year, fit the stop area for both choices. There is a possibility that more modules could be placed, however, 12 modules are considered the maximum amount since there is no bus stop area data available with the driving cycles. The choice between both power ratings depends on the availability of power that can be delivered, the preference of battery size for the PV system, and the number of chargers that is willing to be used. The 200 kW charger needs more modules and has a larger range of needed battery size values but needs fewer chargers at driving cycles. 150 kW charger needs fewer modules, a smaller battery size, more chargers, and less power to make the chargers work.

Figures 7.21-7.25 show the neutrality for each driving cycle used. The figures show that the PV modules installed can at least meet half of the yearly energy demand for one electric bus. The results show that the PV system can meet a higher percentage of the demand for the 150 kW charger. The module amount at the 150 kW charger could have two additional modules placed at the stop when looking at the waiting time of 30 seconds. The effect of 12 modules for a charger of 150 kW that charges 30 seconds is shown in figure 7.23. The Energy-Neutrality when 12 modules are used shows that for half the driving cycles, the power demand is met or even exceeded. It is hard to decide on the number of modules for this situation due to the lack of data about possible grid capabilities at specific times. This means that information about congestion possibility is unknown when 12 modules are used. The seasons are important to consider, however. The coefficient is only reflecting the yearly supply and demand. The winter months for example can not supply the chargers sufficiently alone, while the PV system generates excess energy in the summer. Figure 7.26 shows an example of this.

There are stops at which the waiting times are longer than usual. Crowded places, or important points where the majority of people need to be have a longer waiting time than normal stops. The Energy-Neutrality coefficient for power ratings and waiting times at which 12 modules are sufficient is shown in figures 7.21-7.25. It can be seen that at least 40% of the yearly demand can be met for waiting times of 40 and 50 seconds when 150 kW and 200 kW chargers are used. 200kW charger that charges for 40 seconds charges the battery the fastest and causes the most SOC addition to the battery when compared to the 150 kW charger that charges for 50 or 60 seconds. The choice at stops with a longer waiting time can be either a 150 kW charger that charges slower with less dependency on the grid or a 200 kW charger that charges faster but is more dependent on the grid can be chosen.

## 7.7. Energy Consumption results and discussion

This section will discuss the energy consumption differences, for the preferred charger ratings, when opportunity charging is used compared to an electric bus with wired charging. The comparison is done with the bus weight due to fewer components when wireless charging is used ( $E_{wired} - E_{opp}$ ), the bus weight when a minimum amount of chargers is used ( $E_{wired} - E_{minstops}$ ), and finally the energy consumption difference when the smallest battery is used ( $E_{wired} - E_{minbat}$ ). The values given in the tables 7.5 and 7.6 are obtained from the average of the measurement values shown in Appendix A.2.

The tables are results that show daily energy consumption differences.

The tables show that the weight differences, due to lesser components for opportunity charging result in an energy consumption drop of 1.5 kWh to 1 kWh. The reduced battery size at a minimum amount of operational stops shows that the battery weight difference results in an additional energy consumption difference. The additional energy savings span from 0.3 kWh to approximately 1 kWh for the 200 kW chargers. This range goes from 0.4 kWh to 0.6 kWh for the 150 kW charger. The energy consumption difference at minimum battery size values when the 200 kW charger is used ranges from 14 kWh to 8.56 kWh. The 150 kW charger has an energy consumption range of 12.66 to 4.884 kWh when a minimum battery size is used.

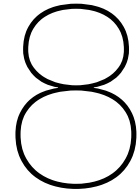
The results show that the energy consumption savings are usually between 2 kWh to 1 kWh when a minimum amount of chargers are used regardless of the charger power rating. The results indicate that there is less energy consumption of the bus when a 200 kW charger is implemented. This result is expected since smaller battery sizes are needed when a 200 kW charger is used. The differences in energy consumption between the charger ratings become more significant when the minimum battery size is implemented at waiting times of 40 to 30 seconds.

Table 7.5: The energy consumption result of the 200 kW charger with different waiting times at stops.

Energy consumption difference:	Time: 60 sec	Time: 50 sec	Time: 40 sec	Time: 30 sec
$E_{wired} - E_{opp}$	1.528 kWh	1.363 kWh	1.3662 kWh	1.273 kWh
$E_{wired} - E_{minstops}$	2.4887 kWh	1.88 kWh	1.66 kWh	1.7092 kWh
$E_{wired} - E_{minbat}$	14.02 kWh	13.1446 kWh	11.94 kWh	8.5593 kWh

Table 7.6: The energy consumption result of the 150 kW charger with different waiting times at stops.

Energy consumption difference:	Time: 60sec	Time: 50 sec	Time: 40 sec	Time: 30 sec
$E_{wired} - E_{opp}$	1.0182 kWh	1.0865 kWh	1.0043 kWh	1.052 kWh
$E_{wired} - E_{minstops}$	1.64 kWh	1.4427 kWh	1.2414 kWh	1.45 kWh
$E_{wired} - E_{minbat}$	12.66 kWh	11.01 kWh	7.9126 kWh	4.884 kWh



## Conclusion

This paper describes the electric powertrain design of an electric bus that is charged with inductive chargers at bus stops. The powertrain model input is the difference between the driving cycle speed from the Arnhem trolleybus grid and the speed of the powertrain model. The difference between the driving cycles and the powertrain model's speed is reduced using a PI controller, which serves as a driver model. This model also implements regenerative braking, namely series braking, to mimic electric vehicles' regenerative braking capabilities. The battery model used is an equivalent circuit model, namely the DP model. The DP model components depend on SOC and are thus represented by lookup tables. The electrical machine used is the PMSM, due to its high efficiency at low speeds. This is convenient for an electric bus that operates within a city. The electrical machine is modeled by implementing its torque speed characteristics together with an efficiency coefficient. This model also accounts for the electric bus's auxiliary and HVAC load demand. A thermodynamic heat exchange model is used between the bus and its environment to determine the auxiliary and HVAC data.

The inductive chargers in this paper are modeled as a power input with system efficiency. The wirelessly charged bus's weight is lighter than a plug-in-charged bus. The weight difference at different power ratings is implemented by proportionally scaling the charger pads to achieve the required power rating. The feasibility of PV as an input source at bus stops is additionally investigated. This is done with a PV output model. The model uses the 'AstroSemi 365W' mono-crystalline panels from Astronergy. The module has a 365 Wp rated power and 19.7% efficiency at STC.

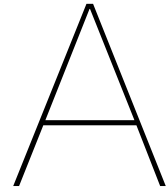
Opportunity charging is investigated by using different scenarios. The first scenario looks at the situation when every stop has a charger that is operational. The second scenario looks at the situation when a minimum amount of stops are used. The minimum amount is chosen to ensure that the electric bus can operate solely with opportunity charging throughout the day. These scenarios are tested with power ratings from 200kW to 100kW with charging times spanning from 30 seconds to 60 seconds. Different driving cycles have different energy consumption results for the electric bus. This results in different amounts of chargers for each driving cycle. The smallest average battery size observed is 51.5 kWh all stops have chargers. The result for the minimum amount of stops case indicates that fewer chargers are needed for high power ratings and longer charging times. The battery size however does not have a large drop, the size reduction spans from 25kWh to 0.

The PV feasibility results show that a standalone PV system placed on a bus stop is not sufficient. This is why a grid-tied PV system is needed with a battery as storage. The results show that the charger demand is especially harder to meet with a standalone PV system for months outside the summer. The results also show that for a grid-tied PV system, the power ratings of 200kW and 150kW are the most suited for opportunity charging. Opportunity charging is convenient when the charging time is low. The power ratings of 200kW and 150kW enable a charging time of 30 seconds. Also, the module amounts needed for 200kW and 150kW chargers that charge 30 seconds are sufficient to place in the area designated for stops in the Netherlands. The area mentioned considers the smallest area given by sources, since there are no location data available for the stops at the driving cycle data, thus the

specific knowledge of how much space there is for PV modules at stops is not present in this paper. The choice of power rating depends on the availability of power that can be delivered, the preference of battery size for the PV system, and the number of chargers that can be placed. 200kW chargers, need fewer chargers but are more dependent on the grid, while 150kW need more chargers and are less dependent on the grid. The 200kW charger usage results in less energy consumption when the bus operates in comparison to a 150kW charger. This difference ranges from 0.8kWh to 0.25kWh daily when a minimum number of chargers is used. The difference in energy consumption at a minimum battery size between both charger power ratings span from approximately 4kWh to 2kWh. These numbers represent the daily difference in energy consumption.

There are some stops at which the bus must wait longer than usual. This means that longer charging is possible at these stops. For this situation, a 200kW charger that charges for 40 seconds and a 150kW charger with 40 to 50 seconds charging times can also be considered. These power ratings and waiting times have module amounts that fit the area available at bus stops. The Energy-Neutrality ratio, which shows the yearly ratio between charger demand and PV system input shows a minimum of 0.4 for the discussed power ratings and waiting times. The lower bound for the Energy-Neutrality coefficient for 200kW and 150kW chargers with a charging time of 30 seconds is 0.5. This value could go up to 1 depending on the number of charges the charger needs to do throughout the day. This amount differs per driving cycle.

This paper can be improved by obtaining more detailed data about the passenger amount that enters or leaves the bus, the area at which the stops are, data about the traffic light placement, and grid data. The passenger data enables a more realistic analysis per driving cycle since the passenger amount is a factor that influences the bus weight throughout the driving cycle. This paper assumed the worst-case scenario where the bus operates at maximum passenger capacity throughout the day. The data about traffic light placement can prevent the possibility of seeing a traffic light as a stop. This paper lacks traffic light data and thus uses assumptions to distinguish a traffic light from a bus stop. These assumptions could result in an overestimation of the bus stop amount during a driving cycle. The data with the area available at stops improves the analysis of the PV feasibility analysis. The possibility of larger stop areas exists and this paper assumed the smallest area presented by sources to assume the worst case. The grid data availability helps with the congestion analysis. This paper tries to limit the PV input to prevent possible congestion. This influences the module amount determination. The grid data could make the module determination more accurate.



# Appendix

## A.1. Driving Cycles

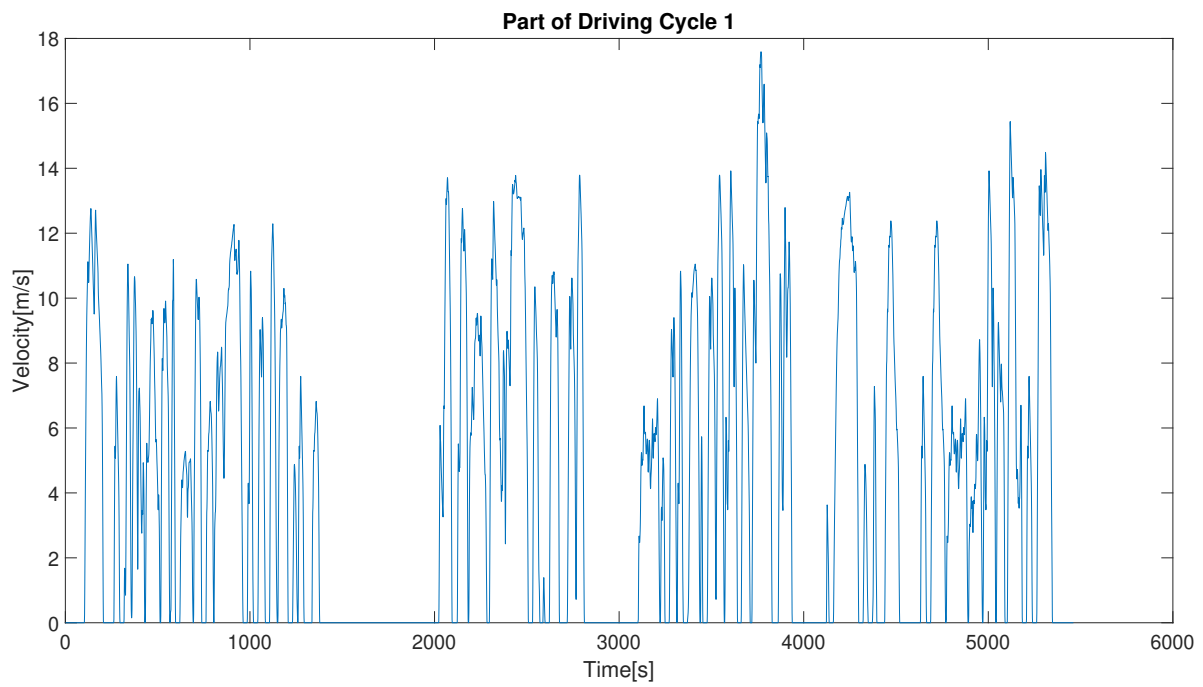


Figure A.1: Partial plot of driving cycle 1

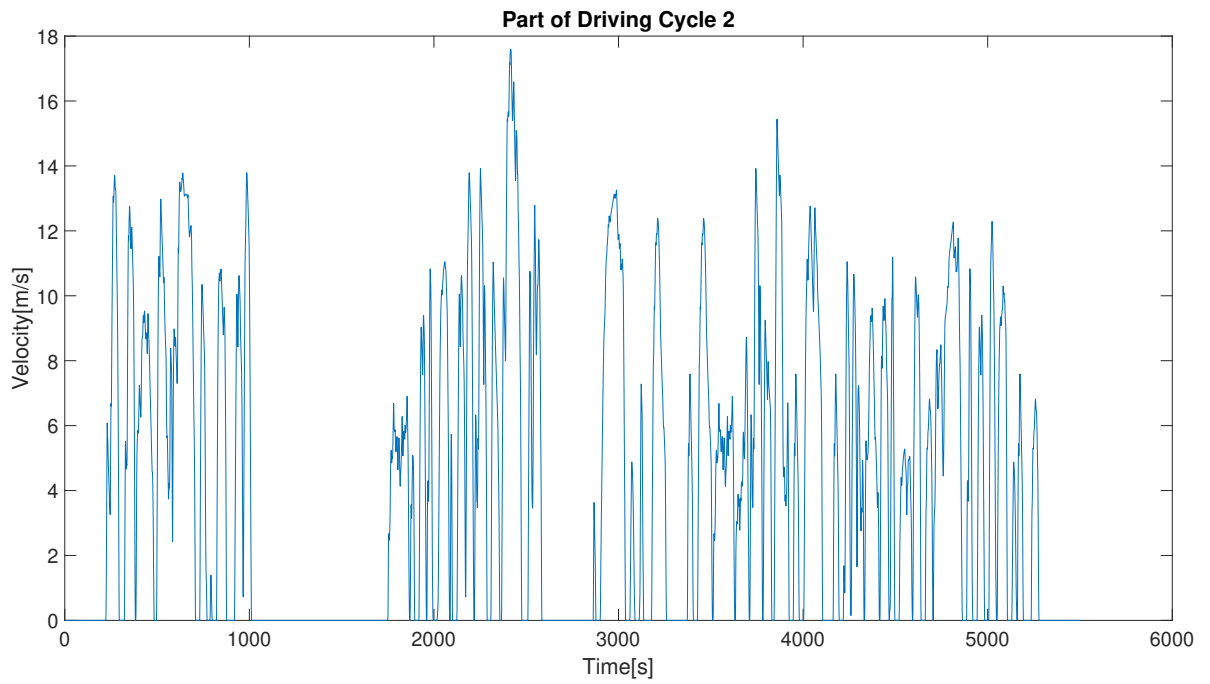


Figure A.2: Partial plot of driving cycle 2

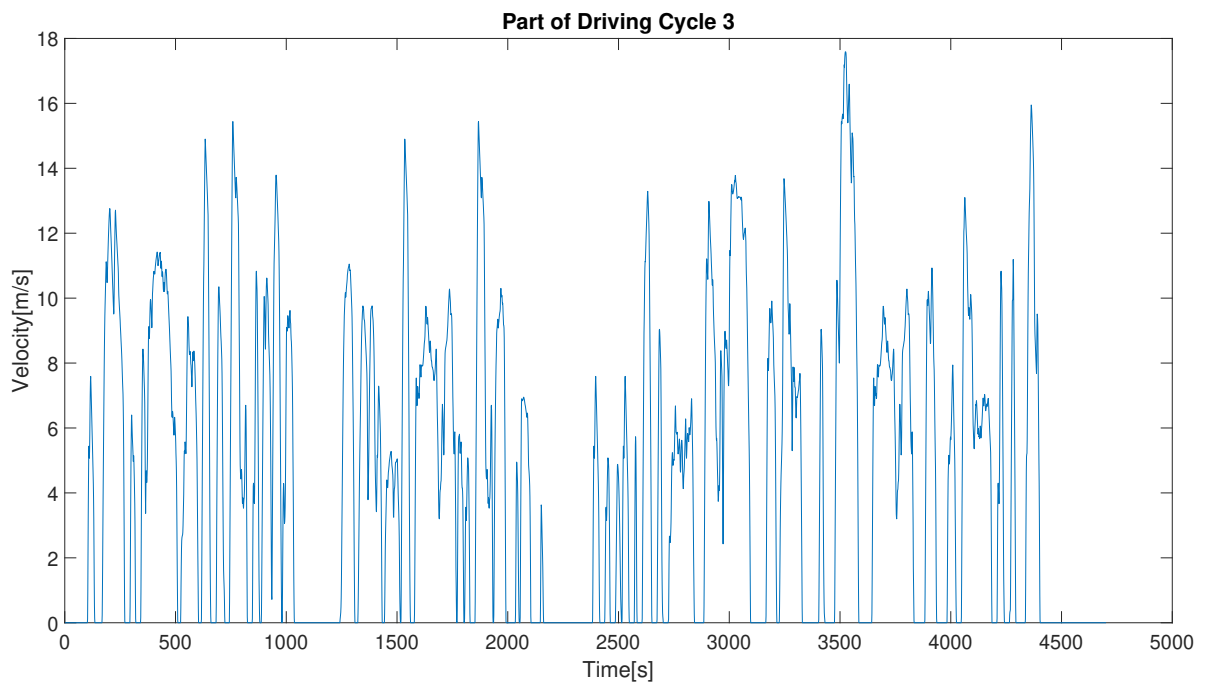


Figure A.3: Partial plot of driving cycle 3

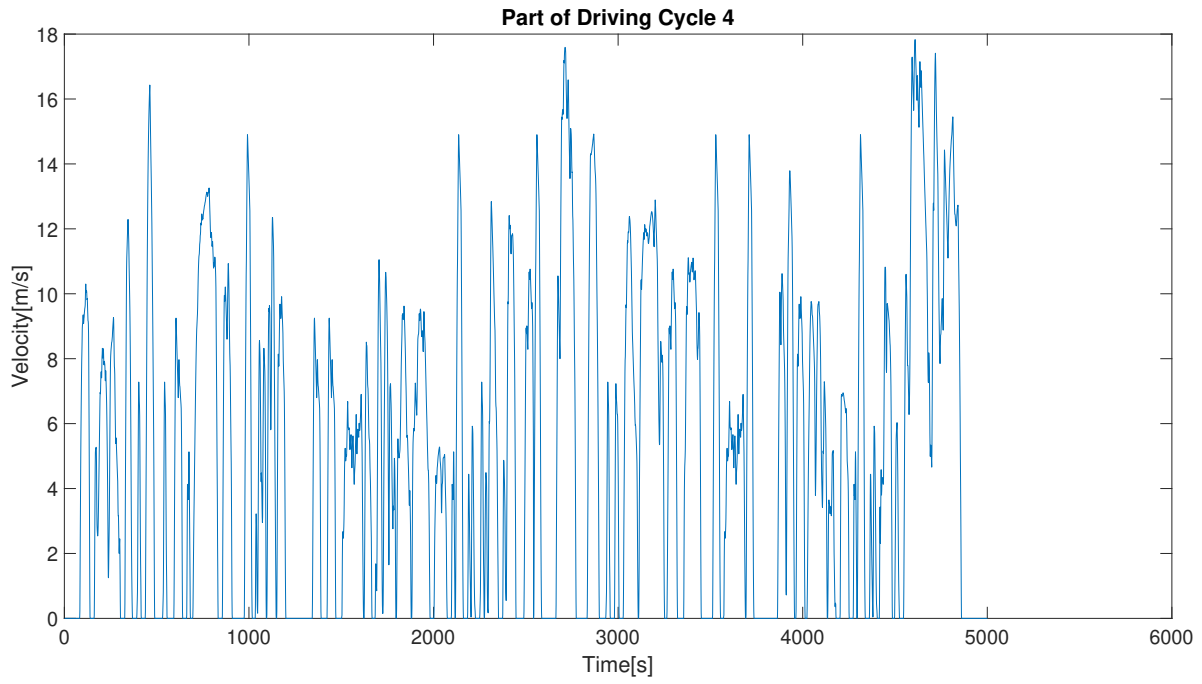


Figure A.4: Partial plot of driving cycle 4

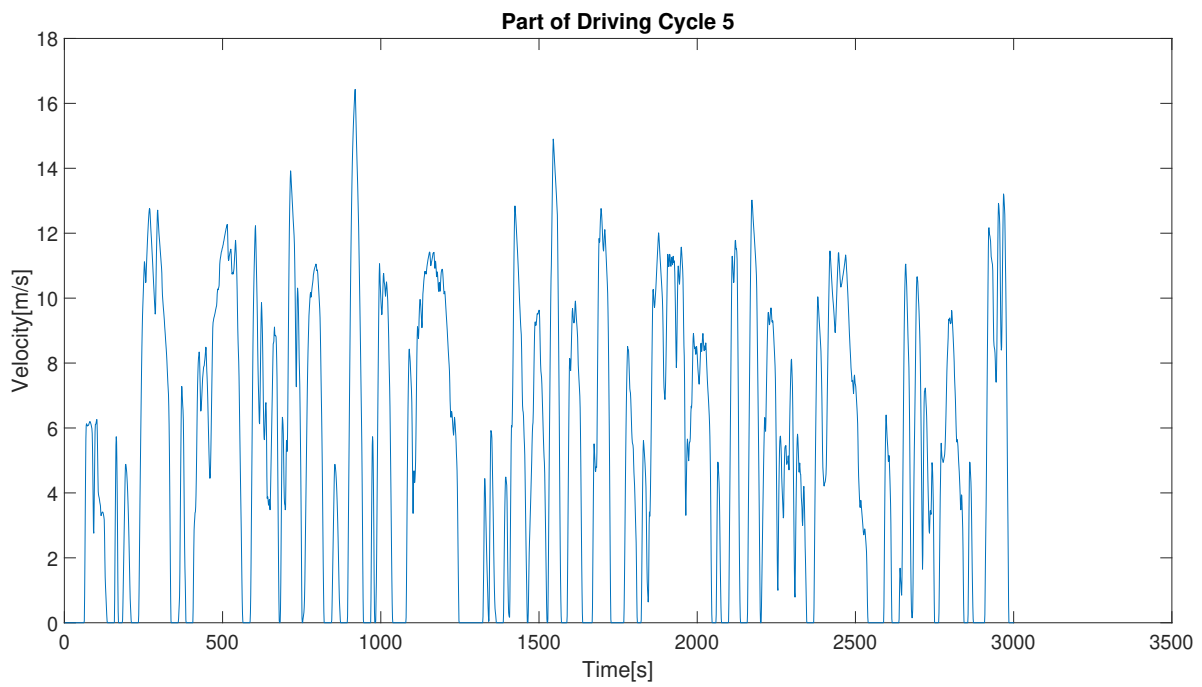


Figure A.5: Partial plot of driving cycle 5

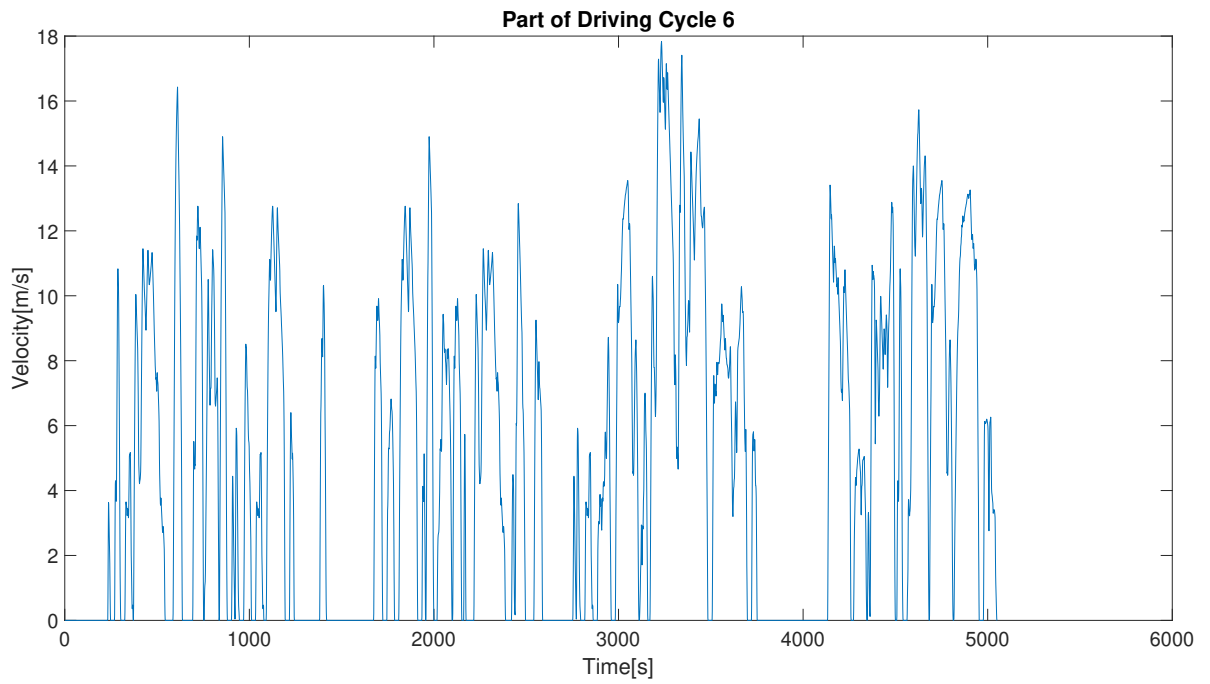


Figure A.6: Partial plot of driving cycle 6

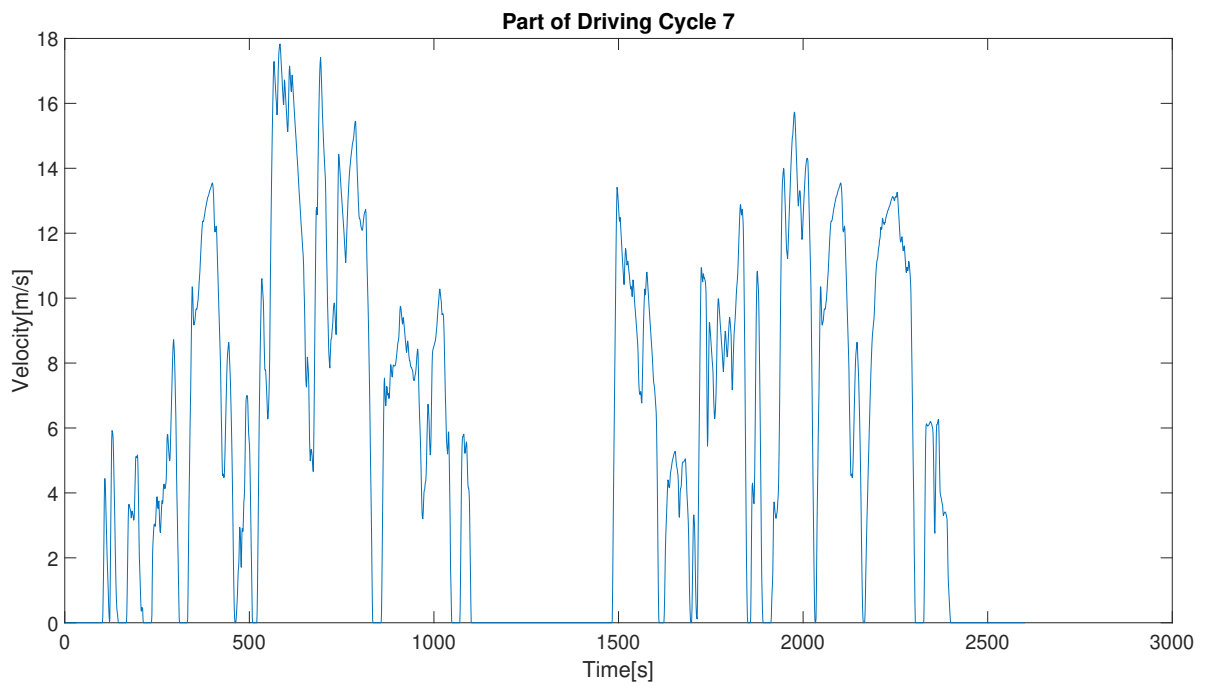


Figure A.7: Partial plot of driving cycle 7

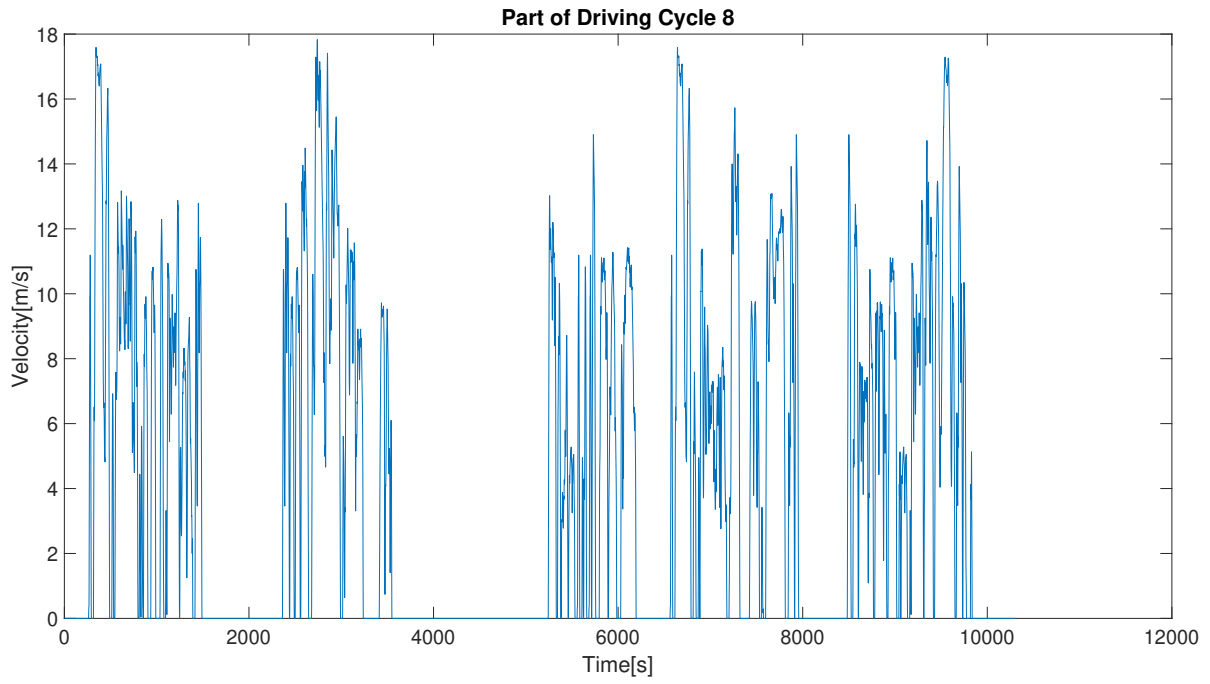


Figure A.8: Partial plot of driving cycle 8

## A.2. Energy Consumption

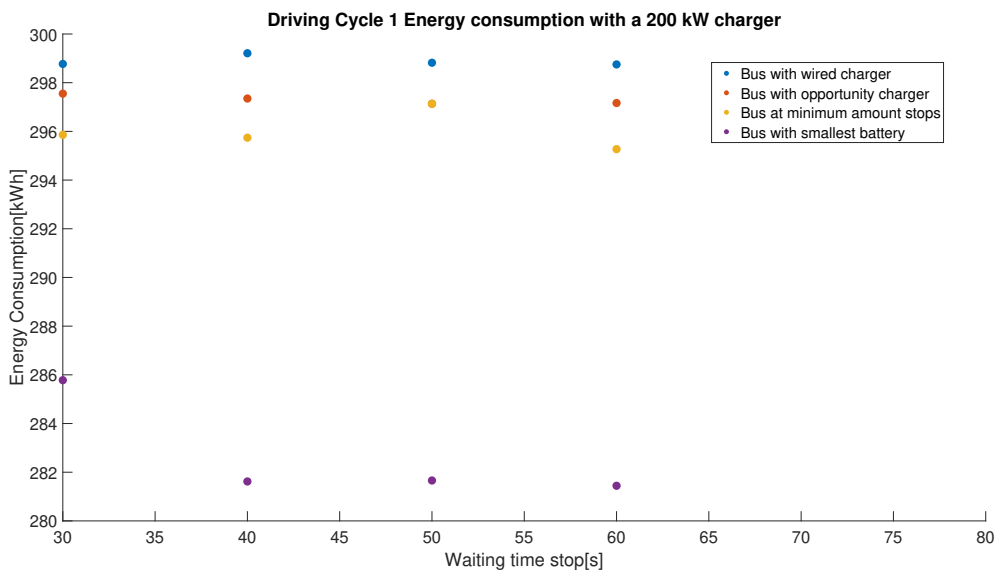


Figure A.9: Energy consumption plot of driving cycle 1 with a 200 kW charger.

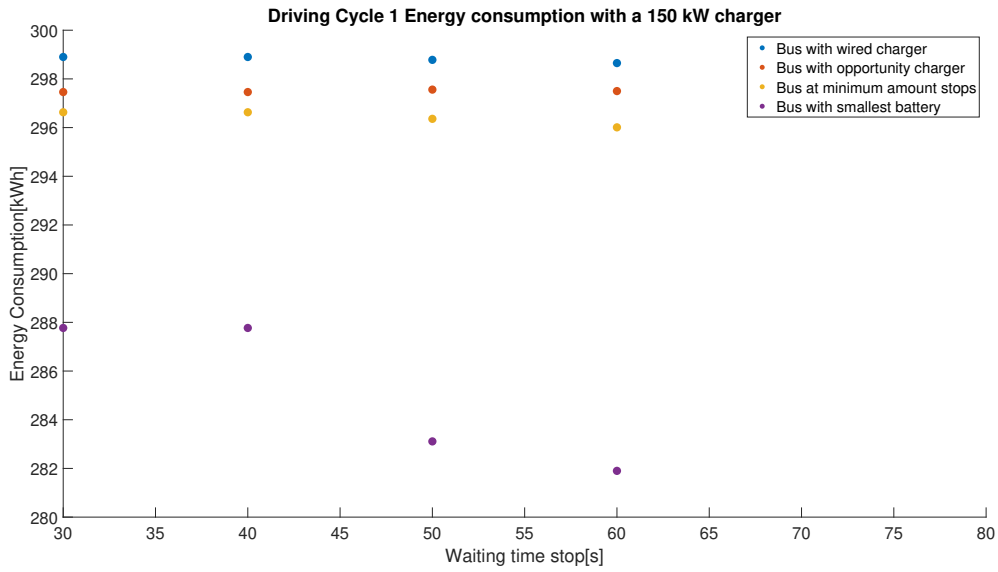


Figure A.10: Energy consumption plot of driving cycle 1 with a 150 kW charger.

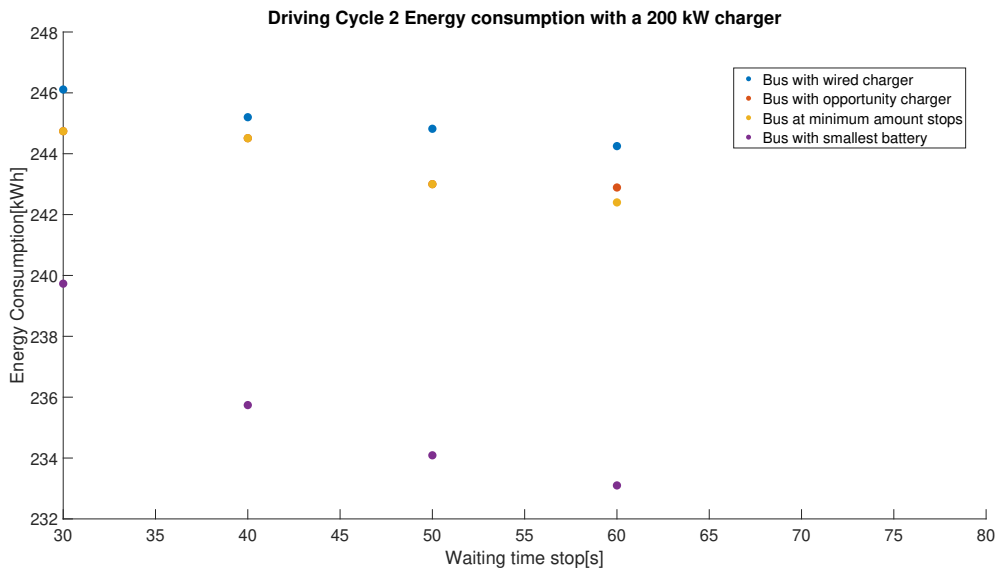


Figure A.11: Energy consumption plot of driving cycle 2 with a 200 kW charger.

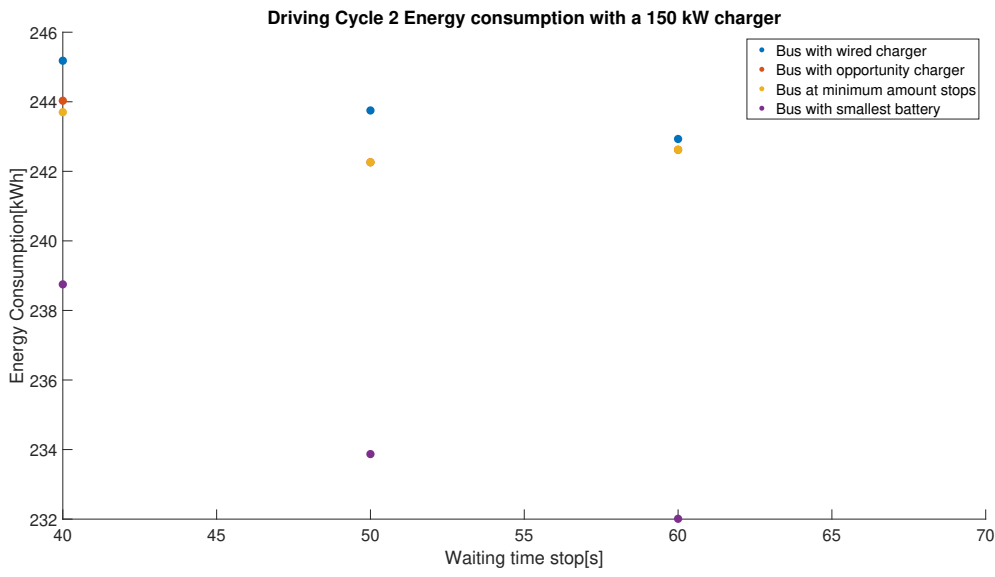


Figure A.12: Energy consumption plot of driving cycle 2 with a 150 kW charger.

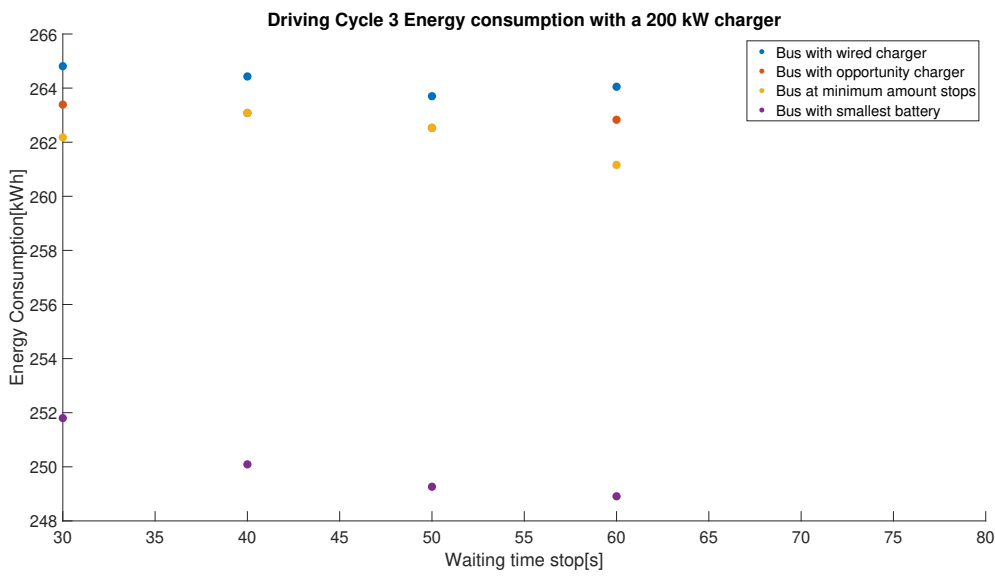


Figure A.13: Energy consumption plot of driving cycle 3 with a 200 kW charger.

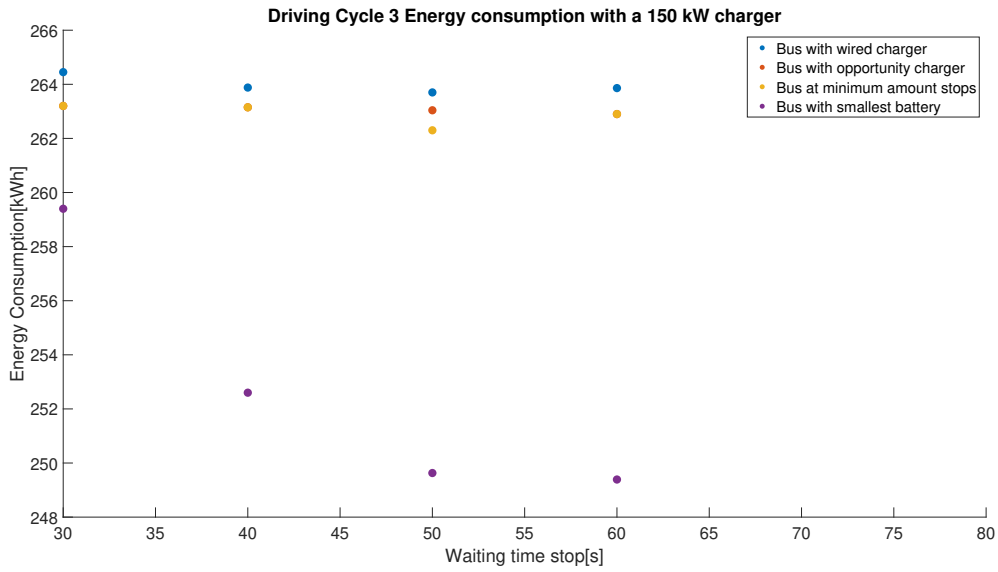


Figure A.14: Energy consumption plot of driving cycle 3 with a 150 kW charger.

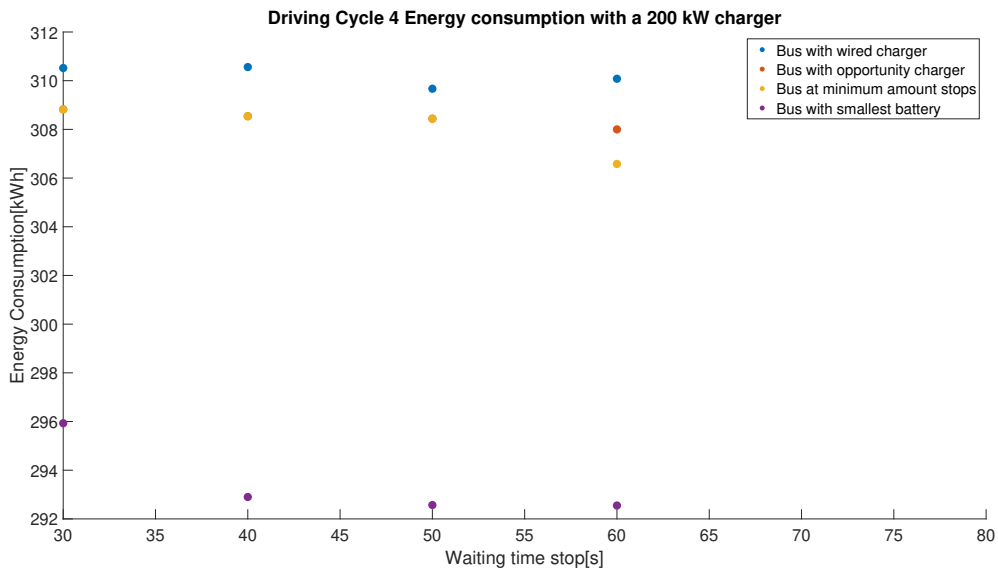


Figure A.15: Energy consumption plot of driving cycle 4 with a 200 kW charger.

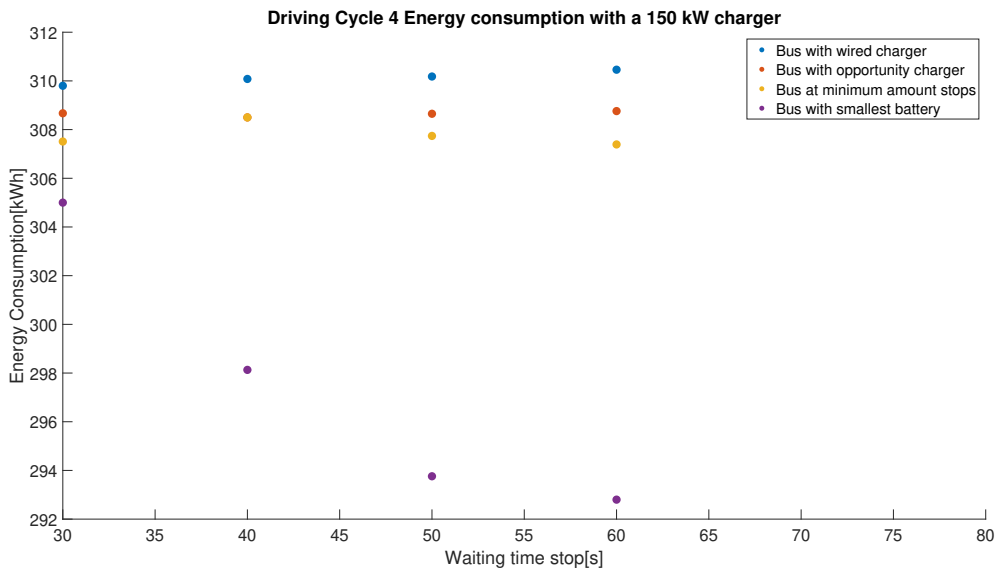


Figure A.16: Energy consumption plot of driving cycle 4 with a 150 kW charger.

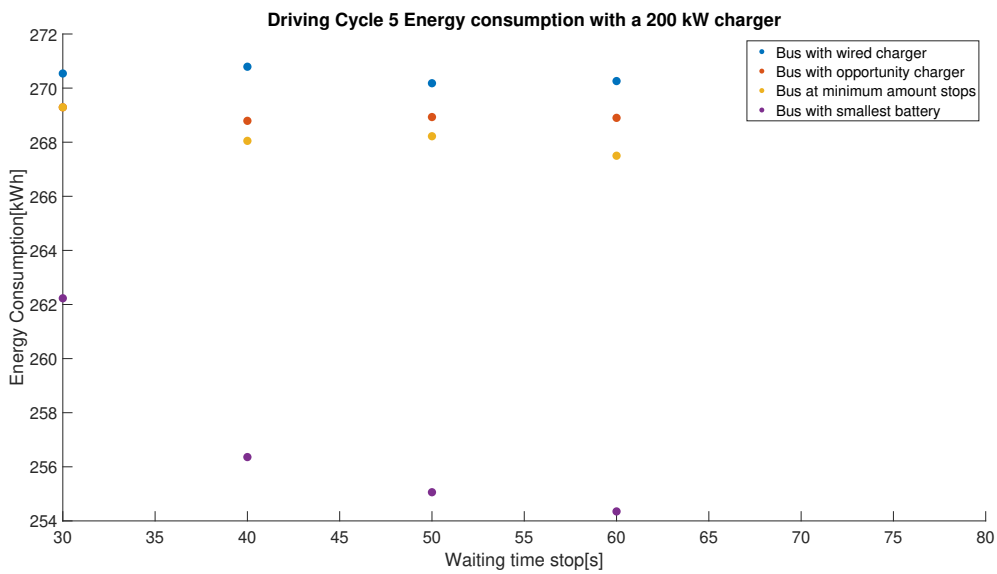


Figure A.17: Energy consumption plot of driving cycle 5 with a 200 kW charger.

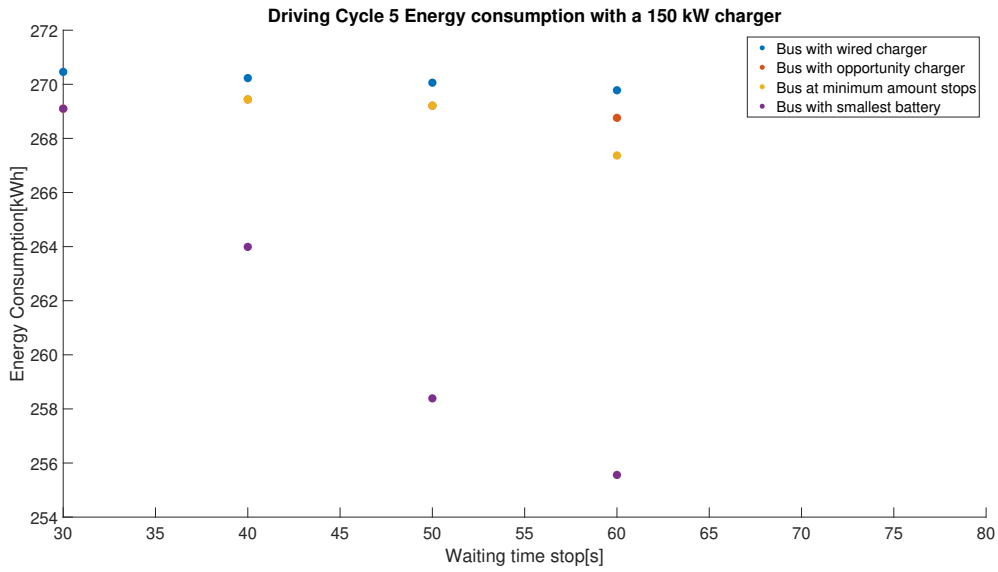


Figure A.18: Energy consumption plot of driving cycle 5 with a 150 kW charger.

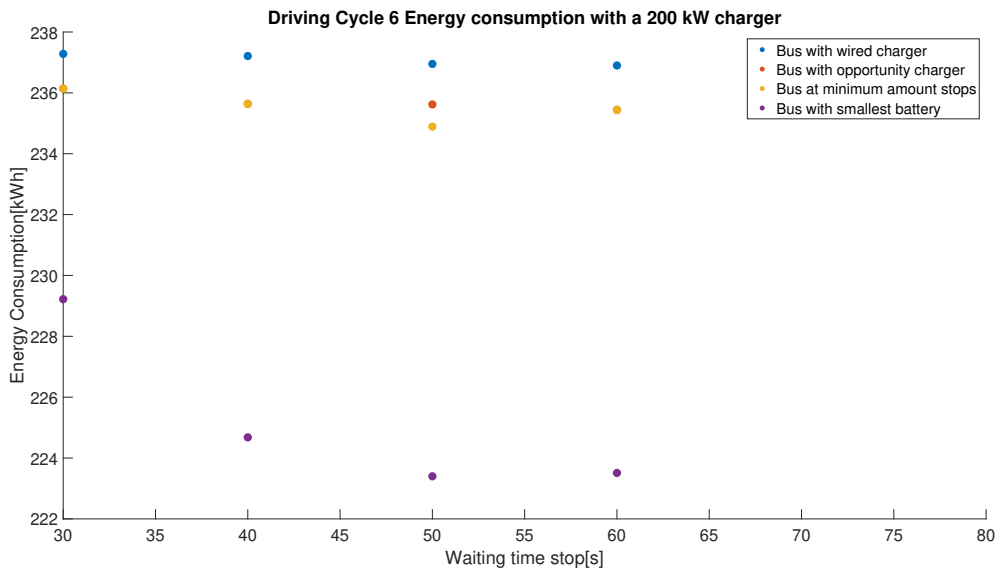


Figure A.19: Energy consumption plot of driving cycle 6 with a 200 kW charger.

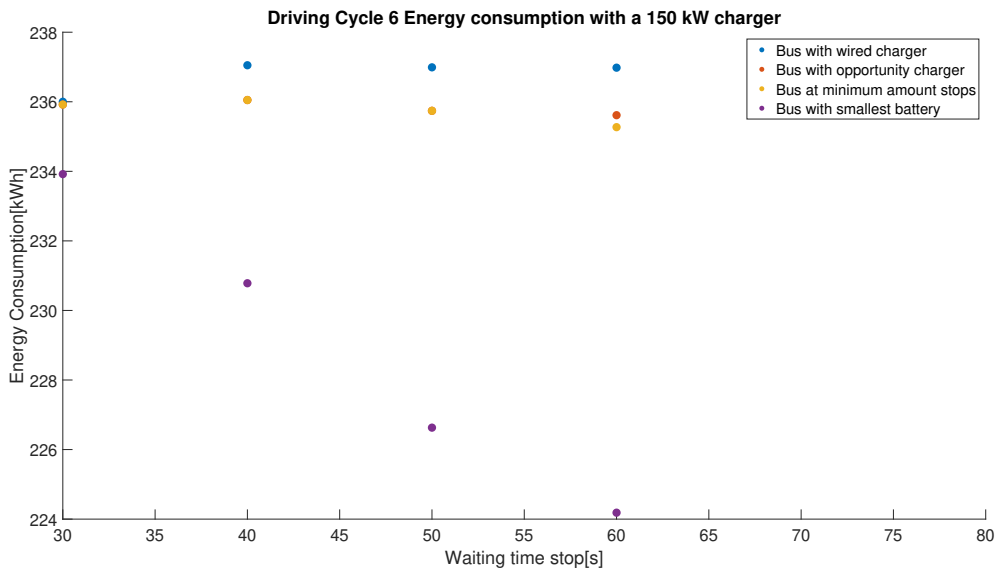


Figure A.20: Energy consumption plot of driving cycle 6 with a 150 kW charger.

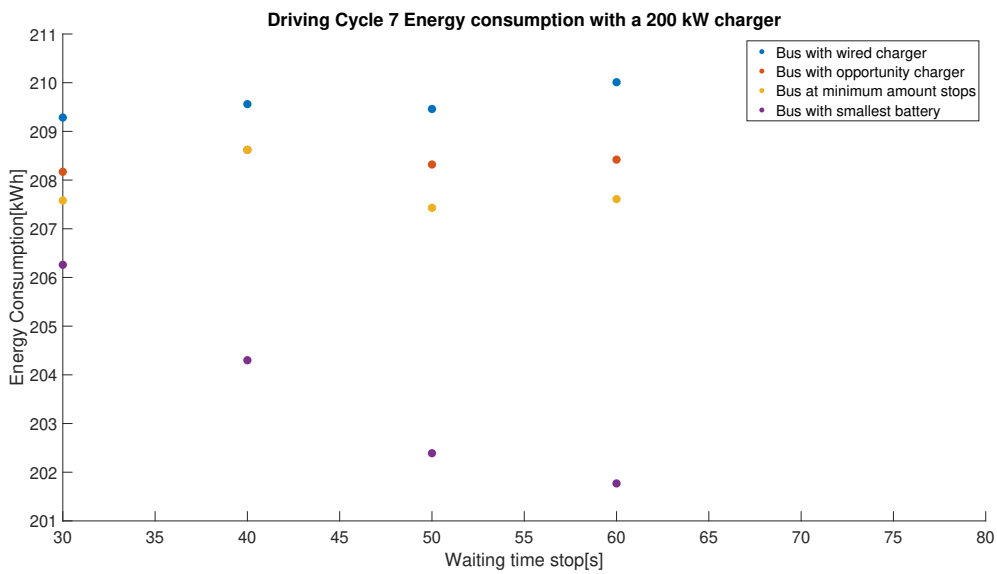


Figure A.21: Energy consumption plot of driving cycle 7 with a 200 kW charger.

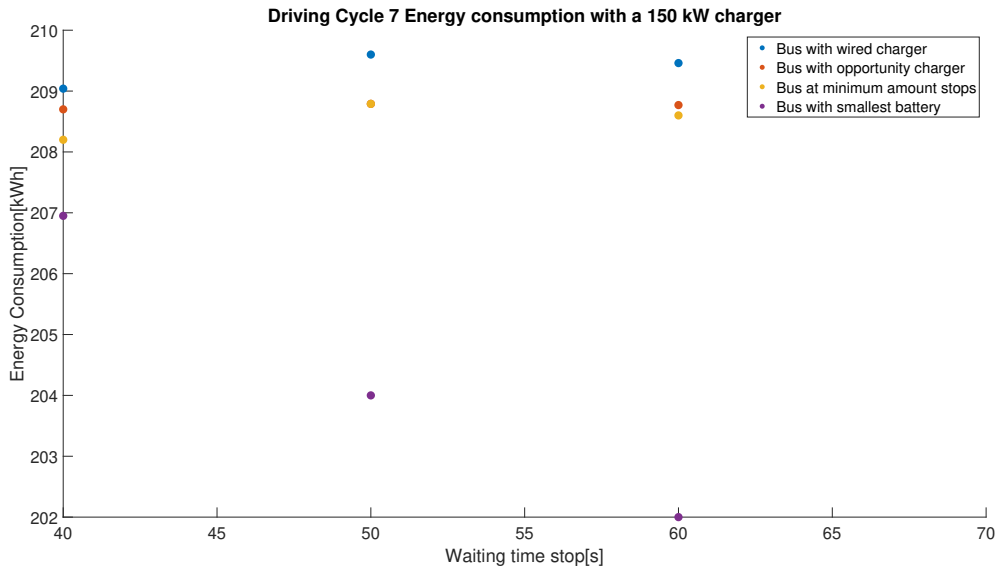


Figure A.22: Energy consumption plot of driving cycle 7 with a 150 kW charger.

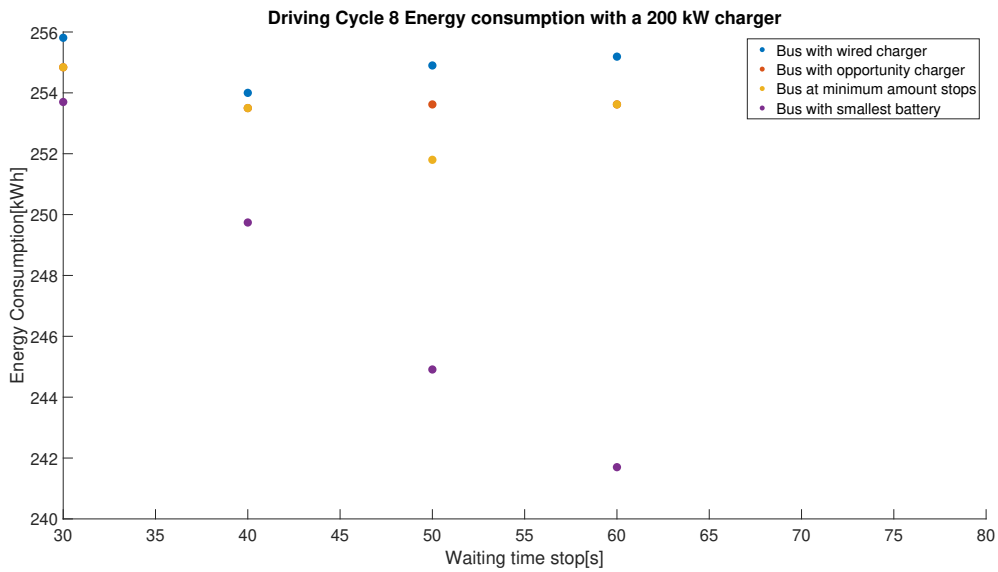


Figure A.23: Energy consumption plot of driving cycle 8 with a 200 kW charger

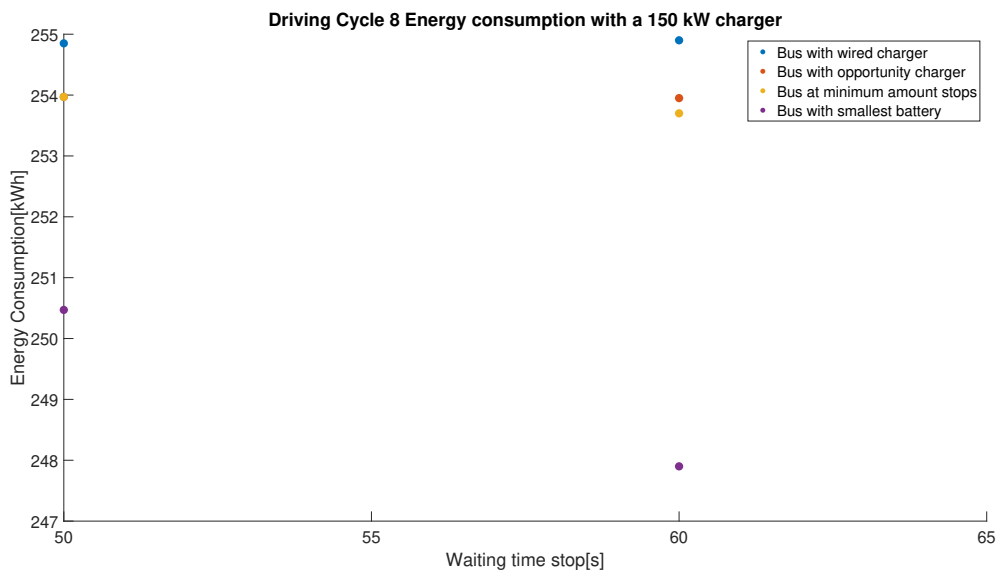


Figure A.24: Energy consumption plot of driving cycle 8 with a 150 kW charger



# Bibliography

- [1] URL: <https://www.studocu.com/bo/document/facultad-nacional-de-ingenieria/mecanica-tecnica/lecture-2-lateral-dynamics/27273998>.
- [2] N Abhay. "Modelling of Electric Powertrain for Heavy-Duty BEV". In: (2020). URL: <https://repository.tudelft.nl/islandora/object/uuid:009a6801-cf71-4490-9046-326113bce762?collection=education>.
- [3] *Abri Bushokje City*. URL: <https://www.skwshop.nl/bushokjes/abri-bushokje-city>.
- [4] Hussein Basma et al. "Comprehensive energy modeling methodology for battery electric buses". In: *Energy* 207 (2020), p. 118241.
- [5] Hussein Basma et al. "Comprehensive energy modeling methodology for battery electric buses". In: *Energy* 207 (2020), p. 118241. ISSN: 0360-5442. DOI: <https://doi.org/10.1016/j.energy.2020.118241>. URL: <https://www.sciencedirect.com/science/article/pii/S0360544220313487>.
- [6] Hussein Basma et al. "Energy consumption and battery sizing for different types of electric bus service". In: *Energy* 239 (2022), p. 122454. ISSN: 0360-5442. DOI: <https://doi.org/10.1016/j.energy.2021.122454>. URL: <https://www.sciencedirect.com/science/article/pii/S0360544221027031>.
- [7] Zicheng Bi et al. "Plug-in vs. wireless charging: Life cycle energy and greenhouse gas emissions for an electric bus system". In: *Applied Energy* 146 (2015), pp. 11–19.
- [8] *Blog: Congestion in the electricity grid*. Apr. 2023. URL: <https://smartcity-atelier.eu/allgemein/blog-congestion-in-the-electricity-grid/?cn-reloaded=1>.
- [9] Dr. Aviva Brecher and Mr. David Arthur. *Review and Evaluation of Wireless Power Transfer (WPT) for Electric Transit Applications*. URL: [https://www.transit.dot.gov/sites/fta.dot.gov/files/FTA\\_Report\\_No.\\_0069\\_0.pdf](https://www.transit.dot.gov/sites/fta.dot.gov/files/FTA_Report_No._0069_0.pdf).
- [10] BYD. *Superior Technology*. URL: <https://en.byd.com/bus/bus-technology/>.
- [11] Anthony Calabro et al. "Performance of 200-kW Inductive Charging System for Range Extension of Electric Transit Buses". In: *2019 IEEE Transportation Electrification Conference and Expo (ITEC)*. 2019, pp. 1–5. DOI: 10.1109/ITEC.2019.8790490.
- [12] Yung-Kang Robert Chin. "A permanent magnet synchronous motor for an electric vehicle - design analysis". In: 2004.
- [13] Davide Cittanti et al. "Modeling Li-ion batteries for automotive application: A trade-off between accuracy and complexity". In: *2017 International Conference of Electrical and Electronic Technologies for Automotive*. 2017, pp. 1–8. DOI: 10.23919/EETA.2017.7993213.
- [14] Olaf Czogalla and Ulrich Jumar. "Design and control of electric bus vehicle model for estimation of energy consumption". In: *IFAC-PapersOnLine* 52.24 (2019), pp. 59–64.
- [15] Karolis Dambrauskas et al. "A method for efficiency determination of permanent magnet synchronous motor". In: *Energies* 13.4 (2020), p. 1004.
- [16] Ibrahim Diab et al. "A Complete DC Trolleybus Grid Model With Bilateral Connections, Feeder Cables, and Bus Auxiliaries". In: *IEEE Transactions on Intelligent Transportation Systems* 23.10 (2022), pp. 19030–19041. DOI: 10.1109/TITS.2022.3157080.
- [17] Ibrahim Diab et al. "Placement and sizing of solar PV and Wind systems in trolleybus grids". In: *Journal of Cleaner Production* 352 (2022), p. 131533. ISSN: 0959-6526. DOI: <https://doi.org/10.1016/j.jclepro.2022.131533>. URL: <https://www.sciencedirect.com/science/article/pii/S0959652622011520>.

- [18] Mehrdad Ehsani et al. "Modern electric, hybrid electric, and fuel cell vehicles". In: (2018), Pages:44–50, 97–98.
- [19] Maurizio Di Paolo Emilio. *Wireless charging for evs*. Oct. 2022. URL: <https://www.powerelectronicsnews.com/wireless-charging-technology-for-evs/>.
- [20] *Factsheet bushalte Bergambacht*. URL: <https://www-crow-nl.tudelft.idm.oclc.org/>.
- [21] Jurgen Garche et al. *Encyclopedia of electrochemical power sources*. Newnes, 2013.
- [22] EMMA ARFA GRUNDITZ. "Traction Motor for a Battery Electric City Bus". In: (2021).
- [23] John G Hayes and Kevin Davis. "Simplified electric vehicle powertrain model for range and energy consumption based on EPA coast-down parameters and test validation by Argonne National Lab data on the Nissan Leaf". In: *2014 IEEE Transportation Electrification Conference and Expo (ITEC)*. IEEE. 2014, pp. 1–6.
- [24] Hongwen He, Rui Xiong, and Jinxin Fan. "Evaluation of Lithium-Ion Battery Equivalent Circuit Models for State of Charge Estimation by an Experimental Approach". In: *Energies* 4.4 (2011), pp. 582–598. ISSN: 1996-1073. URL: <https://www.mdpi.com/1996-1073/4/4/582>.
- [25] Hongwen He et al. "Comparison study on the battery models used for the energy management of batteries in electric vehicles". In: *Energy Conversion and Management* 64 (2012), pp. 113–121.
- [26] *INTIS inductive energy transfer systems at a glance*. URL: <https://www.intis.de/wireless-power-transfer.html>.
- [27] Mustafa Karamuk. "A survey on electric vehicle powertrain systems". In: *International Aegean Conference on Electrical Machines and Power Electronics and Electromotion, Joint Conference*. 2011, pp. 315–324. DOI: 10.1109/ACEMP.2011.6490617.
- [28] Kk. *Opportunity charging - the new industry standard for power supply to agvs, Amr amp; Co.* Aug. 2022. URL: <https://www.wiferion.com/en/opportunity-charging-industry-standard-power-supply-agvs-amr/>.
- [29] Antti Lajunen. *Comparison of Different Powertrain Configurations for Electric City Bus*. URL: <https://ieeexplore-ieee-org.tudelft.idm.oclc.org/stamp/stamp.jsp?tp=&arnumber=7007032&tag=1>.
- [30] King Long. *Electric Vehicles*. URL: [https://www.king-long.com/electric-vehicles\\_cl](https://www.king-long.com/electric-vehicles_cl).
- [31] Mercedes-Benz. *Technische brochures*. URL: [https://www.mercedes-benz-bus.com/nl\\_NL/buy/services-online/download-technical-brochures.html#content/headline](https://www.mercedes-benz-bus.com/nl_NL/buy/services-online/download-technical-brochures.html#content/headline).
- [32] Ilyès Miri, Abbas Fotouhi, and Nathan Ewin. "Electric vehicle energy consumption modelling and estimation—A case study". In: *International Journal of Energy Research* 45.1 (2021), pp. 501–520.
- [33] *Momentum Dynamics - Wireless Charging for Electric Vehicles*. URL: <https://inductev.com/>.
- [34] Optare. *Our Vehicles, Ultra lightweight and efficient*. URL: <https://www.optare.com/our-vehicles/>.
- [35] Proterra. *Revolutionizing transit, The Proterra ZX5 Electric Transit Bus*. URL: <https://www.proterra.com/products/transit-buses/>.
- [36] Claudio Rossi et al. "Simplified parameters estimation for the dual polarization model of lithium-ion cell". In: *ELECTRIMACS 2019*. Springer, 2020, pp. 129–144.
- [37] Saietta. *Heavy Duty eDrives*. URL: <https://www.saietta.com/applications/commercial-vehicles>.
- [38] *Sanyo NCR18650GA 3350mAh - 10A - CN*. URL: <https://eu.nkon.nl/sanyo-18650ga.html>.

- [39] Bram Scheurwater. *The potential of renewable energy sources for powering of trolleybus grids: An Arnhem case-study*. Nov. 2020. URL: <https://repository.tudelft.nl/islandora/object/uuid:39e1cfd8-1b53-415a-bfb5-62f09f9edd37?collection=education>.
- [40] Arno HM Smets et al. *Solar Energy: The physics and engineering of photovoltaic conversion, technologies and systems*. UIT Cambridge, 2015.
- [41] Solaris. *Zero emmissions powertrains, product catalogue*. URL: [https://www.solarisbus.com/public/assets/content/pojazdy/2021/2021/EN\\_Zeroemisyjne\\_1920\\_x\\_1080.pdf](https://www.solarisbus.com/public/assets/content/pojazdy/2021/2021/EN_Zeroemisyjne_1920_x_1080.pdf).
- [42] D Thiruvonasundari and K Deepa. "Electric vehicle battery modelling methods based on state of charge—review". In: *J. Green Eng* 10.1 (2020), pp. 24–61.
- [43] *Wireless charging market for electric vehicles 2023-2033: Technology, players and forecasts*. Oct. 2022. URL: <https://www.idtechex.com/en/research-report/wireless-charging-market-for-electric-vehicles-2023-2033-technology-players-and-forecasts/896>.
- [44] *Wireless charging of EVs*. URL: [https://ocw.tudelft.nl/wp-content/uploads/eCARS2x\\_Lecture\\_Notes\\_L4-1.pdf](https://ocw.tudelft.nl/wp-content/uploads/eCARS2x_Lecture_Notes_L4-1.pdf).